GIA NEWS FROM RESEARCH

The report indicates the status of a research project that is still ongoing within GIA.
Comments on this and other reports and their direction are warmly welcomed as are offers of collaboration.
Contact information can be found in the “about the authors” section on page 70.

AN IN-DEPTH GEMOLOGICAL STUDY OF BLUE SAPPHIRES FROM THE BAW MAR MINE (MOGOK, MYANMAR)

Wasura Soonthorntantikul, Wim Vertriest, Victoria Liliane Raynaud-Flattot, Supharart Sangsawong, Ungkhana Atikarnsakul, Charuwan Khowpong, Vararut Weeramonkhonlert and Vincent Pardieu

Figure 1: Rough and faceted blue sapphires from Baw Mar (North) mine, Mogok, Myanmar. Photo: V. Pardieu © GIA.

INTRODUCTION

High quality blue sapphires have been mined in Myanmar for centuries (Kane & Kammerling 1992, Themelis 2001, Hughes 1997). Until the end of the 20th Century, sapphires were mined from the Mogok Stone Tract, mainly in the western area near Kyatpin and around Mogok town. Towards the end of the 20th Century blue sapphire mining extended to the west around Kyauk Pya That, Kabaing and Kin, to the north around Barnard Myo and in the Chaung Gyi valley, and in the east around Peint Pyit village (Themelis 2008, Hughes 2016).

Between 2011 and 2016 new production from Baw Mar area started to reach the market and attracted the attention of gemologists visiting the region (Phyo Kan Nyunt et al., 2013). GIA field gemologists visited Baw Mar operations in 2013, 2014, and 2015. It was evident the mine was not only the highest altitude mine in the whole of the Mogok area but also one of Mogok's largest mining operations. Its sapphire production is interesting and challenging for gemologists as, its sapphire characteristics (chemistry and internal features) are slightly different from the classic Burmese sapphires.

The aim of this research project is to expand our knowledge of these gemstones which can be a challenge in terms of origin determination. During the field expeditions and subsequent laboratory work it became clear that even within the same mine, sapphires can look different to one another depending on the area where they are mined; samples from the southern area are generally lighter in color than the sapphires recovered from the northern part of the mine.

In this study, we analyzed samples collected at the office (located near the mining site where the production was sorted) during two separate expeditions. The samples were mined from opposite parts of the mine, southern and northern, respectively. The general gemological characteristics; inclusions, UV-VIS and IR spectra and trace element chemistry are covered. A description of the mine, mining techniques employed and preliminary geological observations are also provided. Most of the data collected reveals sufficient information to differentiate between the two sampled areas within the same mine. It is clear that the Baw Mar sapphires formed in a complex geological environment with the potential to produce a range of qualities (high to low), various inclusion scenes and variable trace element concentrations.

CONTENTS

PART I: GIA FIELD EXPEDITION AND FIELD DESCRIPTION

1.1 FIELD DESCRIPTION

The GIA Field Gemology department visited the Baw Mar sapphire mine during GIA Field Expeditions FE46 on 22/09/2013, FE50 on 23/02/2014 and FE75 on 26/12/2015. The mine produces sapphires from a primary and secondary deposit and is located in the hills to the north of Kyatpyin in the western part of Mogok. It covers a large area and shows clear evidence of some form of strip mining, combined with underground workings.

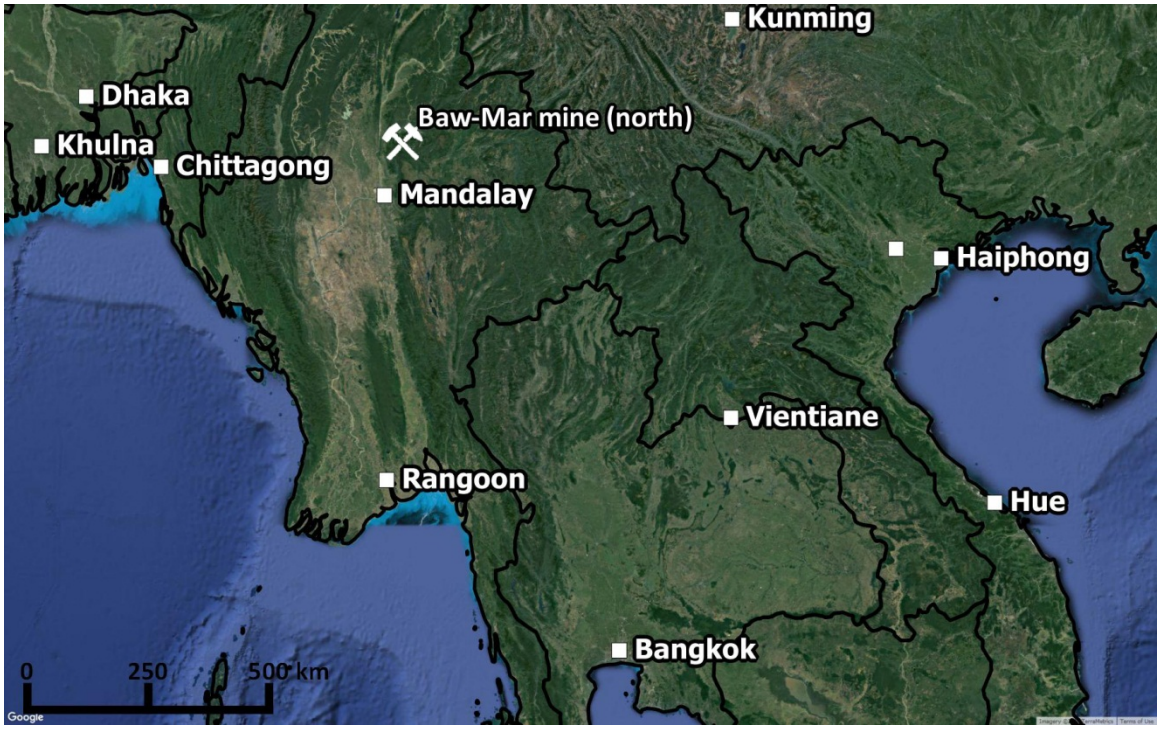

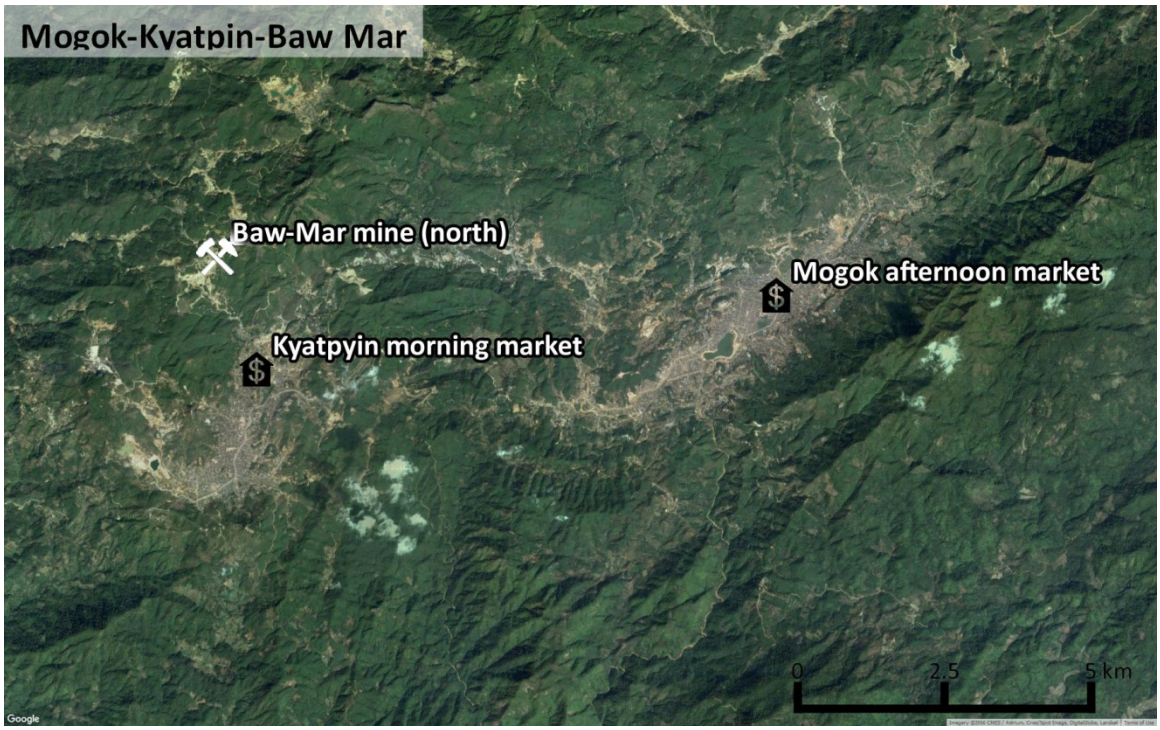

Currently, the northern part of the mine generates the majority of the production. The miners in this part of the mine work in a primary deposit which they exploit during the dry season. Secondary/detritic deposits are mainly worked during the rainy season because the washing process requires a substantial amount of water. However every visit made showed the dynamic nature of the mining environment via the visible changes witnessed at the mining site. Specific areas of the mine, and even the gems recovered, possess slightly different properties to areas and stones located in a different area of the same mine. This study focusses on two sets of samples collected during separate visits (2013 and 2015), from separate areas in the mine (Baw Mar North and South). All the samples were obtained at the mine sorting office located near the mining site.

Figure 2: View of the northern part of the Baw Mar sapphire mine in December 2015. Two types of mining are evident: In the foreground miners are washing the gem rich ground with high pressure water cannons jets while in the background the blue tent marks where miners are tunneling into the sapphire rich rocks. White zones containing corundum can be seen on the stepped strip wall center right in the photo. Photo by Vincent Pardieu © GIA.

Figure 3: View of the southern part of the Baw Mar sapphire mine in December 2015. The main activity involved washing gem rich ground from the area using high pressure water canon jets and a pulsating jig. Photo by Vincent Pardieu © GIA.

1.2 GEOLOGICAL DESCRIPTION

In the Baw Mar North area where sapphires are mined in primary type deposit, the sapphires are found in zones that are easy to spot. These zones consist of lighter colored material, contrasting with the gray-brownish host-rock surrounding it. The contact zone is formed by a layer of brown mica. The zones are very irregular, but easily differentiated from the surrounding rocks. The corundum bearing zones are common and are on average 1 meter wide, but there is a large variation in the width. The zones were estimated to be about 9-10 meters apart, but this is highly irregular. Corundum itself is found throughout the entire white layer.

Based on these observations, we *suspect* that the sapphires formed in intrusive dikes. These dikes are likely of syenitic composition (high Al/Si ratio). Syenites are intrusive rocks that are deficient in quartz; the main mineral usually being feldspar. These rocks have been known to host sapphires in other localities (Groat, 2014; Kievlenko, 2003). The dikes intruded the gneiss host rock and an alteration zone made of biotite formed at the contact zone/point.

Figure 4: The white sapphire containing area is about 2 meters wide and contrasts strongly with the brownish gneisses around it. Photo by Stanislas Detroyat © GIA.

The quality and size of the corundum crystals formed varies greatly. Some corundum zones contained corundum crystals measuring over 15 cm. These minerals were heavily fractured and opaque. Gem quality crystals were usually smaller (2 to 8 mm), but they occurred in similar zones. As far as we could observe, one zone contained corundum of a single quality. Miners use this consistent trait to decide which zones they will exploit. For example, miners will never put a lot of resources into excavating a zone that is characterized by large opaque corundum crystals because it is highly unlikely that they will find any gem-quality material in the same zone. On average, one in ten zones is exploited.

Figure 5: Wim Vertriest holds a sample of matrix hosting blue sapphires, fresh from the mine. Photo by V. Pardieu © GIA.

Figure 6: Closer view of the sapphires in their matrix seen in the previous photo. Photo: V. Pardieu © GIA.

Figure 7: Left: Miner holding non gem-quality sapphires, including some in matrix. Right: Mine owner Daw Kyi OO Mint holding a tray of rough and faceted sapphires. Photos by V.Pardieu © GIA.

The gem-bearing zones consist of pure white material containing a relatively high amount of water. When exposed to dryer air and higher temperatures (e.g. during travel or in the lab), it starts to dry and begins to crumble. The sapphires are embedded in this white mass. They are clearly visible as their striking blue color contrasts very strong with the white matrix. Some rust-brown zones that look like weathering zones where fluids circulated are also evident throughout the matrix. The fluids were probably saturated in iron and deposited limonite-goethite crusts in the most permeable zones, giving rise to the rust-colored stains. This white rock is separated from the gray-brown gneiss by a layer of very brittle brown to orange mica that can be several centimeters thick. Some mica-crystals are very well developed and measure over 10 cm.

Based on very limited field observations and some discussions with the miners, it seems that finer mica around the white zones and purer white matrix result in higher quality sapphires. The size of the mica crystals at the contact zone seem to be related to the size of the corundum crystals, but inversely related to the quality of the corundum (large mica at the rim indicates large, low quality corundum within the white matrix; small mica is associated with small gem-quality sapphire).

Figure 8: Sapphire mining at Baw Mar North. The miner is using simple hand tools. Photo: V. Pardieu © GIA.

Figure 9: Feldspar-kaolin matrix containing sapphires. The rim consists of dark mica. Photo by W. Vertriest © GIA.

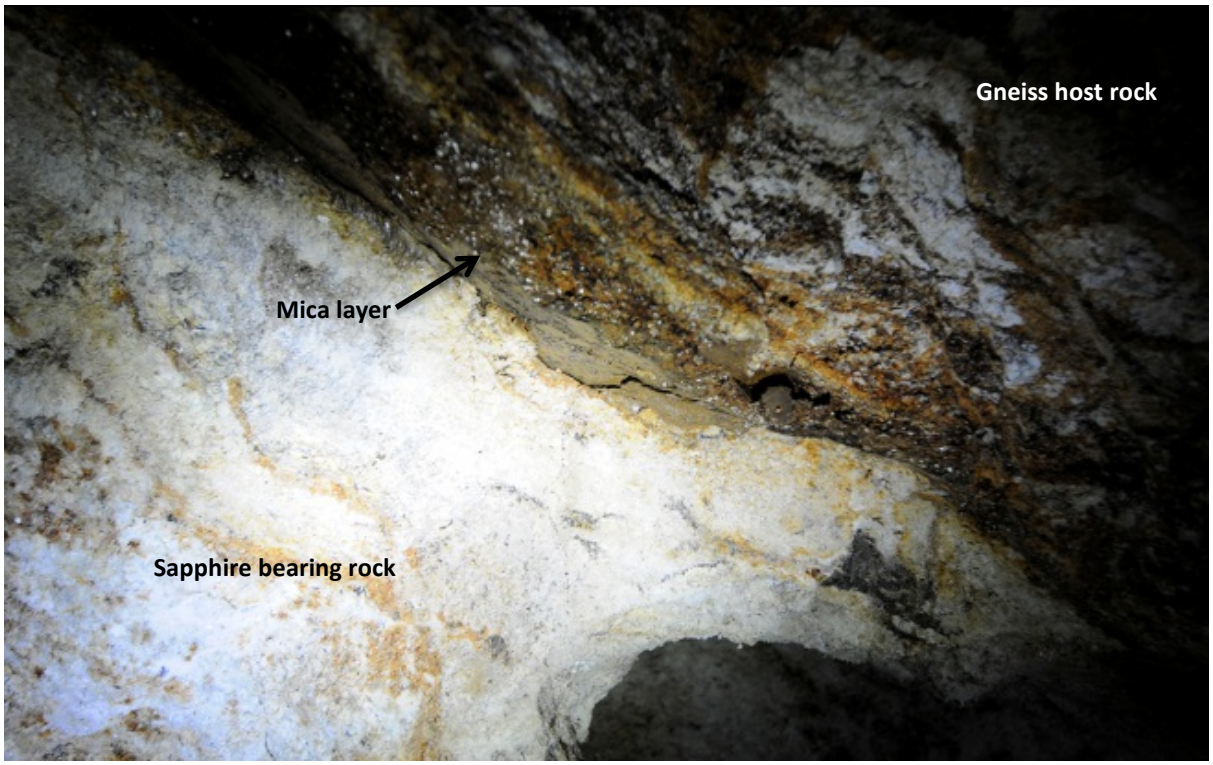

Figure 10: Sapphire bearing rock, mica layer and gneiss host rock. Photo by W. Vertriest © GIA.

1.2.1 MATRIX ANALYSIS

We collected some matrix samples in the mine and brought them to the lab for analysis. The matrix of two samples was analyzed with Raman spectroscopy at GIA Bangkok.

One specimen of matrix consisted entirely of Na-feldspar (albite), while the other sample was associated with minerals that resulted from the hydrothermal alteration of feldspars (dickite).

NOTE: Raman spectroscopy of these samples is very difficult because theyare not polished or cut. This causes high scattering and irregular reflections. Another disadvantage is that Raman cannot quantify the mineral concentrations in the matrix. Other techniques (e.g. X-ray diffraction) may be more suitable for obtaining an overview of the composition of the matrix, but the detection limit of these techniques is usually too low to correctly detect all the trace minerals. An advantage of Raman spectroscopy is that every individual grain can be analyzed.

Figure 11: The first sample (100318470691) showing sapphire crystals in their albite matrix host. The sample width is around 55mm. Photo by Wim Vertriest© GIA.

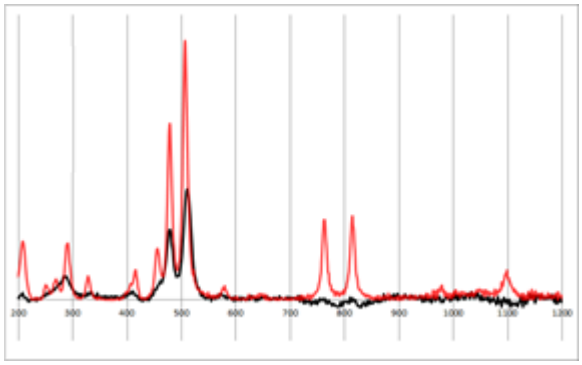

Figure 12: Mineral A (black spectrum) in the first sample compared to the reference spectrum of albite from the RRUFF database (red spectrum).

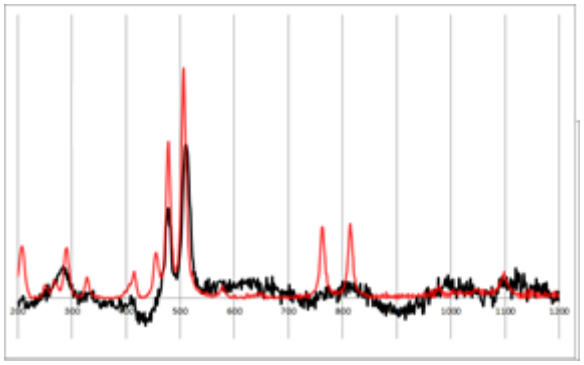

Figure 13: Mineral B (black spectrum) in the first sample compared to the reference spectrum of albite from the RRUFF database (red spectrum).

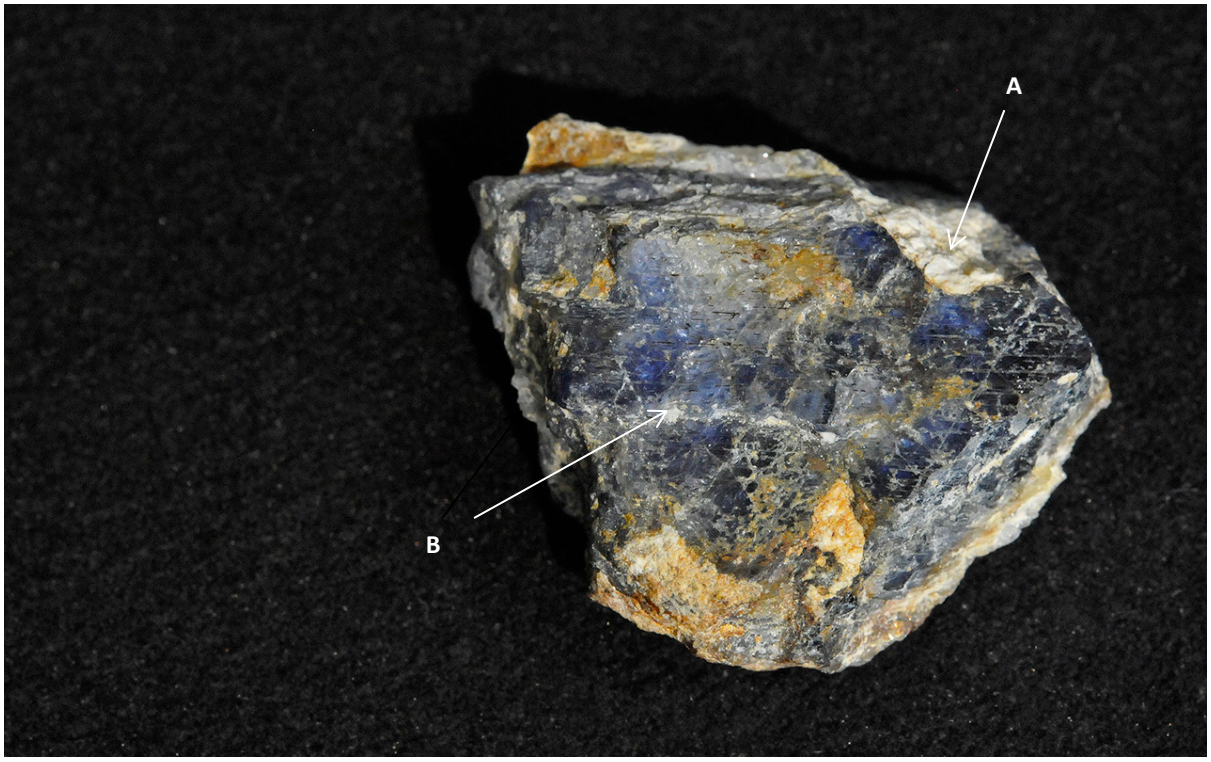

Figure 14: The second sample (100318470694) showing a sapphire crystal associated with dickite. The sample width is around 23mm. Photo by Wim Vertriest© GIA.

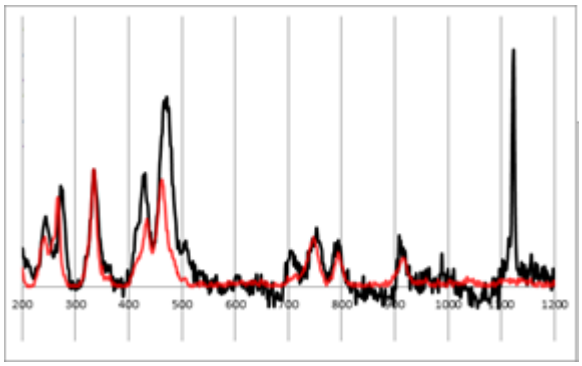

Figure 15: Mineral A (black spectrum) in the second sample compared to the reference spectrum of dickite from the RRUFF database (red spectrum).

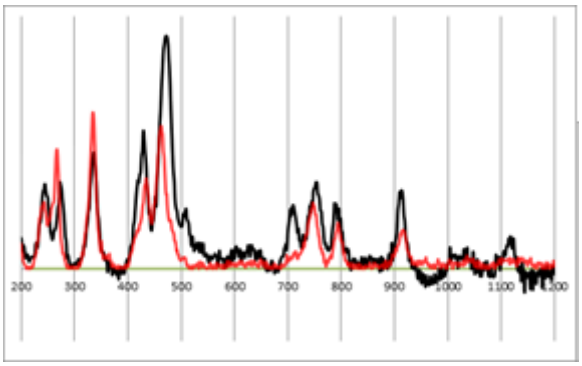

Figure 16: Mineral B (black spectrum) in the second sample compared to the reference spectrum of dickite from the RRUFF database (redspectrum).

1.2.2 MINING TECHNIQUES

Mining at Baw Mar (North or South) is either carried out by washing the sapphire rich ground (alluvial, colluvial or in-situ primary deposits) using mainly high pressure water cannons and passing the ore through pulsating jigs. During the dry season mining in primary deposits is performed by digging tunnels into sapphire bearing rocks. These rocks are first exposed by excavators, which strip away all the waste rock. No explosives are used, because the weathered gneisses and other rocks offer little resistance. The mine tunnels are lightly supported by some wooden structures and the miners depend on a rudimentary system to blow in additional air to help them breath. Miners use very simple hand-tools, mainly picks, to dig through the rocks. This is most likely because the rocks containing the sapphires are very weak as a result of extreme weathering/alteration. The chunks of sapphire-bearing rock are then brought up to the surface and processed.

Figure 17: Washing the sapphire rich rocks with water cannons at Baw Mar North. Photo: V. Pardieu © GIA.

Figure 18: A miner working in Baw Mar with an iron bar in order to loosen the sapphire bearing rocks. Photo by Wim Vertriest © GIA.

PART II: MATERIALS AND METHODS

2.1 SAMPLE FABRICATION:

In this work, the samples were collected from two areas in Baw Mar mine during GIA field expeditions FE46 and FE75. Based on the GPS coordinates of these two mining area, the samples collected from FE46 were denoted as originating from the Northern area in Baw Mar mine (N), whereas those from FE75 were denoted as originating from the mines' Southern area (S).

All 64 samples were fabricated in GIA's Bangkok Laboratory by Jonathan Muyal and Victoria Liliane Raynaud-Flattot (Table 1). These samples were fabricated for two different purposes:

i) 29 samples from the Northern area and 25 samples from the Southern area were selected to document their inclusions because their quantity prevented the collection of high quality optical data. In order to optimize the study of their internal features, one or more windows were polished regardless of their orientation to the c-axis.

ii) 7 samples from the Northern part and 3 samples from the Southern part were selected as 'spectra quality samples'. These samples needed to possess a sufficiently large and clean area in order to enable high quality reference spectra to be collected down the c-axis, and/or perpendicular to the c-axis. In this study, 3 out of 7 samples from the Northern area and all 3 samples from the Southern area were fabricated with one set of polished surfaces perpendicular to the c-axis, while another 4 samples from the Northern area were fabricated with one set of polished surfaces parallel to the c-axis.

Optical path lengths of the wafers were measured with a Mitutoyo Series 395 spherical micrometer with an accuracy of 2 microns.

Table 1: Details of the samples studied. 'N' refers to the samples from Northern area of Baw Mar mine and 'S' from the Southern area of the mine.

GIA Reference #	Weight (carats)	Polished wafer orientation	Path length (mm)	Image (Transmitted light)
For spectroscopic study				
100305165**161-N**	0.340	parallel to c-axis	1.148	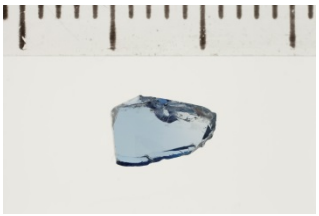
100305165**177-N**	1.457	perpendicular to c-axis	3.332	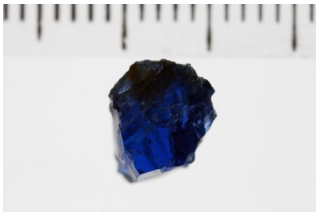

GIA Reference #	Weight (carats)	Polished wafer orientation	Path length (mm)	Image (Transmitted light)
100305165**188-N**	0.350	parallel to c-axis	1.231	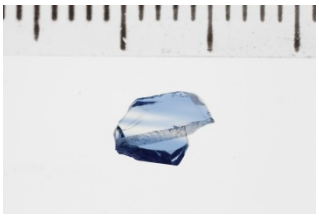
100305165**189-N**	0.260	parallel to c-axis	1.185	
100305165**190-N**	0.227	parallel to c-axis	1.008	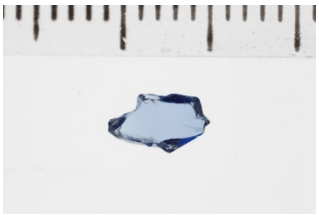
100305165**202-N**	0.217	perpendicular to c-axis	0.217	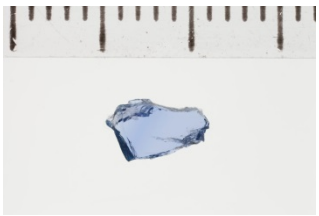
100305165**203-N**	0.183	perpendicular to c-axis	0.836	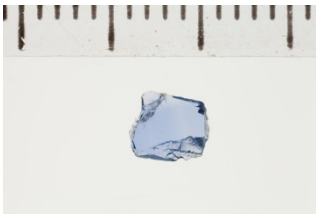
100318470**716-S**	0.666	perpendicular to c-axis	0.696	
100318470**741-S**	0.263	perpendicular to c-axis	0.666	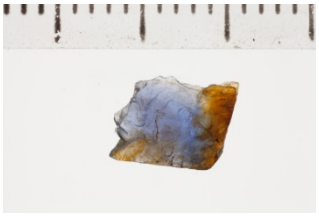

GIA Reference #	Weight (carats)	Polished wafer orientation	Path length (mm)	Image (Transmitted light)
100318470**763-S**	0.096	perpendicular to c-axis	0.405	
For Inclusions Study				
100305165**159-N**	0.518	unoriented	1.770	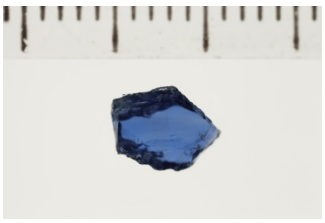
100305165**160-N**	0.448	unoriented	1.800	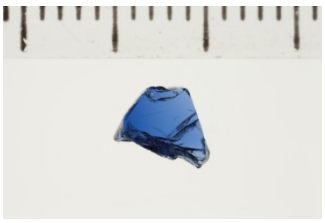
100305165**163-N**	0.742	unoriented	0.990	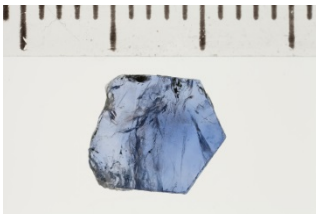
100305165**165-N**	2.754	unoriented	4.190	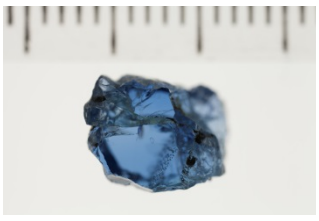
100305165**166-N**	1.578	unoriented	1.770	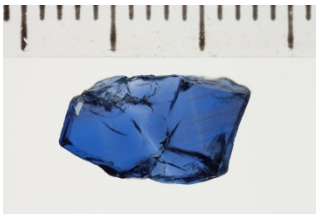

GIA Reference #	Weight (carats)	Polished wafer orientation	Path length (mm)	Image (Transmitted light)
100305165**168-N**	0.738	unoriented	3.020	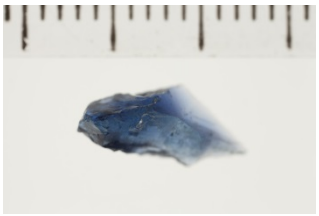
100305165**170-N**	0.573	unoriented	1.670	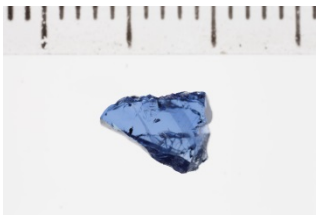
100305165**171-N**	0.328	unoriented	1.650	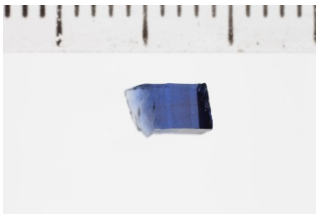
100305165**172-N**	0.203	unoriented	2.21	
100305165**173-N**	0.263	unoriented	1.660	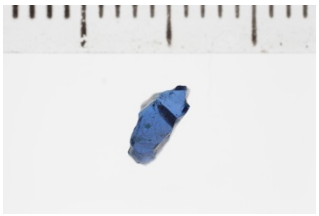
100305165**174-N**	2.539	unoriented	4.815	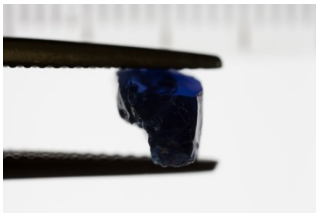
100305165**175-N**	0.770	unoriented	3.040	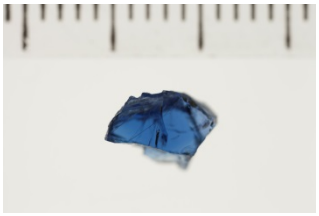

GIA Reference #	Weight (carats)	Polished wafer orientation	Path length (mm)	Image (Transmitted light)
100305165**176-N**	1.127	unoriented	2.700	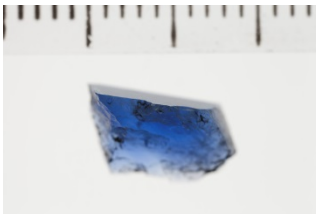
100305165**178-N**	1.226	unoriented	2.390	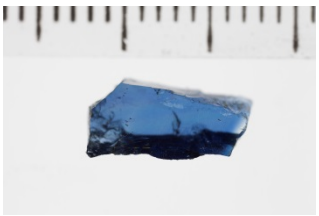
100305165**179-N**	0.563	unoriented	1.570	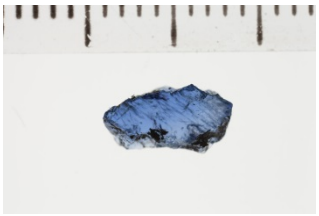
100305165**181-N**	0.285	unoriented	1.080	
100305165**183-N**	0.277	unoriented	1.850	
100305165**186-N**	1.470	unoriented	2.900	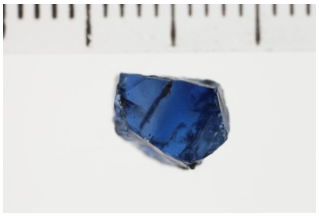
100305165**191-N**	0.119	unoriented	0.640	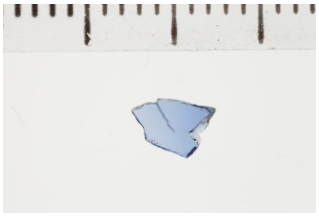

GIA Reference #	Weight (carats)	Polished wafer orientation	Path length (mm)	Image (Transmitted light)
100305165**192-N**	0.419	unoriented	1.550	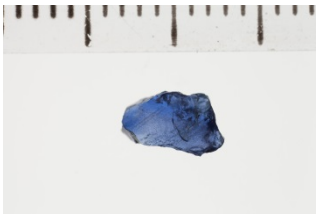
100305165**195-N**	0.370	unoriented	1.310	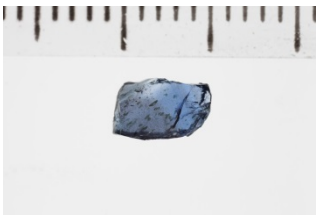
100305165**200-N**	0.381	unoriented	1.890	
100305165**201-N**	0.347	unoriented	2.090	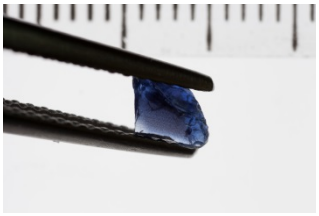
100305165**205-N**	1.728	unoriented	4.810	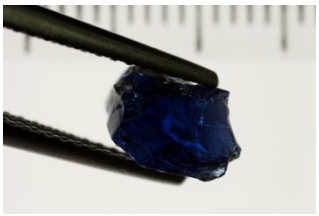
100305165**206-N**	1.510	unoriented	2.600	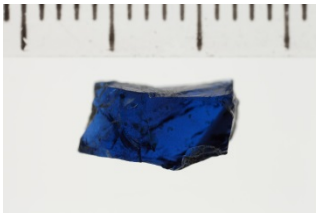
100305165**207-N**	1.056	unoriented	2.750	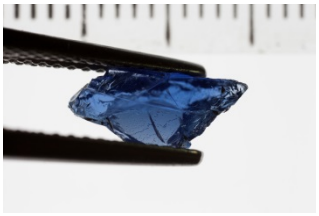

GIA Reference #	Weight (carats)	Polished wafer orientation	Path length (mm)	Image (Transmitted light)
100305165**208-N**	2.339	unoriented	3.920	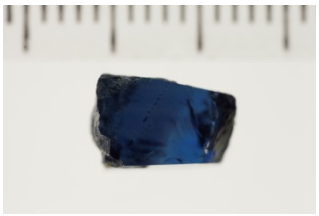
100305165**210-N**	1.233	unoriented	2.350	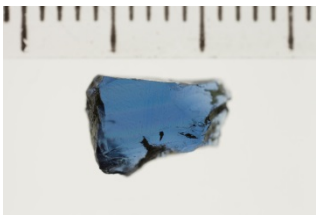
100305165**213-N**	0.306	unoriented	1.960	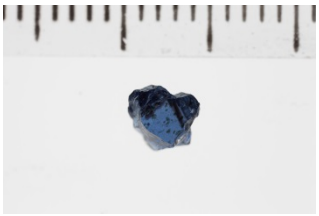
100318470**711-S**	1.402	unoriented	1.870	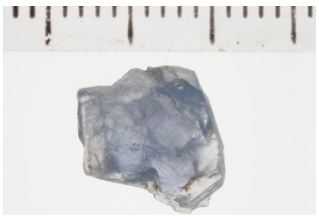
100318470**712-S**	4.266	unoriented	3.880	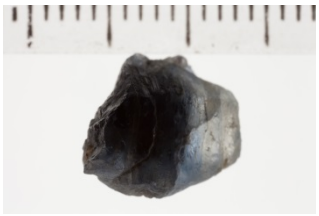
100318470**714-S**	1.367	unoriented	4.250	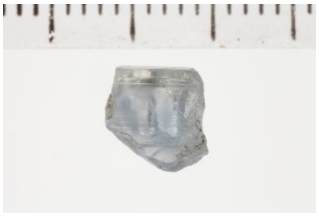
100318470**715-S**	2.318	unoriented	4.600	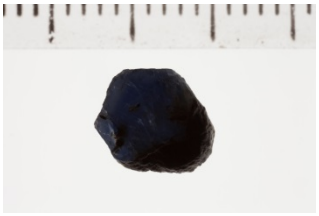

GIA Reference #	Weight (carats)	Polished wafer orientation	Path length (mm)	Image (Transmitted light)
100318470**718-S**	2.114	unoriented	2.980	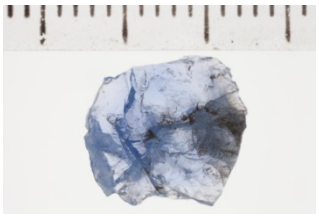
100318470**719-S**	1.320	unoriented	3.010	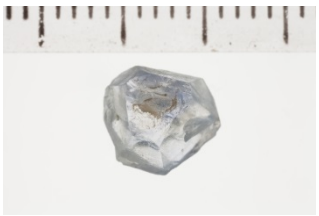
100318470**720-S**	0.944	unoriented	0.944	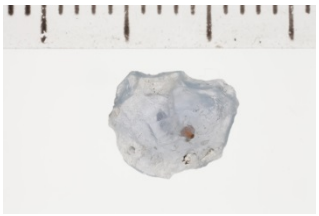
100318470**721-S**	3.301	unoriented	3.301	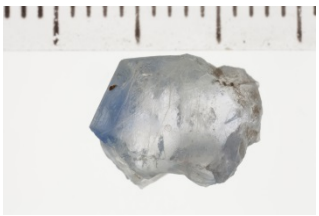
100318470**722-S**	1.749	unoriented	4.020	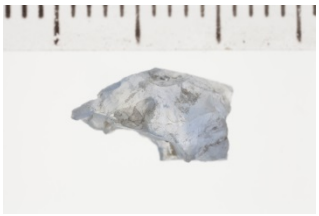
100318470**723-S**	1.281	unoriented	2.560	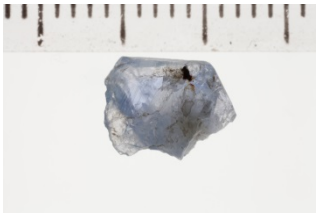
100318470**725-S**	1.022	unoriented	1.550	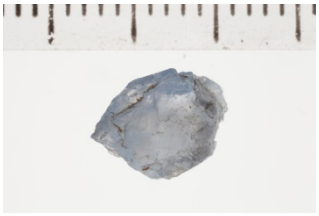

GIA Reference #	Weight (carats)	Polished wafer orientation	Path length (mm)	Image (Transmitted light)
100318470**727-S**	0.590	unoriented	1.550	
100318470**728-S**	0.701	unoriented	2.680	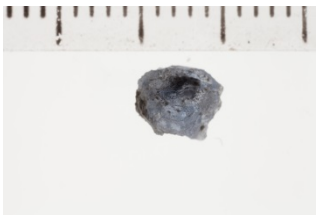
100318470**739-S**	0.958	unoriented	2.150	
100318470**745-S**	0.519	unoriented	2.230	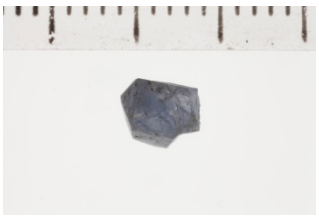
100318470**746-S**	0.689	unoriented	2.910	
100318470**749-S**	0.469	unoriented	1.440	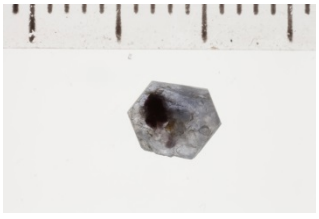
100318470**750-S**	0.343	unoriented	1.850	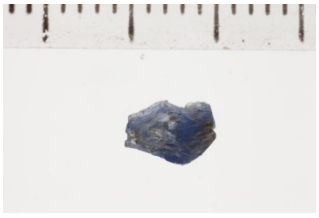

GIA Reference #	Weight (carats)	Polished wafer orientation	Path length (mm)	Image (Transmitted light)
100318470**752-S**	0.375	unoriented	1.990	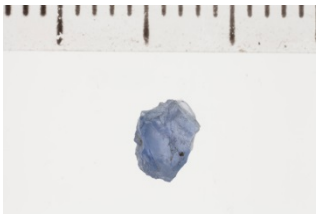
100318470**754-S**	0.638	unoriented	3.250	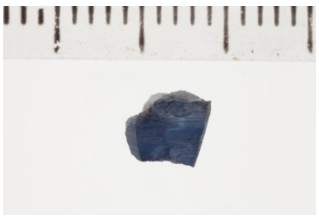
100318470**755-S**	0.945	unoriented	3.280	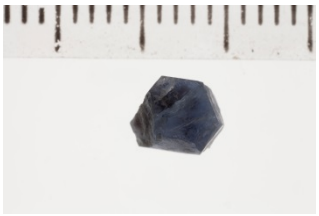
100318470**756-S**	0.498	unoriented	1.780	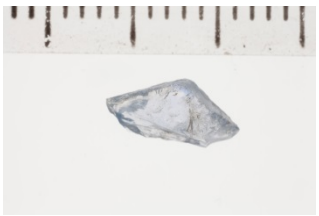
100318470**757-S**	0.406	unoriented	2.110	
100318470**760-S**	0.442	unoriented	1.830	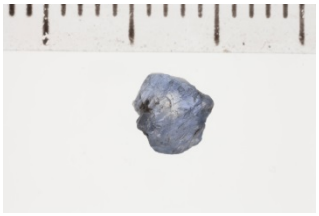
100318470**762-S**	0.117	unoriented	0.690	

2.2 INSTRUMENTATION:

2.2.1 SAMPLE PHOTOGRAPHY

A Canon EOS 5D camera, with a Canon Macro MP-E 65 mm lens adapted to a camera stand, was used to document the color of the samples. In order to produce consistent results for each sample, the photographs were taken under exactly the same lighting conditions, with the reference samples being placed in a Logan Electric Tru-View 810 Color Corrected Light Box (5000 K lamp). A neutral density filter was used to calibrate the camera light box combination to produce a neutral gray. High-resolution reference photographs were then collected using transmitted light. As the reference photos were taken of wafers cut perpendicular or parallel to the c-axis, the color of the samples in the photographs taken using transmitted light may be considered as representative of the color of a nearly pure o-ray or e-ray, respectively.

Photomicrographs of internal features were captured at different magnifications with a Nikon SMZ 18 system and a Nikon SMZ 1500 system using dark-field, bright-field, diffused and oblique illumination, together with a fiber-optic light source when necessary. It should be noted that the field of view information in the captions was calculated by taking the magnification power of the microscope into consideration.

2.2.2 UV-VIS-NIR SPECTROSCOPY

Ultraviolet-visible-near infrared (UV-Vis-NIR) spectra were collected with a Hitachi U-2910 spectrophotometer specially modified at GIA to include a rotatable polarizer to allow the separate collection of both the ordinary (O-) and extraordinary (E-) rays. A wavelength resolution of 1.5 nm was used. The spectra obtained were corrected by calculating the reflection loss from the index of refraction data and the data was converted to show their absorption coefficients (α, cm^{-1}) using $\alpha = 2.303A/d$, where *A* is absorbance and *d* is the path length in centimeters.

2.2.3 FOURIER TRANSFORM INFRARED ABSORPTION (FTIR) SPECTROSCOPY

FTIR spectroscopy was performed using a Thermo Nicolet 6700 FTIR spectrometer equipped with an XT-KBr beam splitter and a mercury-cadmium-telluride (MCT) detector operating with a 4× beam condenser accessory. Resolution was set at 4 cm^{-1} with 1.928 cm^{-1} data spacing. The spectra obtained were converted to be absorption coefficients (α, cm^{-1}) using $\alpha = 2.303A/d$.

2.2.4 RAMAN SPECTROSCOPY

To identify mineral inclusions, Raman spectra were obtained using a Renishaw inVia Raman microscope fitted with a 514 nm argon-ion laser. The spectra were collected in the range of 100 and 1500 cm^{-1}. The accumulation was set at a minimum of 5 until the signal to noise ratio of the spectra was adequate. The calibration was performed using the 520.5 cm^{-1} line of a silicon wafer. In all cases, the RRUFF database was used as a reference when identifying inclusions. Spectral comparisons were performed using Renishaw Wire (version 3.4) and/or Thermo Galactic 'Spectra ID' (version 3.02) software.

2.2.5 LASER ABLATION-INDUCTIVELY COUPLED PLASMA-MASS SPECTROMETRY (LA-ICP-MS)

Chemical analysis was carried out using LA-ICP-MS technology with a Thermo Fisher Scientific iCAP Q Induced Coupled Plasma-Mass Spectrometer (ICP-MS) coupled with a Q-switched Nd:YAG Laser Ablation (LA) device operating at a wavelength of 213 nm. Laser conditions used were 55 μm diameter laser spots, a fluency of around 10 J/cm^2, and a 15 Hz repetition rate. Twelve spots were analyzed on each wafer. ICP-MS was operated using the forward power at ~ 1350 W and the typical nebulizer gas flow at ~ 1.00 L/min. Helium was used as the carrier gas in the laser ablation unit and the flow rate was set at ~ 0.60 L/min. The criteria for the alignment and tuning sequence were to maximize Be counts and to keep the ThO/Th ratio below 2%. A special set of doped synthetic corundum standards including Be, Mg, Ti, V, Cr, Fe, and Ga were used for quantitative analysis. All elemental measurements were normalized on Al as internal elemental standard. This value approximates to the chemical composition of corundum.

Part III: Results and Discussion

3.1 The internal world of blue sapphires from Baw Mar mine

3.1.1 SAPPHIRES FROM THE NORTHERN AREA OF BAW MAR MINE (FE46):

Standard gemological properties of all 36 samples from the Northern area are consistent with typical corundum: RI of n_ω 1.769-1.770 and n_ε 1.760-1.762, birefringence of 0.008-0.009, and hydrostatic SG of 3.86-4.03. All samples were inert when exposed to long- and short-wave UV radiation.

The samples exhibited medium to strong blue color (Table 1). Under the microscope, the most common inclusions seen in the samples were short needles mixed with minute particles and reflective platelets of either whitish or brownish color (Figure 19, Figure 20, Figure 21, Figure 22, Figure 23 and Figure 24). Reflective and/or brownish irregular platelets, depending on the type of illumination employed, were identified as ilmenite by Raman spectroscopy and the RRUFF database (Figure 21 and Figure 22). Strings of short needles mixed with particles were occasionally observed (Figure 26). Samples also contained z-shaped needles (Figure 27), rounded reflective platelets (Figure 25), and either indistinct or even blue zoning.

Like typical Burmese sapphires [Hughes *et al*., 2017], twinning in either single or multiple planes (Figure 28) was found in most samples, and sometimes associated with white tube-like inclusions. The latter are most likely filled with boehmite as shown by the FTIR spectra, and are usually associated with small fingerprints, tiny stress fissures and irregular whitish features (Figure 29 and Figure 30). Fluid inclusions and thin films in various shapes (Figure 31, Figure 32, Figure 33, Figure 34, Figure 35, Figure 36, Figure 37 and Figure 38) were also a common feature. Irregular (unidentified) whitish material was observed in a few samples (Figure 39). The samples also showed open unhealed fissures, white material along unhealed fissures (either diaspore or boehmite features shown in FTIR spectra) (Figure 40), healed fissures with slender, worm-shaped fluid inclusions (Figure 41 and Figure 42) and with a folded fingerprint-like appearance in some cases (Figure 43, Figure 44 and Figure 45), and planes of tabular negative crystals (Figure 46, Figure 47, Figure 48, Figure 49 and Figure 50).

Some mineral inclusions were also present in the samples as would be expected. In certain samples, crystals located near or exposed to the surface were identified using Raman spectroscopy. The most frequently encountered solid inclusions seen in these samples were feldspars, muscovite mica and unidentified dark green platelets. Feldspar crystals appeared as irregular shaped colorless crystals (Figure 51), while mica appeared as tabular colorless crystals or whitish elongated crystals (Figure 52 and Figure 53). The Raman spectra for the dark green platelets (Figure 55 and Figure 56) referenced via the RRUFF database, partially matched with either chromite (spinel group) or biotite (mica group). Based on their morphology and Raman spectra, the dark green platelets are likely biotite sheets. Kaolinite, confirmed by FTIR and Raman spectroscopy, was also present as white material associated with one elongated colorless crystal (Figure 54). In addition, a white feldspar matrix was identified in the same sample (Figure 58). In one sample, an angular colorless crystal with triangular planes was observed (Figure 57); however, this crystal could not be identified by Raman spectroscopy.

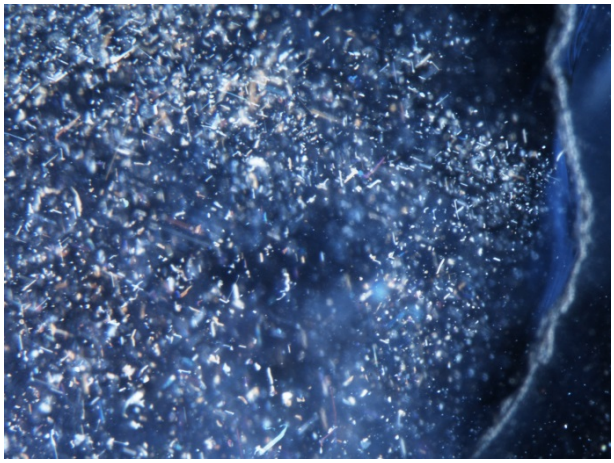

Figure 19: Reflective irregular platelets, likely ilmenite, in sample 163-N using fiber-optic light illumination, field of view (FOV) 1.3 mm. Photo: C. Khowpong © GIA.

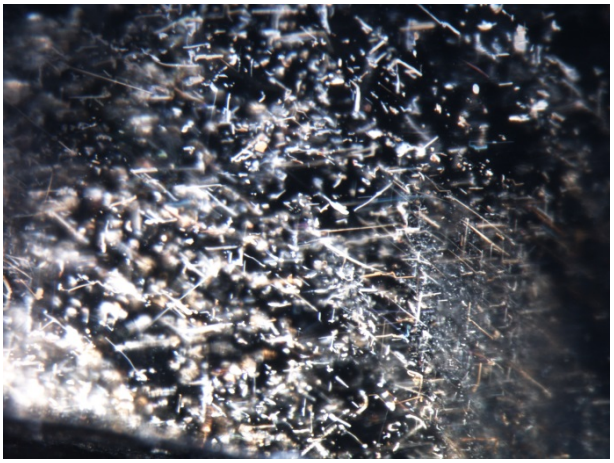

Figure 20: Sample 173-N showing reflective irregular platelets, likely ilmenite, using dark field and fiber-optic light illumination, FOV 1.1 mm. Photo: C. Khowpong © GIA.

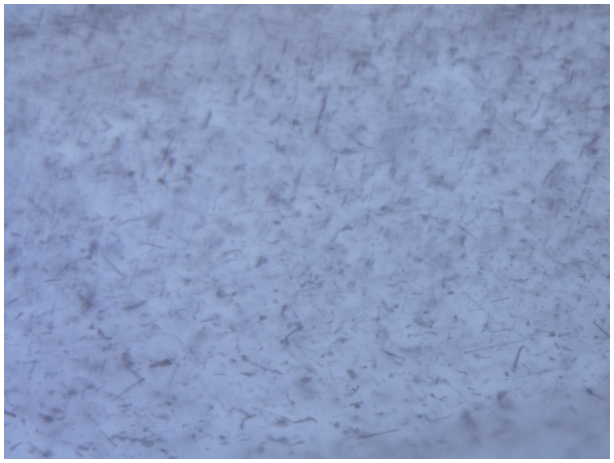

Figure 21: Brownish irregular platelets of ilmenite, identified by Raman spectroscopy (referenced via the RRUFF database), in sample 171-N using dark field and diffused illumination, FOV 1.00 mm. Photo: U. Atikarnsakul © GIA.

Figure 22: Sample 168-N showing black platelets of ilmenite, identified by Raman spectroscopy (referenced via the RRUFF database), using dark field illumination, FOV 2.00 mm. Photo: C. Khowpong © GIA.

Figure 23: Sample 163-N showing iridescent short needles and particles using fiber-optic light illumination, FOV 1.30 mm. Photo: C. Khowpong © GIA.

Figure 24: Hexagonal reflective platelets and irregular platelets in sample 183-N using fiber-optic light illumination, FOV 0.80 mm. Photo: C. Khowpong © GIA.

Figure 25: Rounded reflective platelets in sample 170-N using fiber-optic light illumination, FOV 1.00 mm. Photo: C. Khowpong © GIA.

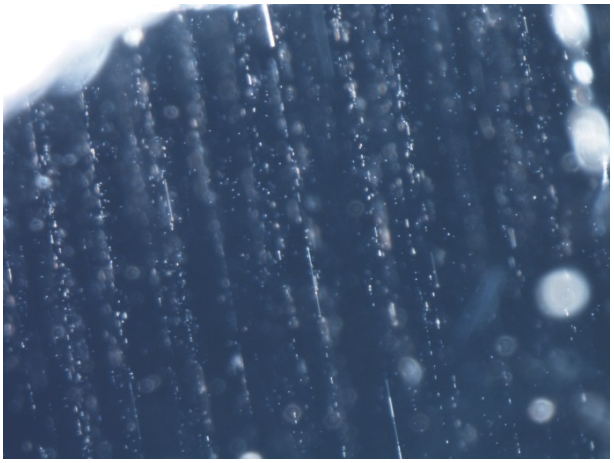

Figure 26: Strings of particles with short needles in sample 189-N using dark field illumination, FOV 1.30 mm. Photo: C. Khowpong © GIA.

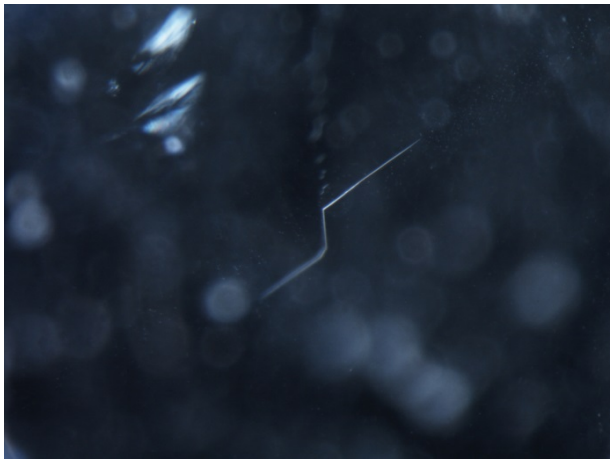

Figure 27: Z-shaped needles in sample 203-N using dark field illumination, FOV 0.90 mm. Photo: C. Khowpong © GIA.

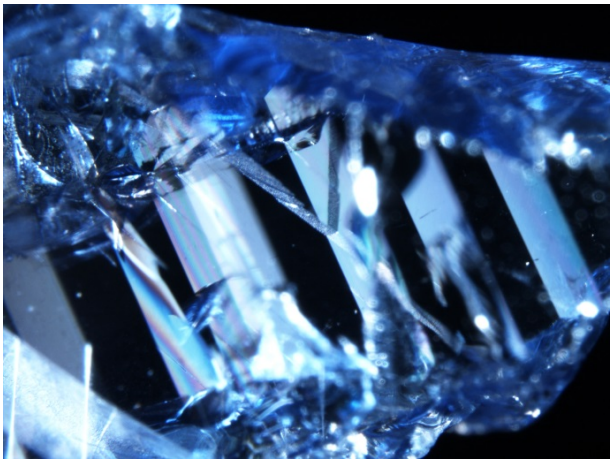

Figure 28: Sample 170-N showing obvious lamellar twinning using fiber-optic light illumination, FOV 4.00 mm. Photo: C. Khowpong © GIA.

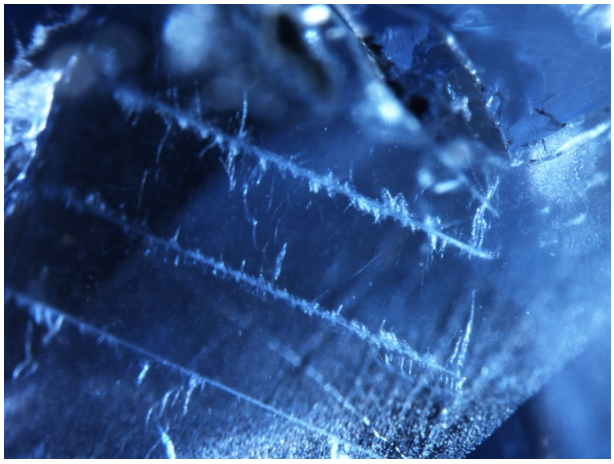

Figure 29: Sample 170-N showing growth tubes containing boehmite, identified by FTIR spectroscopy, with irregular whitish features. The tubes are orientated along twinned planes. Fiber-optic light illumination, FOV 2.00 mm. Photo: C. Khowpong © GIA.

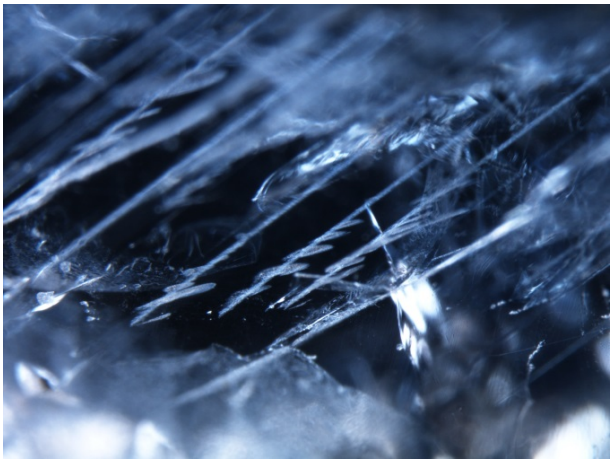

Figure 30: Sample 179-N showing growth tubes containing boehmite, identified using FTIR spectroscopy, with healed fissures, associated with twinned planes using dark field illumination, FOV 2.00 mm. Photo: C. Khowpong © GIA.

Figure 31: Plane of needles and fluid inclusions in sample 159-N using dark field and fiber-optic light illumination, FOV 0.90 mm. Photo: C. Khowpong © GIA.

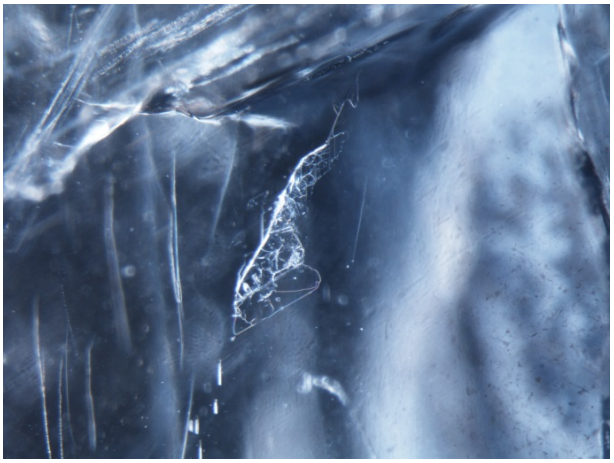

Figure 32: Sample 163-N showing irregular-shaped fluid inclusions and needles using dark field illumination, FOV 1.30 mm. Photo: C. Khowpong © GIA.

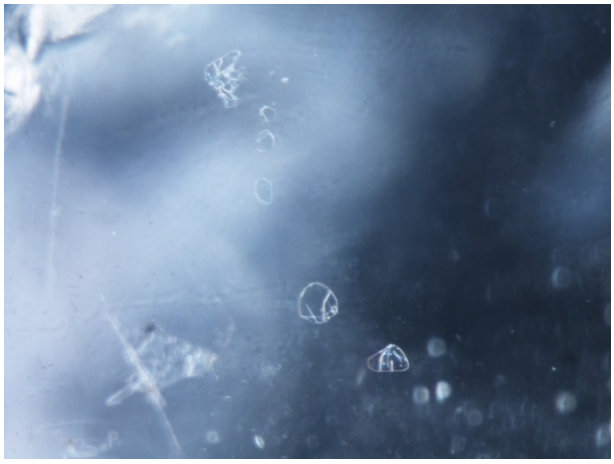

Figure 33: Fluid inclusions in sample 163-N using dark field illumination, FOV 0.90 mm. Photo: C. Khowpong © GIA.

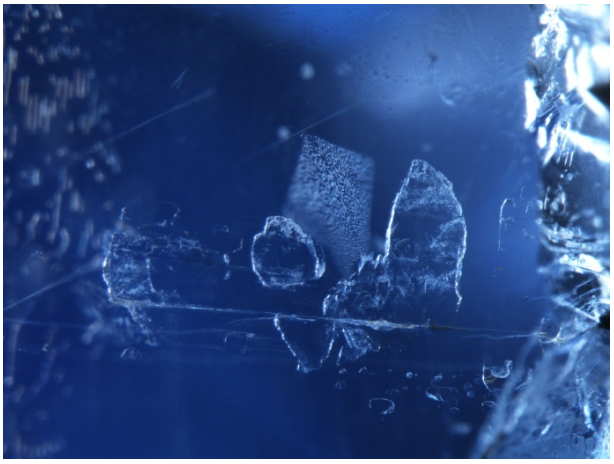

Figure 34: Fluid inclusions in sample 170-N using fiber-optic light illumination, FOV 2.00 mm. Photo: C. Khowpong © GIA.

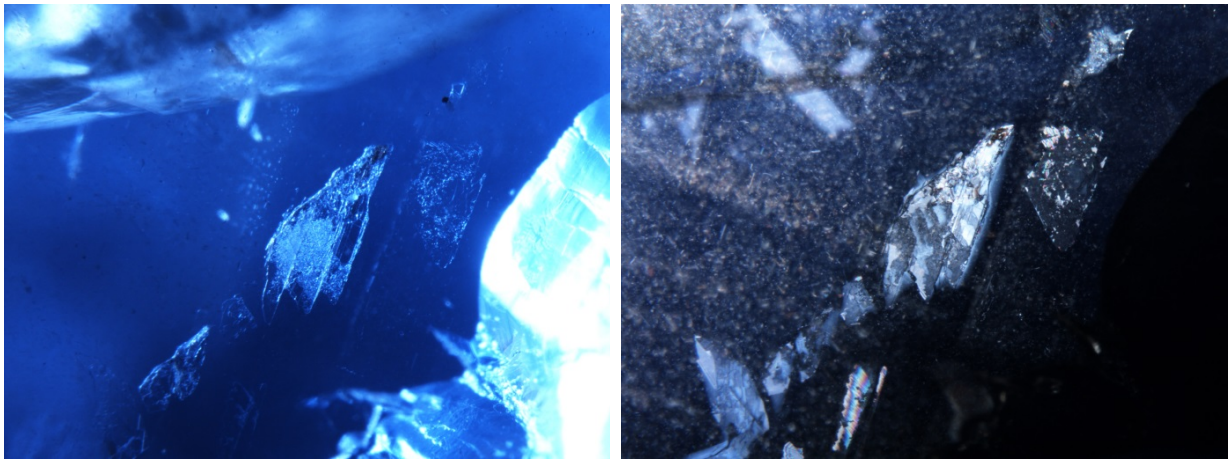

Figure 35: Fluid inclusions in sample 174-N using dark field (left) and fiber-optic light (right) illumination, FOV 2.00 mm. Photos: C. Khowpong © GIA.

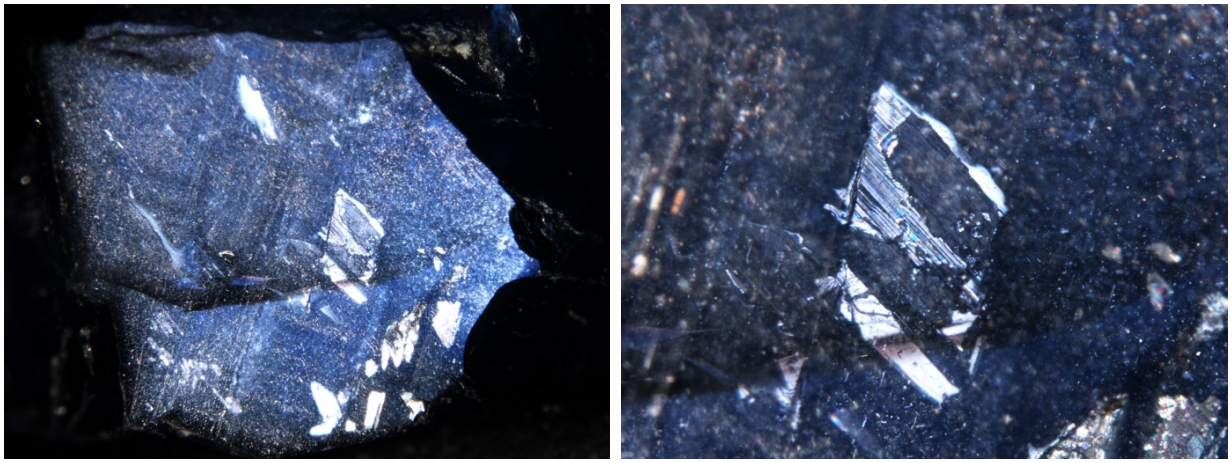

Figure 36: An overview (left) of sample 174-N containing irregular reflective platelets and particles throughout, large thin films (FOV 8.20 mm) and (right) showing the thin film in greater detail (FOV 2.00 mm), using fiber-optic light illumination. Photos: C. Khowpong © GIA.

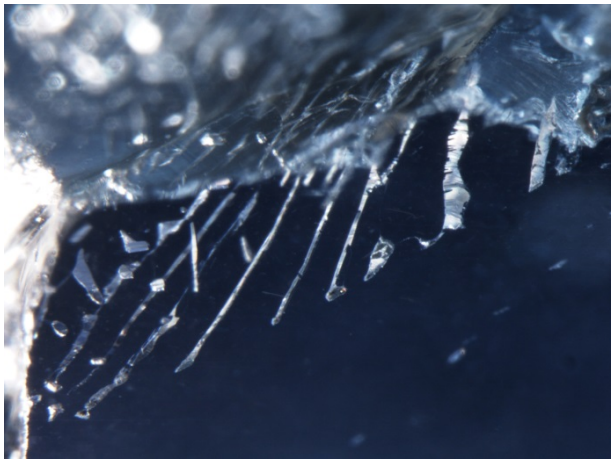

Figure 37: Fluid inclusions in sample 159-N using dark field and fiber-optic light illumination, FOV 1.30 mm. Photo: C. Khowpong © GIA.

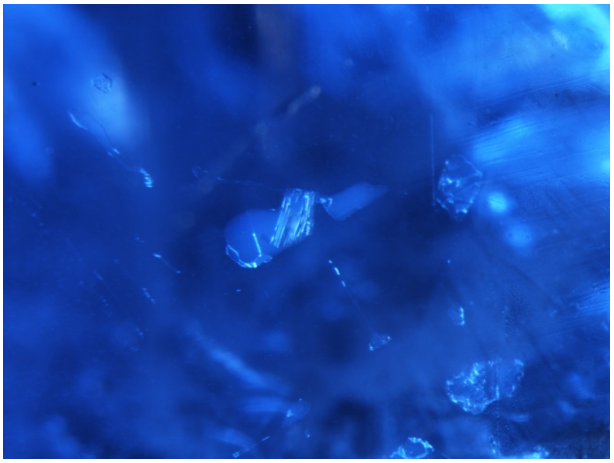

Figure 38: Thin films in sample 176-N using fiber-optic light illumination, FOV 1.30 mm Photo: C. Khowpong © GIA.

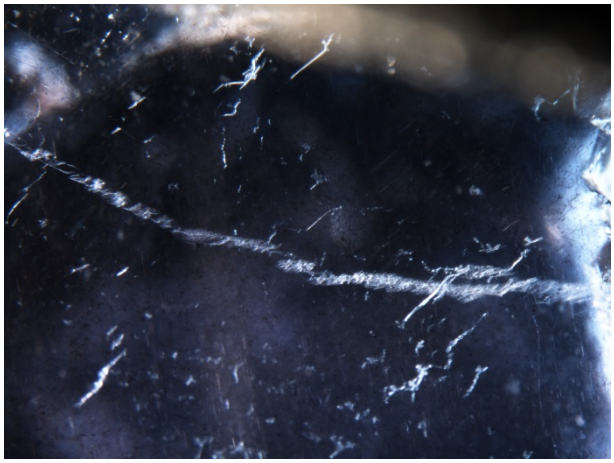

Figure 39: Sample 171-N showing (unidentified) whitish flake or lathe-like inclusions using fiber-optic light illumination, FOV 2.70 mm. Photo: C. Khowpong © GIA.

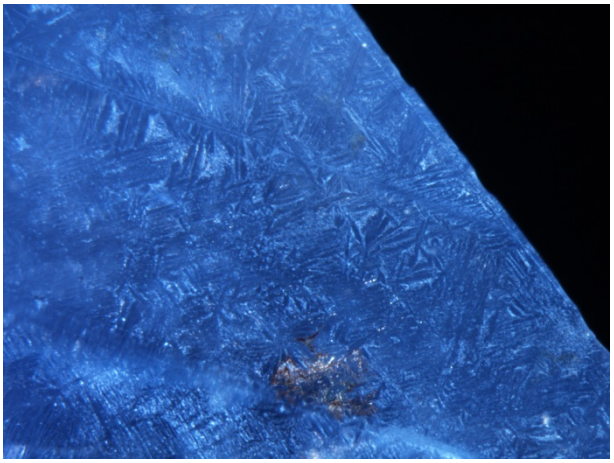

Figure 40: Sample 176-N showing epigenetic material (boehmite, identified by FTIR spectroscopy) along an open fissure using fiber-optic light illumination, FOV 1.60 mm. Photo: C. Khowpong © GIA.

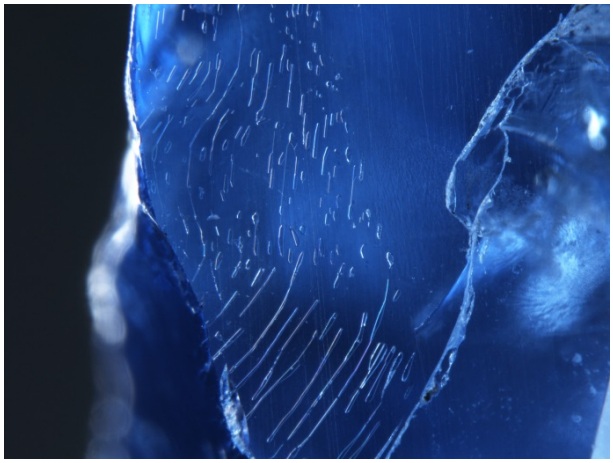

Figure 41: Healed fissure consisting of slender, worm-shaped fluid channels in sample 170-N using dark field illumination, FOV 2.00 mm. Photo: C. Khowpong © GIA.

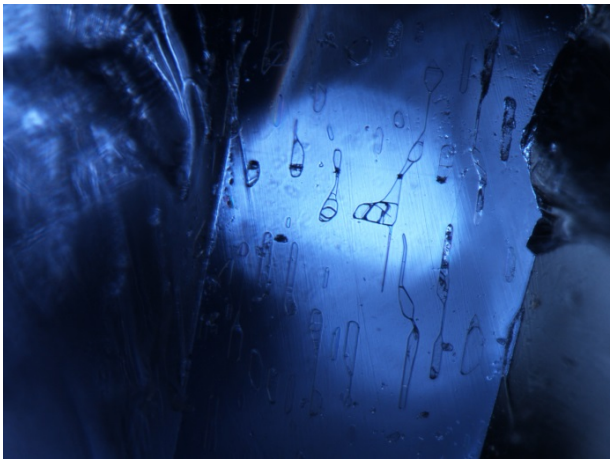

Figure 42: Close-up view of figure 37 showing multi-phases within the channels of the healed fissure in sample 170-N using fiber-optic light illumination, FOV 1.10 mm. Photo: C. Khowpong © GIA.

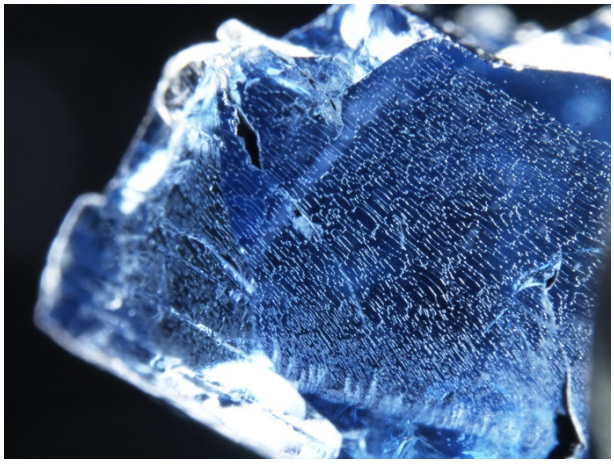

Figure 43: Healed fissure in sample 183-N using dark field illumination, FOV 4.00 mm. Photo: U. Atikarnsakul © GIA.

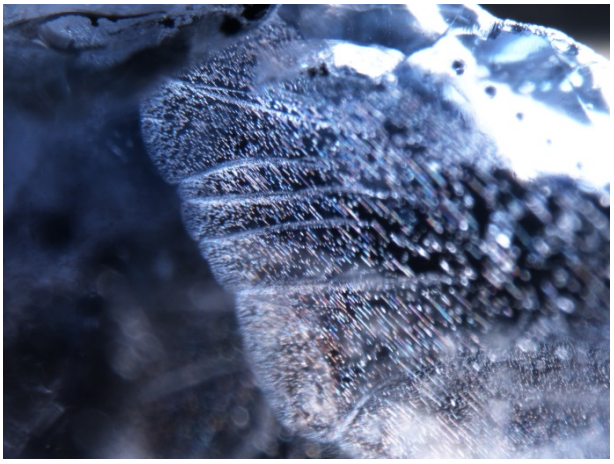

Figure 44: Healed fissure with a folded fingerprint-like appearance in sample 192-N using dark field and fiber-optic light illumination, FOV 2.00 mm. Photo: C. Khowpong © GIA.

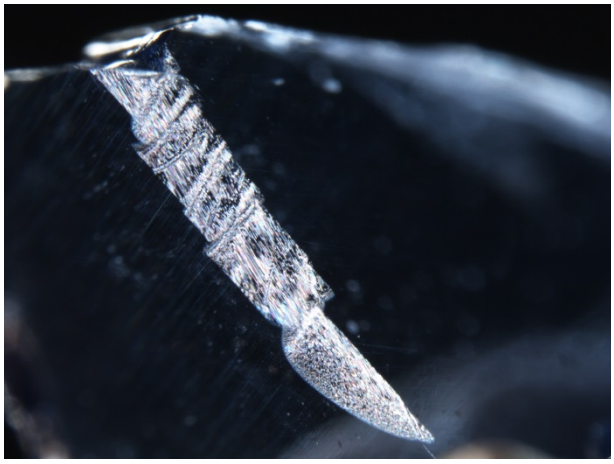

Figure 45: Healed fissure with a folded fingerprint-like appearance in sample 191-N using dark field and fiber-optic light illumination, FOV 2.70 mm. Photo: C. Khowpong © GIA.

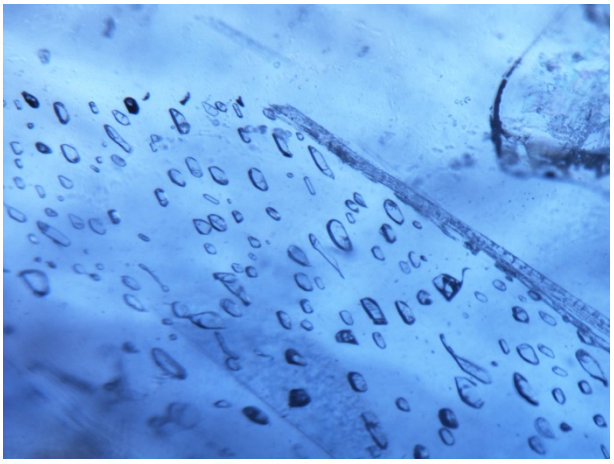

Figure 46: Plane of tabular negative crystals in sample 176-N using dark field illumination, FOV 1.10 mm. Photo: C. Khowpong © GIA.

Figure 47: Sample 165-N showing a plane of tabular negative crystals using dark field illumination, FOV 4.00 mm. Photo: C. Khowpong © GIA.

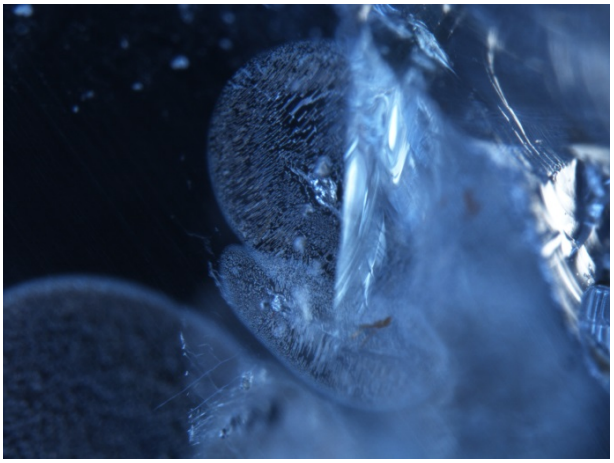

Figure 48: In the same inclusion scene shown in figure 47, some negative crystals are associated with healed fissures in sample 165-N using dark field illumination, FOV 2.00 mm. Photo: C. Khowpong © GIA.

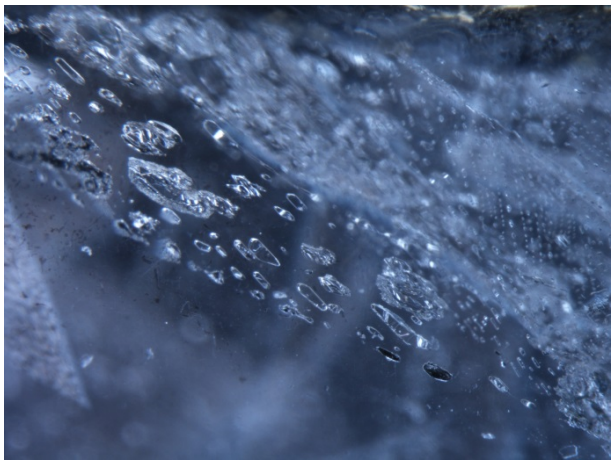

Figure 49: Plane of tabular negative crystals, some with whitish granular planes, in sample 192-N using dark field illumination, FOV 1.60 mm. Photo: C. Khowpong © GIA.

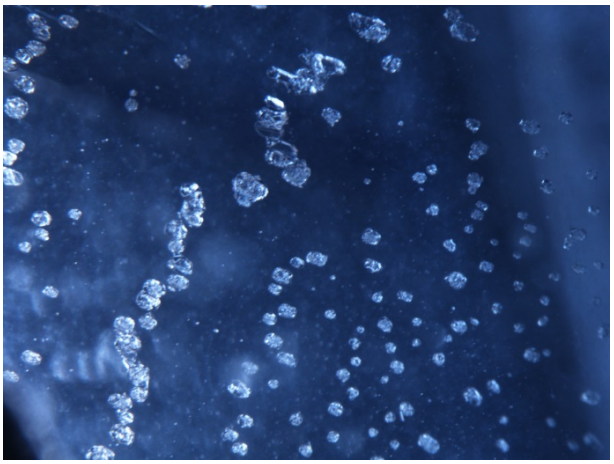

Figure 50: Plane of tabular negative crystals in sample 207-N using dark field illumination, FOV 2.00 mm. Photo: C. Khowpong © GIA.

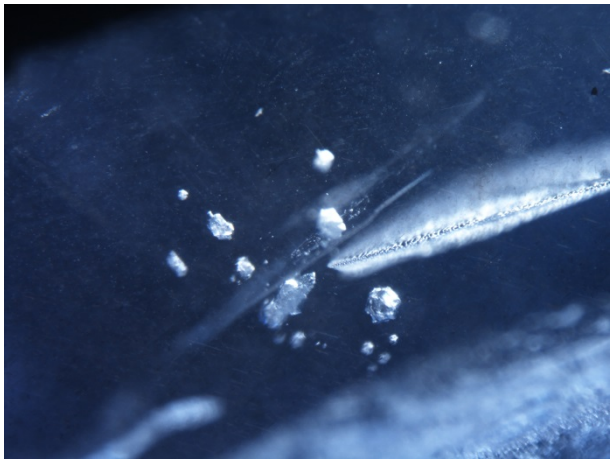

Figure 51: Irregularly shaped colorless crystals of plagioclase feldspar, identified by Raman spectroscopy (referenced via the RRUFF database), in sample 168-N using dark field illumination, FOV 2.00 mm. Photo: C. Khowpong © GIA.

Figure 52: Rows of tabular colorless crystals of mica, identified by Raman spectroscopy (referenced via the RRUFF database), in sample 178-N using dark field and fiber-optic light illumination, FOV 1.60 mm. Photo: C. Khowpong © GIA.

Figure 53: Sample 186-N showing an elongated whitish crystal of mica, identified by Raman spectroscopy (referenced via the RRUFF database), associated with orange material at end using dark field illumination, FOV 2.70 mm. Photo: C. Khowpong© GIA.

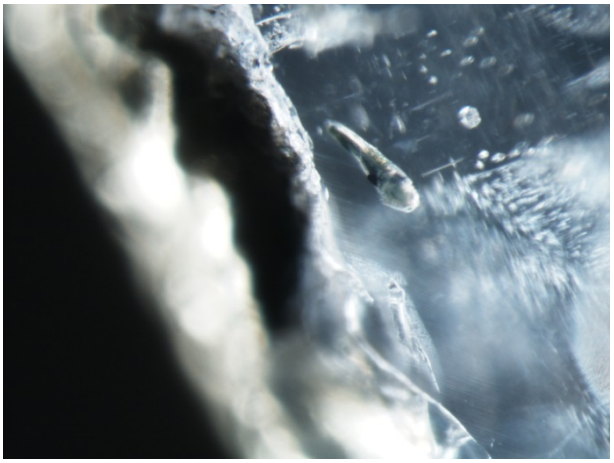

Figure 54: Sample 163-N showing white kaolinite, identified by Raman spectroscopy (referenced via the RRUFF database), associated with an elongated colorless crystal, using diffuse and fiber-optic light illumination, FOV 1.20 mm. Photo: S. Sangsawong © GIA.

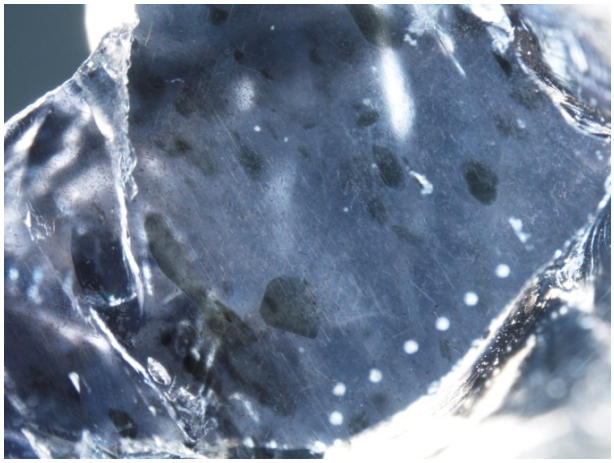

Figure 55: Sample 213-N showing dark green platelets, likely biotite mica, as associated with needles and particles using dark field illumination, FOV 3.10 mm. Photo: C. Khowpong © GIA.

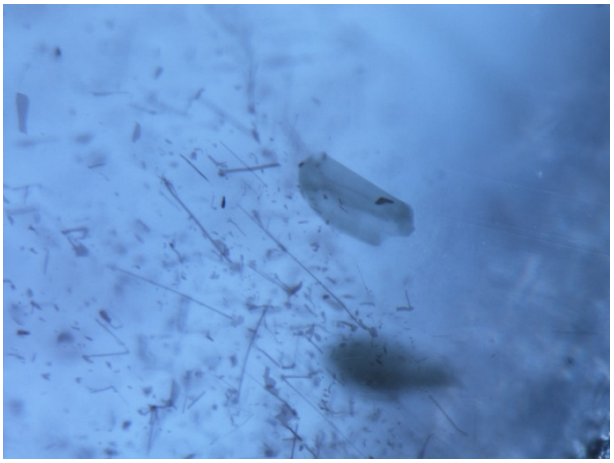

Figure 56: Sample 173-N showing dark green platelets, likely biotite mica sheets, using bright field, diffuse and fiber-optic light illumination, FOV 0.80 mm. Photo: C. Khowpong © GIA.

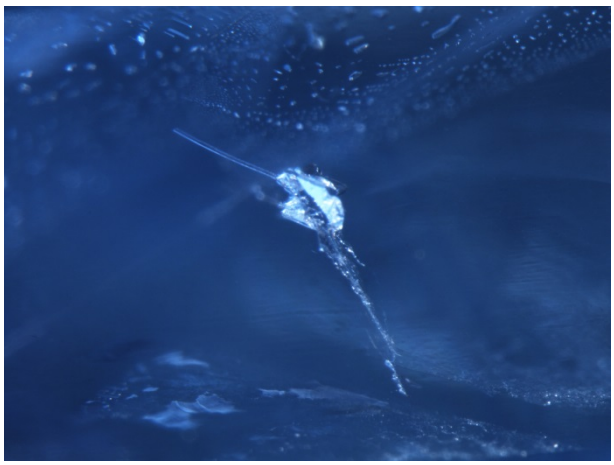

Figure 57: Angular (unidentified) near-colorless transparent crystal with "wings" in sample 176-N using fiber-optic light illumination, FOV 1.10 mm. Photo: C. Khowpong© GIA.

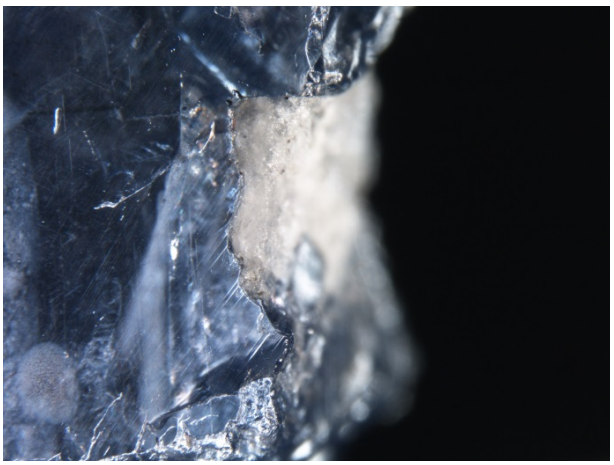

Figure 58 Sample 163-N showing white feldspar matrix, identified by Raman spectroscopy (referenced via the RRUFF database), using dark field and fiber-optic light illumination, FOV 2.70 mm. Photo: C. Khowpong© GIA.

3.1.2 SAPPHIRES FROM THE SOUTHERN AREA OF BAW MAR MINE (FE75):

Standard gemological testing of all 28 samples from the Southern area revealed properties consistent with typical corundum: RI of n_{ω}1.768-1.769 and n_{ε} 1.760-1.761, birefringence of 0.008-0.009, and hydrostatic SG of 3.84-4.02.

Due to the complex geology of the Mogok Stone Tract which includes the Baw Mar mine, blue sapphires from different areas in the mine (FE 46 and FE75) were found to possess different gemological and spectroscopic properties and inclusions. Generally, blue sapphires from the Southern area were of a much lighter color than those from the Northern area (Table 1). The samples from the Southern area sometimes showed very weak to weak orange zoned fluorescence under long-wave UV radiation.

Microscopic observation revealed that the samples from Baw Mar-North and -South share many inclusions commonly seen in classical Mogok blue sapphires [Hughes *et al.* 2017, Gübelin and Koivula 2005, Themelis 2008]. However, it is notable that the samples from the Southern area were relatively more included than those from the Northern area. Under magnification, samples from Southern area in this study frequently showed dense clouds of short rutile needles (Figure 59, Figure 60 and Figure 61), intersecting short needles and/or thin films mixed with particles (Figure 62, Figure 63, Figure 64 and Figure 65) as well as dense clouds of brownish particles mixed with short needles and brownish irregular platelets of ilmenite (Figure 66 and Figure 67). Etch tubes were also seen (Figure 68). Like the blue sapphires from Northern area, the samples from the Southern area typically contained twin planes which were occasionally associated with tube-like inclusions (Figure 69 and Figure 70).

Interestingly, tabular negative crystals surrounded by thin films were often observed in the samples from the Southern area (Figure 71, Figure 72, Figure 73, Figure 74 and Figure 75). When viewed under dark field illumination, small dark inclusions of iron sulfide were sometimes found on tabular negative crystals (Figure 73). Variously shaped thin films (Figure 76, Figure 77, Figure 78 and Figure 79), planes of small tabular negative crystals (Figure 80, Figure 81 and Figure 82), negative crystals of various shapes with fingerprints (Figure 83, Figure 84, Figure 85 and Figure 86), healed fissures (Figure 87 and Figure 88) and whitish epigenetic material along fractures were also observed. The samples in general from Baw Mar mine typically had indistinct or even blue zoning, however, one sample from the Southern area showed saturated straight blue zoning (Figure 89).

Various types of solid inclusions were seen in the blue sapphires from the Southern area. The most frequently observed mineral inclusions found were zircon crystals, unidentified opaque black crystals and feldspars. Transparent colorless crystals of zircon appeared as either single crystals or in groups usually associated with fingerprints or tension fractures (Figure 90, Figure 91 and Figure 92). Unidentified opaque black crystals appeared as rounded crystal, irregular shaped crystal with tension fracture and blocky crystal associated with elongated colorless crystal (Figure 92, Figure 93 and Figure 94). Feldspar showed as transparent irregular shaped colorless crystals (Figure 95). Tabular dark brownish crystals of rutile (Figure 96), triangular and irregularly shaped brownish crystals of biotite mica (Figure 97 and Figure 98) and a dark green crystal of spinel (Figure 99) were also identified. One sample from the Southern area contained unidentified dark green platelets (Figure 101), similar to those observe in samples from the Northern area. In addition, unidentified orange material with tension fractures (Figure 102), unidentified angular crystals with granular planes (Figure 103 and Figure 104) and unidentified orange material associated with cut-through dark opaque crystals of goethite (Figure 105) were observed.

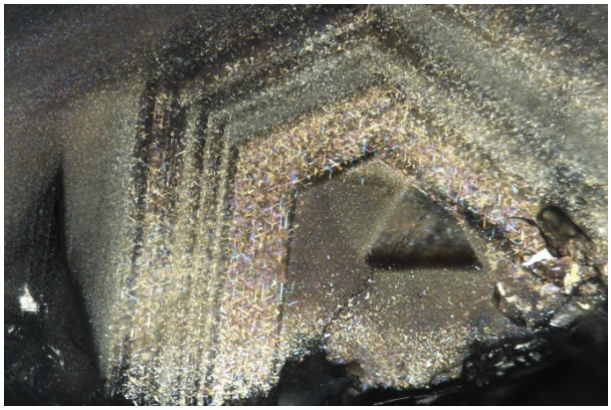

Figure 59: Angular bands of short rutile needles, identified by Raman spectroscopy referenced via RRUFF database, in sample 723-S using fiber-optic light illumination, FOV 2.85 mm. Photo: V. Raynaud © GIA.

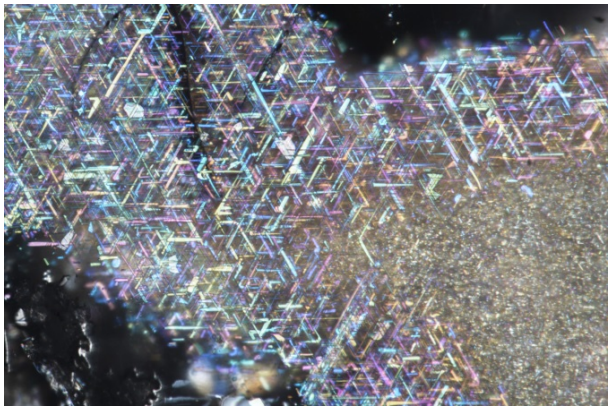

Figure 60: Short rutile needles, identified by Raman spectroscopy referenced via RRUFF database, in sample 754-S using fiber-optic light illumination, FOV 1.05 mm. Photo: V. Raynaud © GIA.

Figure 61: Sample 725-S showing dense short needles using fiber-optic light illumination, FOV 1.05 mm. Photo: V. Raynaud © GIA.

Figure 62: Iridescent short needles mixed with particles in sample 741-S using fiber-optic light illumination, FOV 1.75 mm. Photo: V. Raynaud © GIA.

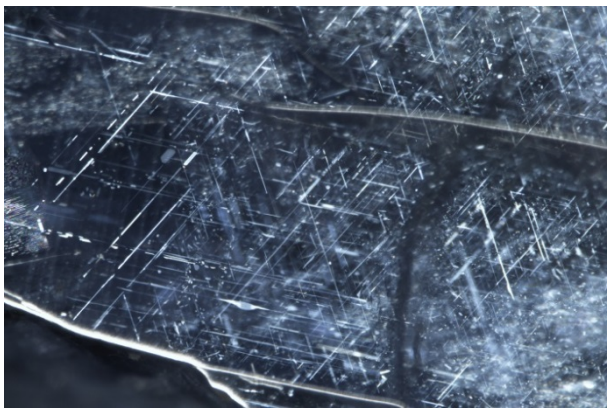

Figure 63: Intersecting needles and thin films in sample 746-S using fiber-optic light illumination, FOV 3.65 mm. Photo: C. Khowpong © GIA.

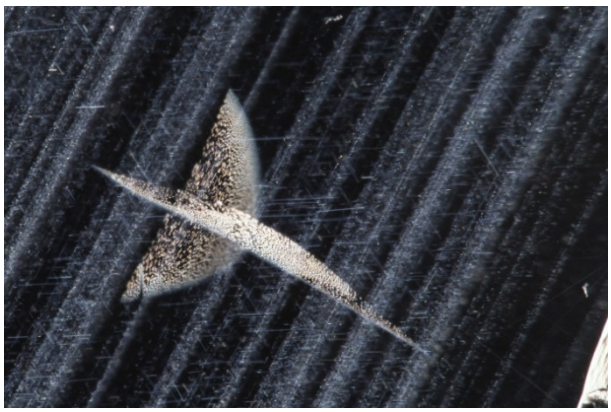

Figure 64: Planar zones of short needles mixed with particles and healed fissures in sample 763-S using dark field illumination, FOV 1.75 mm, Photo: V. Raynaud © GIA.

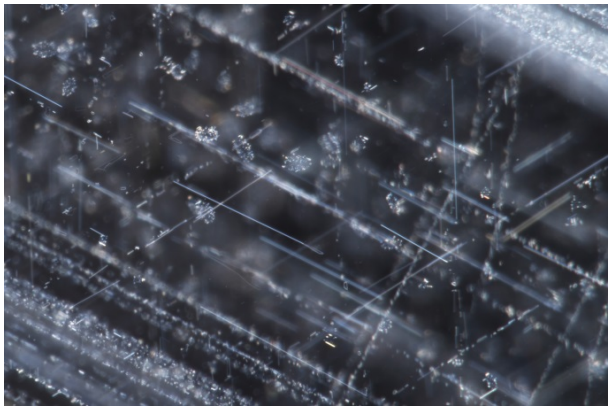

Figure 65: Sample 716-S containing short needles, planar zones of particles and milky thin films, using dark field illumination, FOV 1.05 nm. Photo: V. Raynaud © GIA.

Figure 66: Dense reflective brownish particles, needles and platelets of ilmenite, identified by Raman (referenced via RRUFF database), in sample 749-S using fiber-optic light illumination, FOV 1.40 mm Photo: V. Raynaud © GIA.

Figure 67: Short needles, particles and brownish platelets in sample 741-S using dark field illumination, FOV 1.05 mm. Photo: V. Raynaud © GIA.

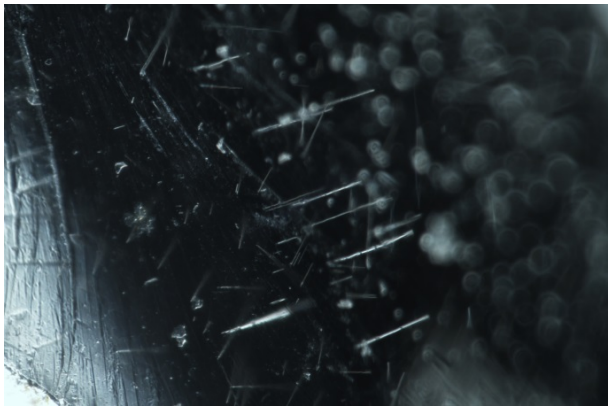

Figure 68: Short needles attached to the unpolished surface of sample 719-S using dark field illumination, FOV 1.20 mm. Photo: C. Khowpong © GIA.

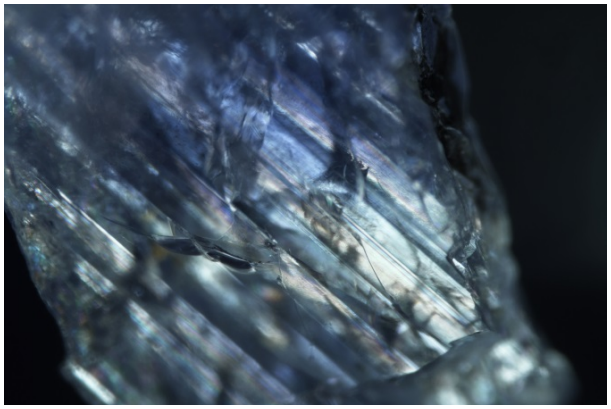

Figure 69: Lamellar twinning in sample 750-S under crossed polarized light, FOV 3.65 mm. Photo: C. Khowpong © GIA.

Figure 70: Growth tubes with fractures, along lamellar twinning, in sample 715-S using fiber-optic light illumination, FOV 2.40 mm. Photo: C. Khowpong © GIA.

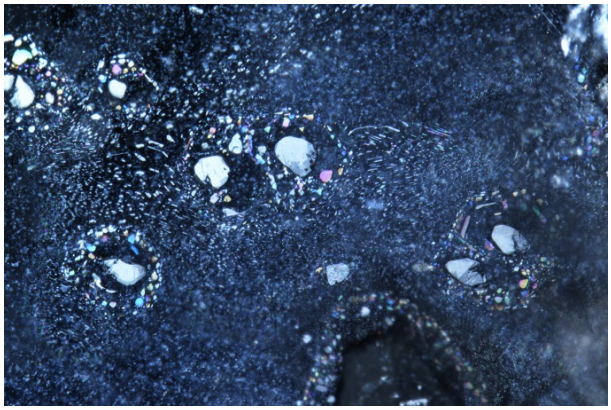

Figure 71: Sample 720-S containing tabular negative crystals surrounded by iridescent thin films as well as platelets throughout, using fiber-optic light illumination, FOV 3.65 mm. Photo: V. Raynaud © GIA.

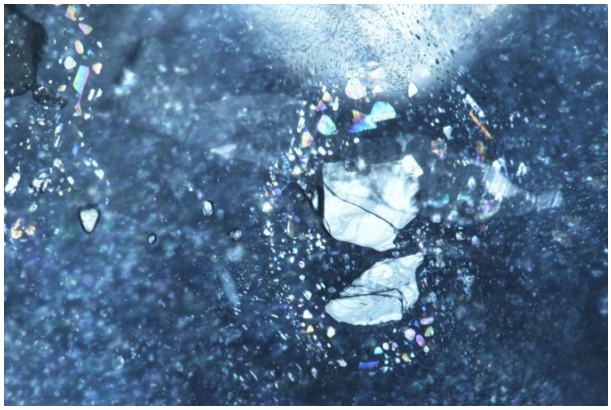

Figure 72: Close-up view of inclusion scene in figure 67, showing tabular negative crystals with planes of thin films in sample 720-S using fiber-optic light illumination, FOV 1.75 mm. Photo: V. Raynaud © GIA.

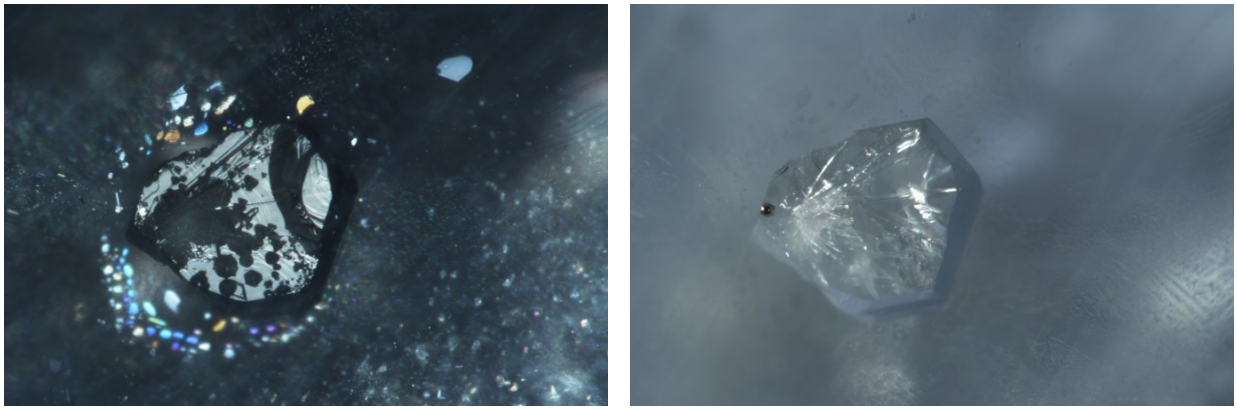

Figure 73: Tabular negative crystal surrounded by thin films in sample 711-S viewed under different illuminations—using fiber-optic light (left) and dark field illumination (right). A negative crystal associated with small dark opaque crystal of iron sulfide can be seen in the image on the right. FOV 1.20 mm. Photo: V. Raynaud © GIA.

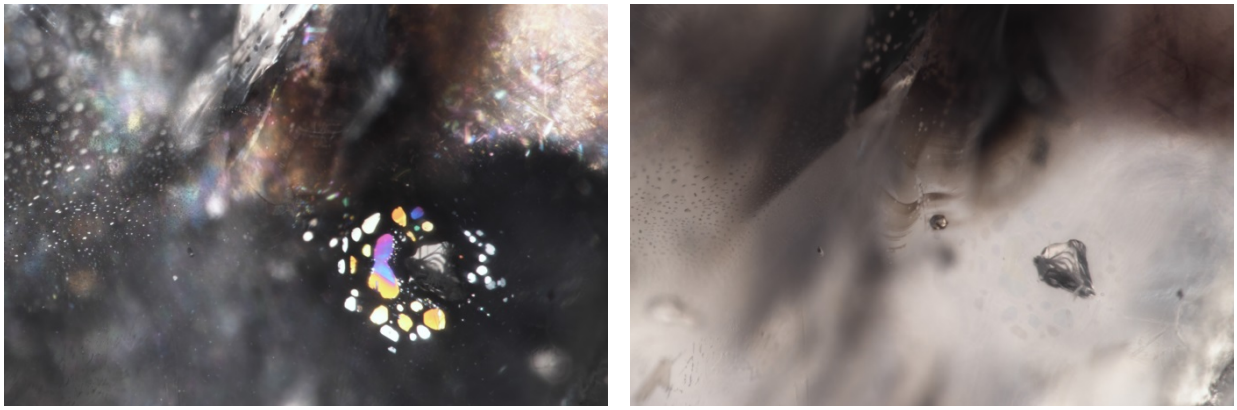

Figure 74: In sample 749-S, tabular negative crystal surrounded by thin films and to the right of each image with dense brownish particles, needles and thin films, viewed under different illuminations—using fiber-optic light (left) and dark field illumination (right). FOV 1.20 mm. Photo: V. Raynaud © GIA.

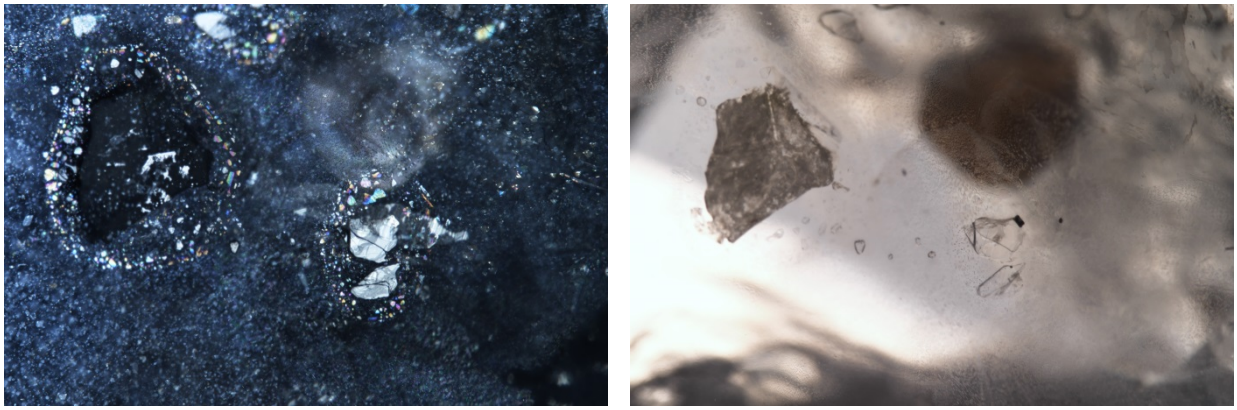

Figure 75: On the left part of each image, a granular whitish crystal of gibbsite, identified by Raman spectroscopy (referenced via the RRUFF database), surrounded with thin films is visible, and on the right of each image, tabular negative crystals surrounded with thin films are visible, viewed under different illuminations in sample 720-S—using fiber-optic light (left) and diffuse light (right) illumination, FOV 3.65 mm. Photo: V. Raynaud © GIA.

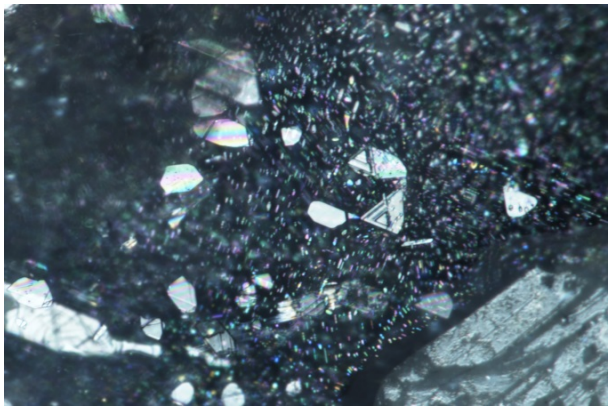

Figure 76: Thin films in sample 711-S using fiber-optic light illumination, FOV 1.05 mm. Photo: V. Raynaud © GIA.

Figure 77: Thin films in sample 739-S using fiber-optic light illumination, FOV 1.75 mm. Photo: V. Raynaud © GIA.

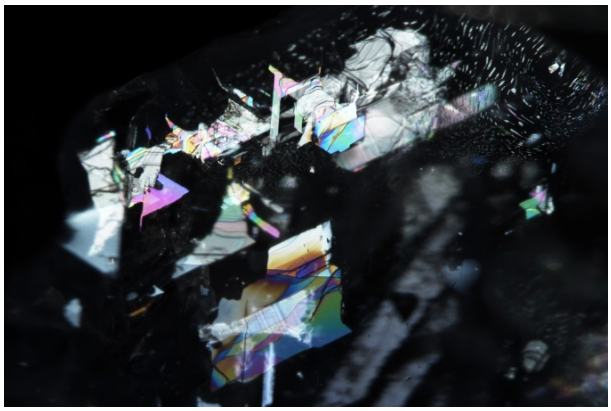

Figure 78: Thin films in sample 723-S using fiber-optic light illumination, FOV 2.85 mm. Photo: V. Raynaud © GIA.

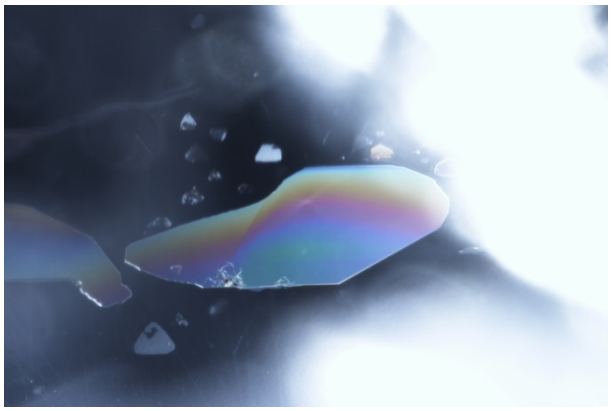

Figure 79: Thin films in sample 756-S using fiber-optic light illumination, FOV 1.40 mm. Photo: C. Khowpong © GIA.

Figure 80: Sample 716-S showing a negative crystal with a gas bubble inside, associated with a plane of small flat negative crystals, using fiber-optic light illumination, FOV 1.20 mm. Photo: V. Raynaud © GIA.

Figure 81: Plane of flat negative crystals in sample 716-S using diffused illumination, FOV 1.05 mm. Photo: V. Raynaud © GIA.

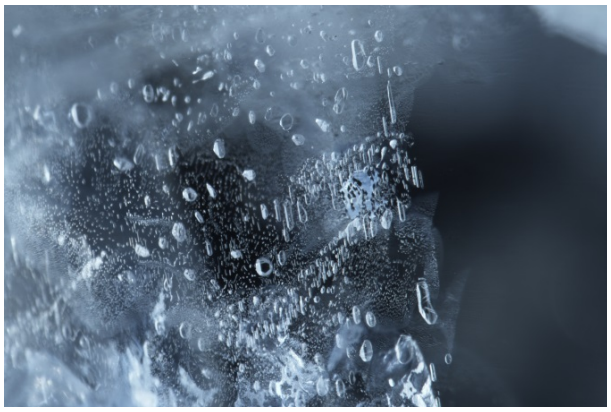

Figure 82: Healed fissure consisting of small tabular negative crystals in sample 721-S using fiber-optic light illumination, FOV 2.40 mm. Photo: C. Khowpong © GIA.

Figure 83; Irregular-shaped negative crystal with healed fissure in sample 721-S using fiber-optic light illumination, FOV 2.40 mm. Photo: C. Khowpong © GIA.

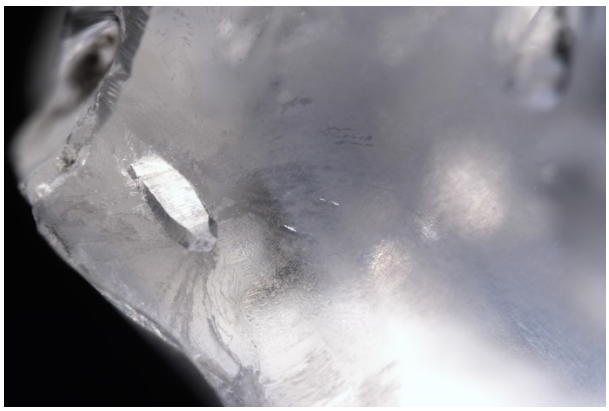

Figure 84: Barrel-shaped negative crystal with healed fissure in sample 714-S using fiber-optic light illumination, FOV 2.85 mm. Photo: V. Raynaud © GIA.

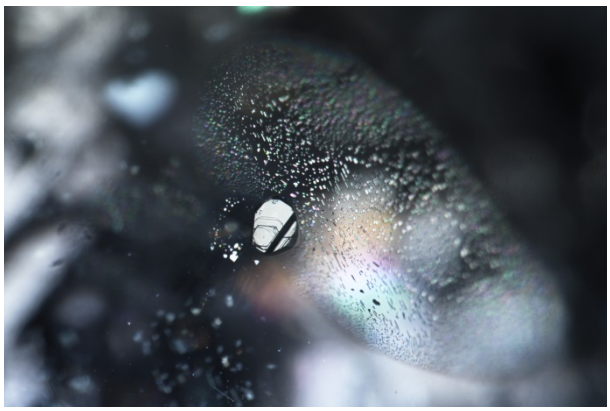

Figure 85: Tabular negative crystal with a healed fissure surrounded by thin films in sample 723-S, using fiber-optic light illumination, FOV 1.75 mm. Photo: V. Raynaud © GIA.

Figure 86: Negative crystal with a healed fissure in sample 721-S using fiber-optic light illumination, FOV 2.85 mm. Photo: C. Khowpong © GIA.

Figure 87: Thread-like healed fissure in sample 762-S using fiber-optic light illumination, FOV 2.00 mm. Photo: C. Khowpong © GIA.

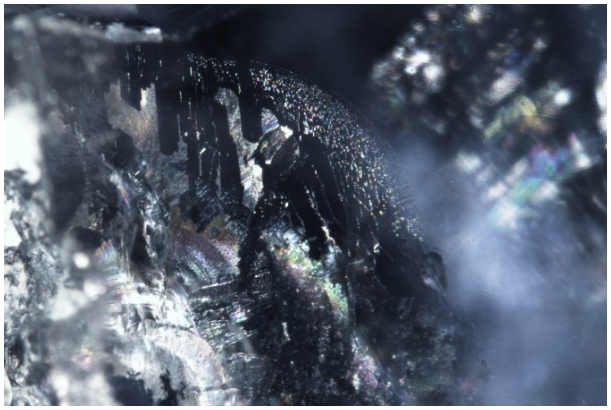

Figure 88: Fluid fingerprint in sample 752-S using fiber-optic light illumination, FOV 2.40 mm. Photo: C. Khowpong © GIA.

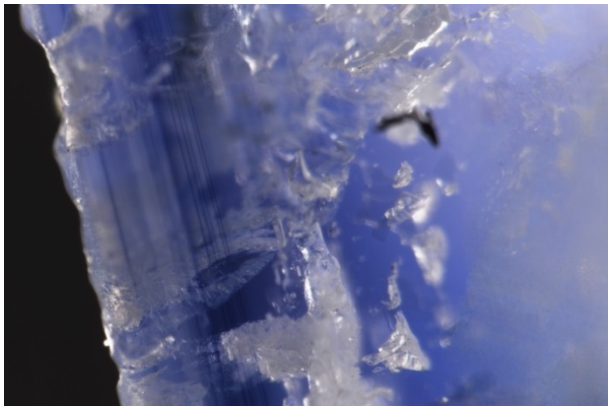

Figure 89: Straight and strong blue zoning and irregularly-shaped negative crystals in sample 754-S under diffused illumination, FOV 1.40 mm. Photo: V. Raynaud © GIA.

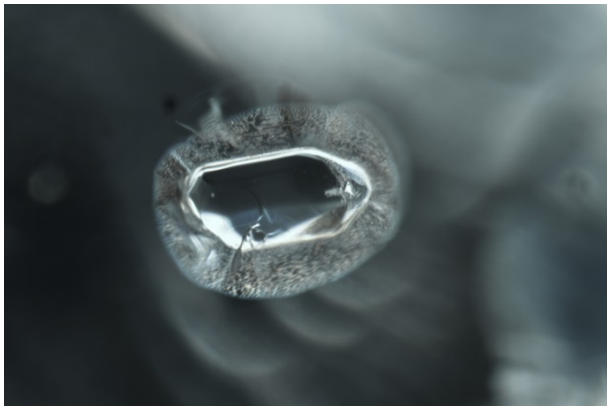

Figure 90: Transparent colorless crystal of zircon, identified by Raman spectroscopy (referenced via the RRUFF database), associated with a healed fissure in sample 719-S using dark field illumination, FOV 1.75 mm. Photo: C. Khowpong © GIA.

Figure 91: Transparent colorless crystal of zircon, identified by Raman spectroscopy (referenced via the RRUFF database), with associated with tension fractures in sample 718-S using fiber-optic light illumination, FOV 1.40 mm. Photo: C. Khowpong © GIA.

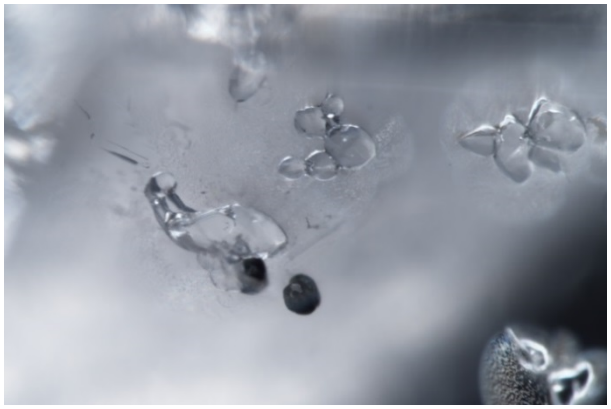

Figure 92: Sample 719-S showing groups of zircon crystals, identified by Raman spectroscopy (referenced via the RRUFF database), with healed fissures, and unidentified opaque black crystals, using dark field illumination, FOV 1.40 mm. Photo: C. Khowpong © GIA.

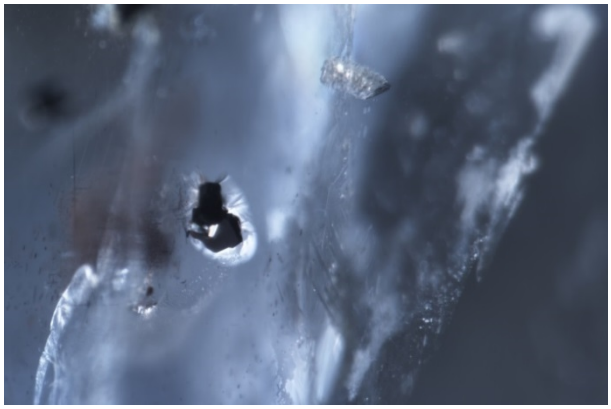

Figure 93: An unidentified opaque black crystal with surrounding tension fracture in sample 712-S using fiber-optic light illumination, FOV 1.05 mm. Photo: C. Khowpong © GIA.

Figure 94: An unidentified opaque black crystal associated with a transparent colorless crystal in sample 719-S, using fiber-optic light illumination, FOV 1.05 mm. Photo: V. Raynaud © GIA.

Figure 95: Irregular-shaped colorless crystals of plagioclase feldspar, identified by Raman spectroscopy (referenced via the RRUFF database), in sample 755-S using dark field illumination, FOV 1.05 mm. Photo: C. Khowpong © GIA.

Figure 96: A bisected tabular dark brownish crystal of rutile, identified by Raman spectroscopy (referenced via the RRUFF database), in sample 728-S using fiber-optic light illumination, FOV 1.05 mm. Photo: C. Khowpong © GIA.

Figure 97: Transparent triangular brownish crystal of biotite mica, identified by Raman spectroscopy (referenced via the RRUFF database), with an associated plane of thin films in sample 749-S using fiber-optic light illumination, FOV 1.20 mm. Photo: V. Raynaud © GIA.

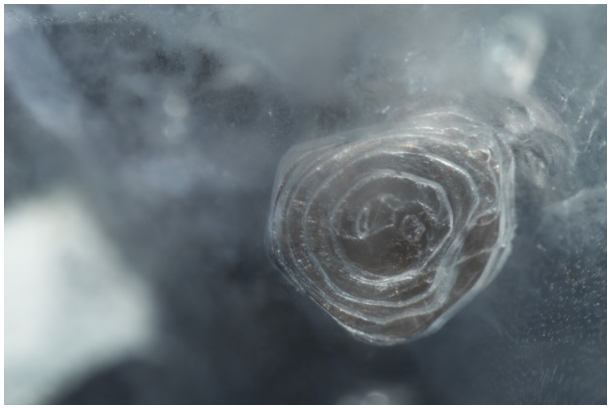

Figure 98: Irregularly-shaped brownish crystal of biotite mica, identified by Raman spectroscopy (referenced via RRUFF database), in sample 720-S using fiber-optic illumination, FOV 2.40 mm. Photo: V. Raynaud © GIA.

Figure 99: A bisected dark green crystal of spinel, identified by Raman spectroscopy (referenced via RRUFF database), in sample 754-S using fiber-optic illumination, FOV 1.20 mm. Photo: V. Raynaud © GIA.

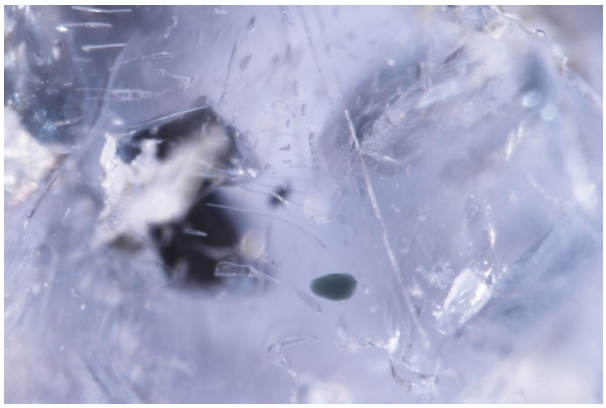

Figure 100: A rounded (unidentified) dark green crystal with associated healed fissure in sample 728-S using fiber-optic light illumination, FOV 1.40 mm. Photo: V. Raynaud © GIA.

Figure 101: Unidentified dark green platelets with associated brownish particles in sample 712-S using fiber-optic light illumination, FOV 1.75 mm. Photo: V. Raynaud © GIA.

Figure 102: Unidentified orangy material with tension fractures in sample 712-S using dark field and fiber-optic light illumination, FOV 1.40 mm. Photo: C. Khowpong © GIA.

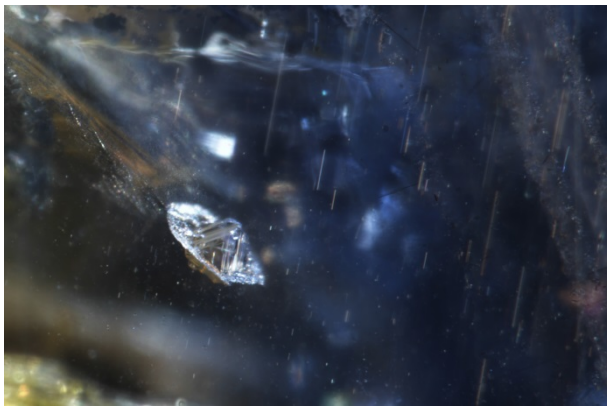

Figure 103: An unidentified angular negative crystal with surrounding granular plane and short needles in sample 741-S using fiber-optic light illumination, FOV 1.05 mm. Photo: V. Raynaud © GIA.

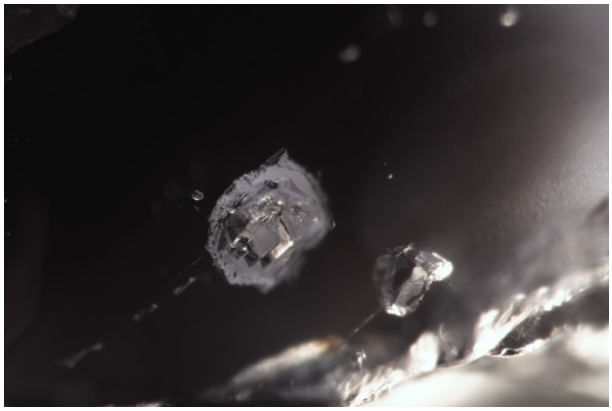

Figure 104: Unidentified angular negative crystals with surrounding granular planes in sample 712-S using dark field illumination, FOV 1.40 mm. Photo: V. Raynaud © GIA.

Figure 105: A bisected black crystal of goethite, identified by Raman spectroscopy (referenced via RRUFF database), and unidentified orange material in sample 715-S using dark field and fiber-optic light illumination, FOV 2.40 mm. Photo: V. Raynaud © GIA.

3.2 Spectroscopy and chemistry of blue sapphires from Baw Mar mines

3.2.1 UV-VIS-NIR SPECTROSCOPY

3.2.1.1 TWO SAMPLES FROM NORTHERN AREA OF BAW MAR MINE (FE46):

Most of the spectral quality samples from the Northern area in Baw Mar mine exhibited similar spectra, and therefore, the spectra of samples 161-N and 188-N were selected as being representative for discussion. The spectra of all wafers are shown in Annex A. In general, UV-Vis-NIR spectra of the samples from the the Northern area revealed strong Fe^{3+} absorption features with a cut-off/shoulder at 330 nm and peaks at 377, 388 and 450 nm, as well as Fe^{2+}-Ti^{4+} intervalence charge transfer features in the way of broad bands centered at 580 nm in the o-ray and at 700 nm in the e-ray. In addition, a weak broad band relating to Fe clusters was observed in the near infrared region.

GIA reference sample 161-N

Figure 106 shows a very strong Fe^{3+} absorption and Fe^{2+}-Ti^{4+} charge transfer features for sample 161-N. The absorption at approximately 330 nm is related to a Fe^{3+}-Fe^{3+} pair interaction, and generally manifests itself as a shoulder; however, this sample showed a cut-off at 330 nm due to the high Fe concentration, long beam path, and/or scattering by particles. The peaks at 377 and 450 nm are associated with a pair of Fe^{3+}-Fe^{3+} ions, whereas the peak at 388 nm results from a single Fe^{3+} ion absorption [Ferguson and Fielding 1971, Ferguson and Fielding 1972, Krebs and Maisch 1971]. A slightly greater peak height was shown by the 377 nm, when compared to the 388 nm, in o-ray, whereas the height of the absorption peak at 377 nm is significantly greater than that of the 388 nm peak in e-ray. The broad band centered at 580 nm in the o-ray and at 700 nm in the e-ray is attributed to Fe^{2+}-Ti^{4+} pair charge transfer, and is responsible for the blue color of the sapphire. In comparison, it is interesting to note that the UV-Vis spectra of a pure synthetic corundum doped with Fe^{2+}-Ti^{4+} [E.V. Dubinsky and J.L. Emmett, 2013], exibits a higher absorption at about 760 nm and longer wavelengths in the o-ray than that of the e-ray for sample 161-N. A pure synthetic doped Fe-Ti spectrum was subtracted from the the spectrum obtained, and the resulting spectrum showed Fe^{3+} absorption features and a broad peak at about 870 nm which is related to Fe clusters [Hughes *et al*., 2017].

To study the correlation between color, UV-Vis-NIR and chemistry data of the sample, LA-ICP-MS was performed on each side of the wafer and the laser spots were positioned in the same areas where the UV-Vis-NIR and FTIR spectra were collected. Six spots were analyzed on each side of the sample, twelve spots in total (Figure 107). It should be noted that the LA-ICP-MS technique only analyzes the components within micron-sized spots, whereas UV-Vis-NIR and FTIR techniques analyze the whole volume of the wafer within the beam path. The homogeneity of the samples should also be taken into consideration when comparing the results between these techniques. Table 2 shows chemical data obtained from LA-ICP-MS for sample 161-N. The values of each trace element were found to be relatively consistent within the 12 spots. A significantly high amount of Fe and some amounts of Mg, Ti and Ga were detected. Beryllium (Be) and zirconium (Zr) are present in negligible concentrations. An insignificant level of Nb was detected which is commonly attributed to minute included particles. Chromium (Cr), vanadium (V) and other high field strength elements, including Hf, Ta, W, Th, were below detection limits.

The amount of Mg is less than that of Ti, and therefore a Ti^{4+} charge compensates for Mg^{2+} leaving some Ti to be paired with Fe^{2+} via a charge transfer interaction to produce blue color in the sample [Emmett et al. 2003]. The visible color of this sample (Figure 107) corresponds with the results obtained from the UV-Vis spectra (Figure 106) and chemical data as analyzed by LA-ICP-MS (Table 2).

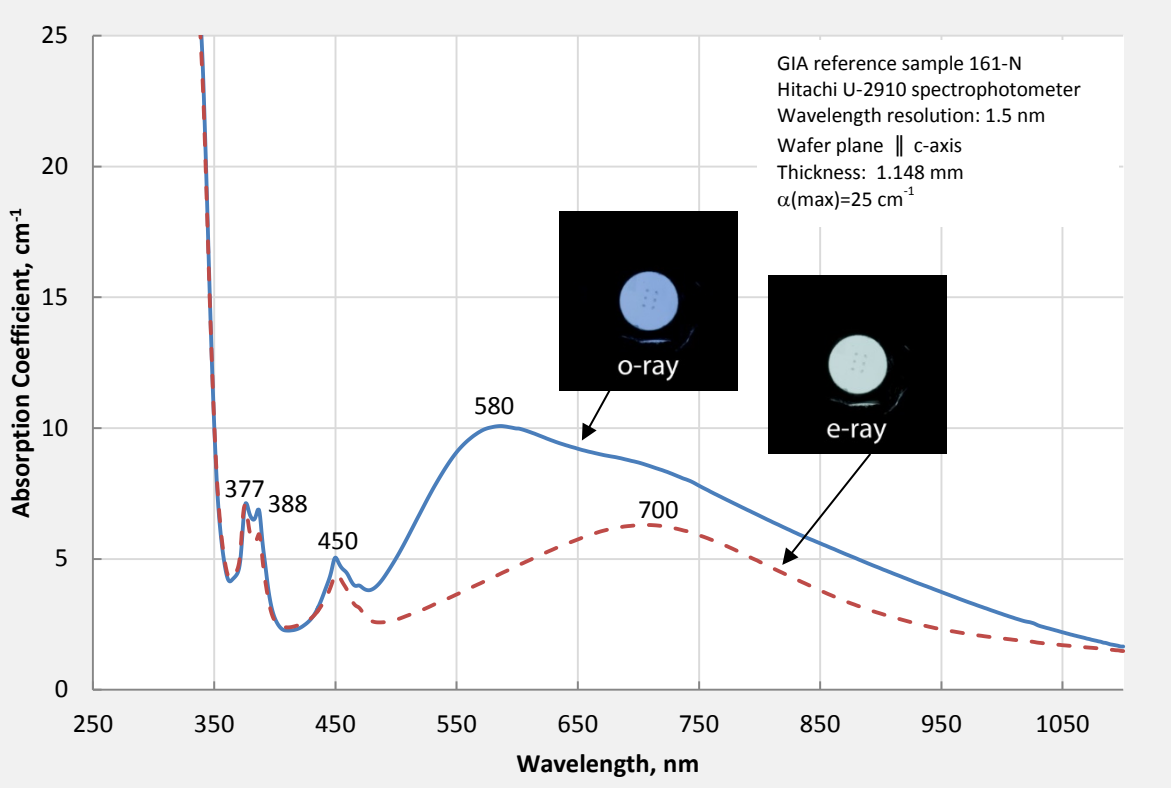

Figure 106: UV-Vis-NIR spectra of sample 161-N with inset color calibrated polarized photos of the beam path area for the o- and e-rays. Optical path length 1.148 mm. Weight 0.340 carat. Color: Even blue.

Figure 107: Sample 161-N showing the positions of 12 spots (6 each side of the wafer) where LA-ICP-MS analysis was conducted for this study. Photo: S. Engniwat © GIA.

Table 2: LA-ICP-MS results in parts per million atoms (ppma) for GIA reference sample 161-N. All spots were positioned within blue areas. 'BDL' stands for 'below detection limit' and 'BQL' for 'below quantification limit'

Sample 161-N Spot number	Concentration in ppma												
	9Be	24Mg	47Ti	51V	53Cr	57Fe	69Ga	90Zr	93Nb	178Hf	181Ta	182W	232Th
SP1 (blue area)	BDL	8.64	15.2	BQL	BDL	1833	22.7	BDL	0.01	BDL	BDL	BDL	BDL
SP2 (blue area)	BDL	8.09	14.1	BDL	BQL	1749	23.1	BDL	0.01	BDL	BDL	BDL	BDL
SP3 (blue area)	BDL	7.42	13.2	BQL	BDL	1826	23.4	BDL	0.01	BDL	BDL	BDL	BDL
SP4 (blue area)	0.32	6.27	12.9	BQL	BDL	1745	24.3	BDL	0.01	BDL	BDL	BDL	BDL
SP5 (blue area)	BDL	6.70	13.5	BQL	BDL	1727	24.3	BDL	0.01	BDL	BDL	BDL	BDL
SP6 (blue area)	BDL	6.53	12.2	BQL	BDL	1749	23.9	BDL	0.01	BDL	BDL	BDL	BDL
SP7 (blue area)	BDL	7.67	13.7	BDL	BQL	1986	21.2	0.01	0.01	BDL	BDL	BDL	BDL
SP8 (blue area)	0.34	8.64	16.6	BQL	BDL	1844	21.2	BDL	BQL	BDL	BDL	BDL	BDL
SP9 (blue area)	0.34	11.2	18.6	BQL	BDL	1950	21.6	BDL	0.01	BDL	BDL	BDL	BDL
SP10 (blue area)	BDL	8.39	15.9	BQL	BDL	1986	22.1	BDL	0.01	BDL	BDL	BDL	BDL
SP11 (blue area)	BDL	9.06	19.6	BQL	BQL	1950	21.7	BDL	BQL	BDL	BDL	BDL	BDL
SP12 (blue area)	BDL	9.31	19.3	BQL	BQL	2037	21.4	0.01	0.01	BDL	BDL	BDL	BDL
Average	-	**8.16**	**15.4**	-	-	**1865**	**22.6**	-	-	-	-	-	-
Standard Deviation	-	**1.39**	**2.6**	-	-	**112**	**1.2**	-	-	-	-	-	-
Detection Limits	*0.07*	*0.04*	*0.74*	*0.10*	*1.25*	*6.87*	*0.06*	*0.00*	*0.00*	*0.00*	*0.00*	*0.00*	*0.00*

Note: The limit of detection (LOD) or detection limit (DL), given by the International Union and Pure and Applied Chemistry (IUPAC) and the American Chemical Society (ACS), expressed as a concentration or quantity, is derived from the smallest measure that can be detected with reasonable certainty for a given analytical procedure. The limit of quantification (LOQ) or quantitation limit (QL) refers to the smallest concentrations which can be quantitatively analyzed with reasonable reliability by a give procedure.

GIA reference sample 188-N

As shown in Figure 108, the UV-Vis-NIR spectra of sample 188-N shows strong Fe^{3+} absorption features with a high shoulder at 330 nm, and peaks at 377, 388 and 450 nm. In this sample, the peak height of 388 nm is greater than that of 377 nm in the o-ray, whereas the peak height at 377 nm is higher than that of the 388 nm peak for the e-ray. The spectra also displayed a broad band centered at 580 nm in the o-ray and at 700 nm in the e-ray attributable to an Fe^{2+}-Ti^{4+} charge transfer. In addition, the o-ray spectrum of the sample shows a weak broad band centered at around 870 nm which is related to Fe clusters [Hughes *et al*., 2017].

LA-ICP-MS was carried out in twelve spots on one side and six spots on the opposite side of sample 188-N, eighteen spots in total (Figure 109). Twelve spots (spots 1-6 and 13-18) were collected in the same area studied by UV-Vis-NIR and FTIR spectroscopy, whereas another six spots (spots 7-9) were positioned in different areas. Table 3 lists the concentrations of trace elements detected by LA-ICP-MS in sample 188-N. This sample had high Fe content as well as some Mg, Ti, V and Ga content. Beryllium (Be), chromium (Cr) and high field strength elements (Zr, Nb, Hf, Ta, W, Th) were generally below detection limits. As the top part of Table 3 shows, spots 1-6 and 13-18, reveal Ti concentrations ($[Ti^{4+}]$) greater than Mg concentrations ($[Mg^{2+}]$), leaving some Ti^{4+} available to form Fe^{2+}-Ti^{4+} pairs. In addition, spots 7-9 were positioned in a colorless area in order to compare the chemistry witjhin color zoning (Figure 109). For spots 7-9 (colorless area, Table 3, bottom), $[Ti^{4+}] < [Mg^{2+}]$, thus all Ti charges compensate for Mg leaving none to form Fe^{2+}-Ti^{4+} pairs. In sample 188-N the chemistry results obtained by LA-ICP-MS correspond with the UV-Vis-NIR spectra and observable visual color (Figure 109).

When comparing the UV-Vis spectra of the o-ray from sample 161-N (Figure 106) with that from sample 188-N (Figure 108), the peak height at 377 nm (attributed to a pair of Fe^{3+}-Fe^{3+} ions) is higher than that at 388 nm (related to a single Fe^{3+} ion) in sample 161-N, whereas the height at 377 nm is lower in sample 188-N. This is possibly due to the greater Fe concentrations in sample 161-N (Table 2) than those in sample 188-N (Table 3).

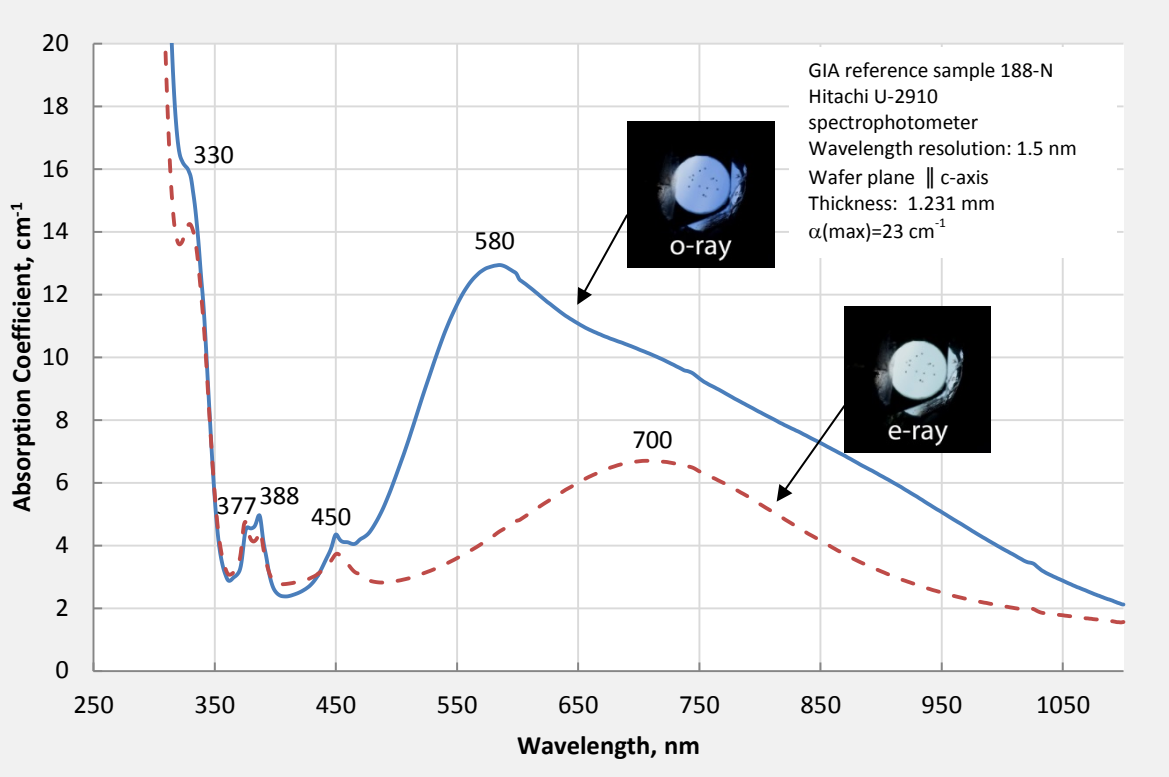

Figure 108: UV-Vis-NIR spectra of sample 188-N with inset color calibrated polarized photos of the beam path area for the o- and e-rays. Optical path length 1.231 mm. Weight 0.350 carat. Color: Blue and colorless.

Figure 109: Sample 188-N showing the location of 15 spots where LA-ICP-MS analysis was conducted on each side of the wafer for this study. Photo: S. Engniwat © GIA.

Table 3: LA-ICP-MS results in ppma for GIA reference sample 188-N. Twelve spots were positioned within blue areas and three spots within colorless areas. 'BDL' stands for 'below detection limit' and 'BQL' for 'below quantification limit'

Sample 188-N Spot number	Concentration in ppma												
	9Be	24Mg	47Ti	51V	53Cr	57Fe	69Ga	90Zr	93Nb	178Hf	181Ta	182W	232Th
SP1 (blue area)	BDL	11.2	17.7	1.81	BDL	1274	26.2	BQL	BDL	BDL	BQL	BDL	BDL
SP2 (blue area)	BDL	14.5	16.2	1.76	BQL	1413	27.3	BDL	BDL	BDL	BDL	BDL	BDL
SP3 (blue area)	BDL	14.6	20.3	1.84	BDL	1289	26.1	BDL	BDL	BDL	BDL	BDL	BDL
SP4 (blue area)	BDL	14.8	20.1	1.23	BDL	1293	26.2	BDL	BDL	BQL	BQL	BQL	0.00
SP5 (blue area)	BDL	13.8	17.1	1.74	BDL	1245	25.5	BDL	BDL	BQL	BDL	BDL	BDL
SP6 (blue area)	BDL	13.5	19.7	1.98	BDL	1384	27.2	BDL	BDL	BDL	BDL	BDL	BDL
SP13 (blue area)	BQL	14.5	19.0	19.0	BDL	1293	26.4	BDL	BDL	BDL	BDL	BDL	BDL
SP14 (blue area)	BDL	15.2	22.7	22.7	BDL	1303	25.7	BDL	BQL	BDL	BDL	BDL	BDL
SP15 (blue area)	BDL	13.3	16.1	16.1	BQL	1274	25.5	BDL	BDL	BDL	BDL	BQL	BDL
SP16 (blue area)	BDL	14.1	13.9	13.9	BDL	1293	24.9	BDL	BQL	BDL	BDL	BQL	BDL
SP17 (blue area)	BDL	13.0	19.8	19.8	BDL	1311	24.4	BDL	BDL	BDL	BDL	BQL	BDL
SP18 (blue area)	BDL	12.1	17.3	17.3	BQL	1373	26.9	BDL	BDL	BDL	BDL	BDL	BDL
Average	-	**13.7**	**18.3**	**9.93**	-	**1312**	**26.0**	-	-	-	-	-	-
Standard Deviation	-	**1.2**	**2.4**	**8.8**	-	**51**	**0.9**	-	-	-	-	-	-
SP7 (colorless area)	BDL	15.9	14.2	1.30	BDL	1336	26.6	BDL	BDL	BDL	BDL	BDL	BDL
SP8 (colorless area)	BDL	16.4	15.6	1.69	BDL	1234	25.0	BDL	BDL	BDL	BDL	BDL	BDL
SP9 (colorless area)	BQL	17.3	11.6	1.70	BDL	1274	24.8	BQL	BDL	BDL	BDL	BQL	BDL
Average	-	**16.5**	**13.8**	**1.56**	-	**1281**	**25.5**	-	-	-	-	-	-
Standard Deviation	-	**0.7**	**2.0**	**0.2**	-	**51**	**1.0**	-	-	-	-	-	-
Detection limit	*0.21*	*0.11*	*1.34*	*0.27*	*2.10*	*7.20*	*0.14*	*0.02*	*0.02*	*0.00*	*0.00*	*0.00*	*0.00*

3.2.1.2 TWO SAMPLES FROM THE SOUTHERN AREA OF BAW MAR MINE (FE75):

Samples 741-S and 763-S were selected as representative of the spectroscopic data obtained from southern area samples for discussion. In general, UV-Vis-NIR spectra of blue sapphires from the Southern area revealed weak to moderate Fe absorption features and evidence of an Fe^{2+}-Ti^{4+} intervalence charge transfer.

GIA reference sample 741-S

The UV-Vis-NIR spectrum of the o-ray for sample 741-S showed typical Fe^{3+} absorption features with a moderately high shoulder at 330 nm, peaks at 377, 387 and 450 nm, and also a band centered at 580 nm attributable to an Fe^{2+}-Ti^{4+} charge transfer (Figure 110). The peak height at 377 nm is comparable with that at 387 nm.

LA-ICP-MS analysis was performed on sample 741-S in the same area that UV-Vis-NIR and FTIR spectroscopy was carried out. Four spots on each side of the wafer, eight spots in total (Figure 111) were tested. Table 4 shows the chemical data results obtained for sample 741-S. Fe, Mg, Ti, Ga and V were present in relatively consistent values for all 8 spots. The Fe concentration was relatively high. After Ti charge compensated Mg, some Ti interacted with Fe to produce the sample's blue color (Figure 111). An insignificant amount of Be was also detected. In addition, Cr, Zr, Nb, Hf, Ta, W, Th were generally found to be below the detection limits. Visual observation of color in sample 741-S (Figure 111) corresponds well with the UV-Vis-NIR spectrum (Figure 110) and chemical data results obtained by LA-ICP-MS (Table 4) spectrometry.

When compared with sample 161-N (Table 2) and sample 188-N (Table 3) from the Northern area of Baw Mar mine, sample 741-S possesses less Fe, slightly higher Ga, and significantly greater quantities of Mg and Ti (Table 4).

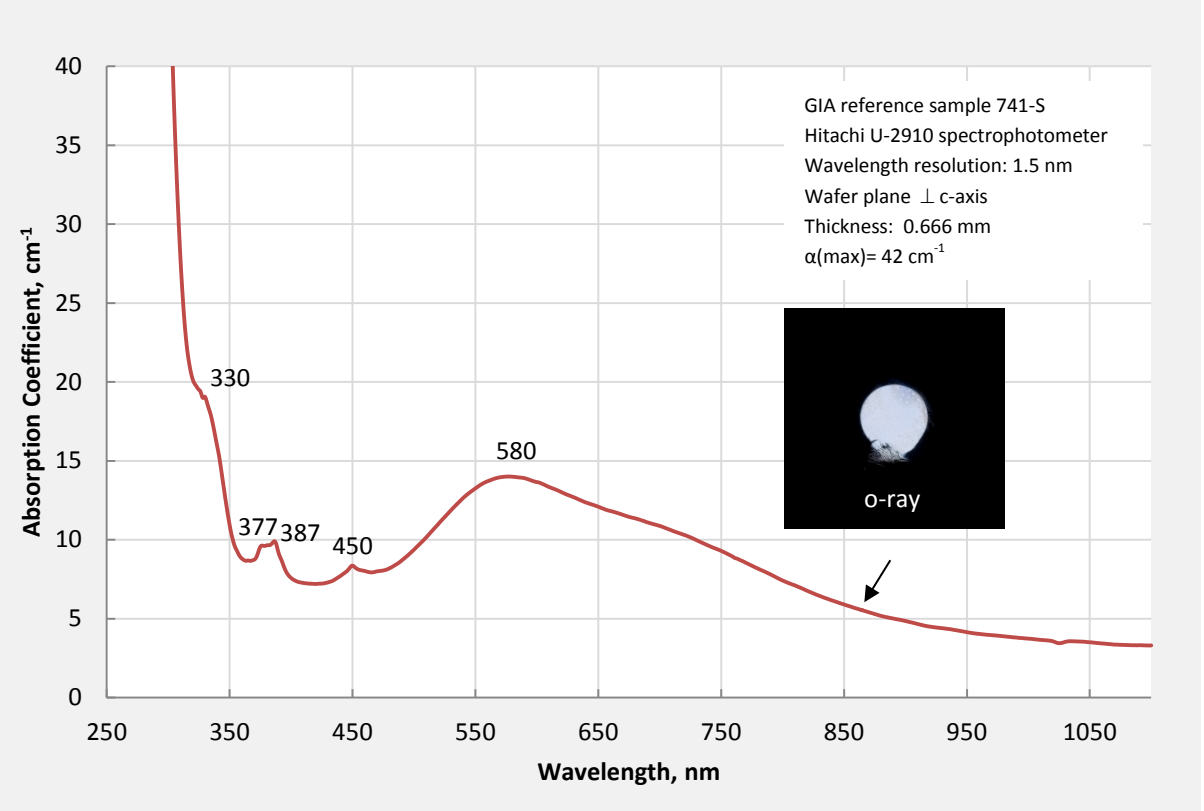

Figure 110: UV-Vis-NIR spectrum of sample 741-S with inset color calibrated polarized photo of the beam path area for the o-ray. Optical path length 0.666 mm. Weight 0.263 carat. Color: Light blue.

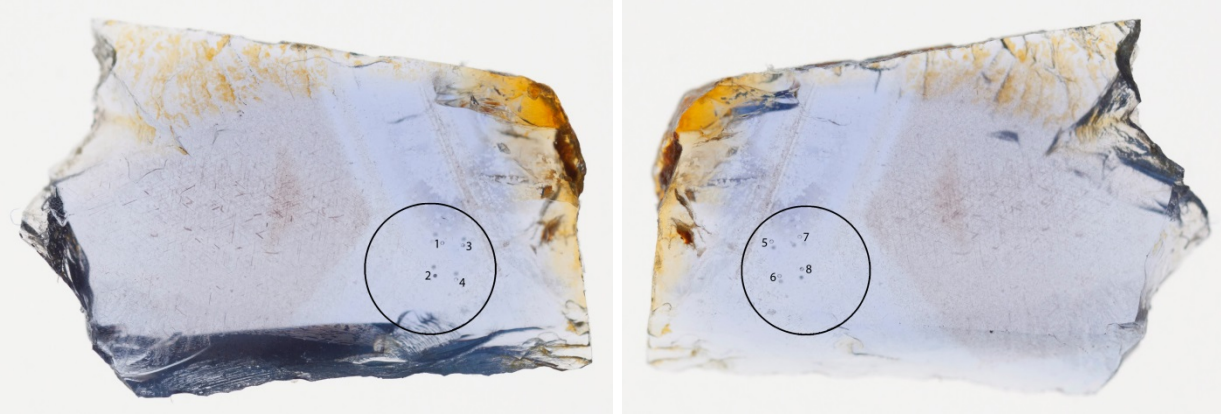

Figure 111: Sample 741-S showing the location of the 8 spots where LA-ICP-MS analysis was conducted on each side of the wafer for this study. Photo: S. Engniwat © GIA.

Table 4: LA-ICP-MS results in ppma for GIA reference sample 741-S. All spots were positioned within a blue area. 'BDL' stands for 'below detection limit'.

Sample 741-S Spot number	Concentration in ppma												
	9Be	24Mg	47Ti	51V	53Cr	57Fe	69Ga	90Zr	93Nb	178Hf	181Ta	182W	232Th
SP1 (blue area)	BDL	36.2	44.3	0.90	BDL	1154	32.2	BDL	BDL	BDL	BDL	0.00	BDL
SP2 (blue area)	0.43	38.4	42.5	1.02	BDL	1150	32.8	BDL	BDL	BDL	BDL	BDL	BDL
SP3 (blue area)	0.34	38.5	43.0	1.09	BDL	1128	32.2	BDL	BDL	BDL	BDL	BDL	BDL
SP4 (blue area)	BDL	36.4	45.1	0.82	BDL	1172	33.1	BDL	BDL	BDL	BDL	BDL	BDL
SP5 (blue area)	BDL	37.4	43.4	0.91	BDL	1110	31.3	BDL	BDL	BDL	BDL	BDL	BDL
SP6 (blue area)	0.18	30.3	37.5	1.02	BDL	1030	29.5	BDL	BDL	0.00	BDL	BDL	BDL
SP7 (blue area)	BDL	31.8	47.3	0.89	BDL	1066	31.0	BDL	BDL	BDL	BDL	BDL	BDL
SP8 (blue area)	BDL	34.2	40.9	0.92	BDL	1103	31.3	0.00	BDL	BDL	BDL	BDL	BDL
Average	-	**34.8**	**42.9**	**0.94**	-	**1101**	**31.4**	-	-	-	-	-	-
Standard Deviation	-	**3.3**	**3.4**	**0.10**	-	**49**	**1.2**	-	-	-	-	-	-
Detection Limits	*0.03*	*0.02*	*0.27*	*0.05*	*0.47*	*3.62*	*0.02*	*0.00*	*0.00*	*0.00*	*0.00*	*0.00*	*0.00*

GIA reference sample 763-S

The UV-Vis-NIR spectrum of the o-ray for sample 763-S revealed weak Fe absorption features including a low shoulder at 330 nm and peaks at 388 and 450 nm; however, no absorption peak at 377 nm was observed (Figure 112). It also showed a weak broad band with approximate center being at 560 nm; however, this weak band has not yet been identified.

LA-ICP-MS analysis was carried out on sample 763-S in the same area that UV-Vis-NIR and FTIR spectroscopy was carried out. Four spots on each side of wafer, eight spots in total (Figure 113) were tested. As shown in Table 5, sample 763-S showed Fe, Mg, Ti, V, and Ga in relatively consistent concentrations. Be was also detected but in negligible amounts. Other trace elements, namely Cr, Zr, Nb, Hf, Ta, W, and Th, were below detection limits or very slightly above. The light blue color in sample 763-S (Figure 113) and UV-Vis-NIR spectrum (Figure 110) do not correspond well with the chemistry (Table 5) possibly owing to the sample's inhomogeneity.

When comparing the chemical data of the samples from the same zone, sample 763-S (Table 5) showed significantly lower Fe concentrations and significantly higher Mg and Ti concentrations than those of sample 741-S (Table 4), while V and Ga concentrations in both samples were comparable.

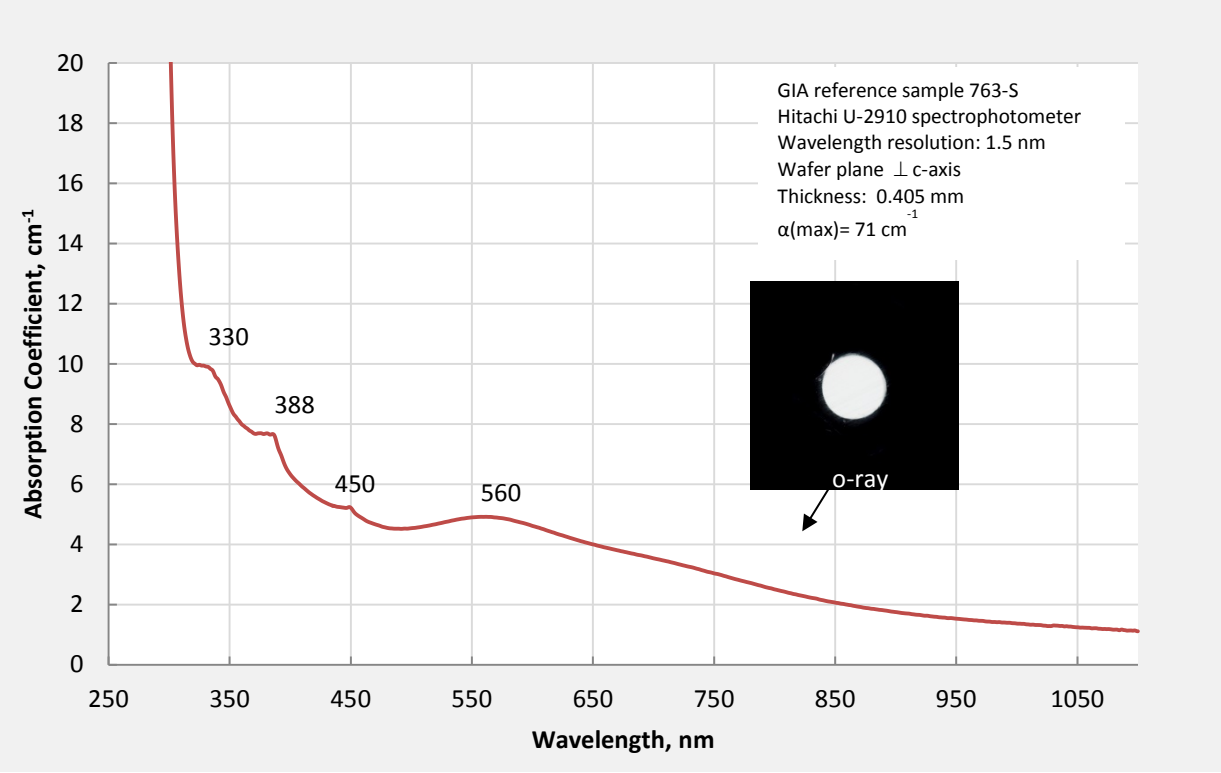

Figure 112: UV-Vis-NIR spectrum of sample 763-S with inset color calibrated polarized photo of the beam path area for the o-ray. Optical path length 0.405 mm. Weight 0.096 carat. Color: Very light blue.

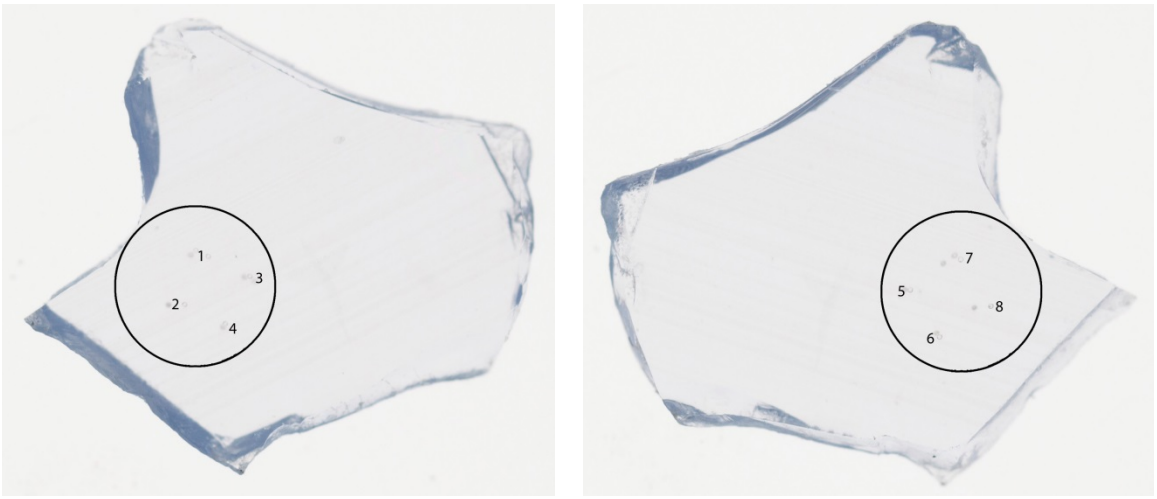

Figure 113: Sample 763-S showing the location of the 8 spots where LA-ICP-MS analysis was conducted on each side of the wafer for this study. Photo: S. Engniwat © GIA

Table 5: LA-ICP-MS results in ppma on GIA reference sample 763-S**.** All spots were conducted in a blue area. 'BDL' stands for 'below detection limit' and 'BQL' for 'below quantification limit'.

Sample 763-S Spot number	Concentration in ppma												
	9Be	24Mg	47Ti	51V	53Cr	57Fe	69Ga	90Zr	93Nb	178Hf	181Ta	182W	232Th
SP1 (light blue area)	0.45	83.2	101	1.68	BDL	486	34.5	0.01	BDL	BDL	BDL	BDL	BDL
SP2 (light blue area)	BDL	87.2	91.6	1.45	BDL	460	31.9	0.00	BQL	BDL	BDL	BDL	BDL
SP3 (light blue area)	0.20	88.9	91.6	1.51	BDL	489	33.9	BDL	BDL	BDL	BDL	BDL	BDL
SP4 (light blue area)	0.38	89.8	95.8	1.58	BDL	478	33.1	BDL	BDL	BDL	BDL	BDL	BDL
SP5 (light blue area)	BDL	79.9	83.9	1.40	BDL	467	33.3	BQL	0.00	0.00	BDL	BDL	0.00
SP6 (light blue area)	BDL	79.5	80.9	1.29	BDL	467	31.6	BDL	0.00	BDL	BDL	BDL	0.00
SP7 (light blue area)	BDL	78.7	76.7	1.47	BDL	471	33.6	BDL	BDL	BDL	BDL	BDL	BDL
SP8 (light blue area)	BDL	80.4	80.9	1.44	BDL	453	31.3	BDL	BDL	BDL	BDL	BDL	BDL
Average	**-**	**82.9**	**85.0**	**1.45**	**-**	**471**	**32.8**	**-**	**-**	**-**	**-**	**-**	**-**
Standard Deviation	**-**	**5.1**	**7.3**	**0.10**	**-**	**12**	**1.1**	**-**	**-**	**-**	**-**	**-**	**-**
Detection Limits	*0.03*	*0.02*	*0.27*	*0.05*	*0.47*	*3.62*	*0.02*	*0.00*	*0.00*	*0.00*	*0.00*	*0.00*	*0.00*

3.2.2 CHEMICAL ANALYSIS OF DIFFERENT SAMPLE AREAS USING LA-ICP-MS

Baw Mar blue sapphires from either the Northern or Southern areas occasionally contained dense clouds of minute whitish and brownish particles. LA-ICP-MS analysis revealed different elements and/or different concentrations of the same elements between the visually inclusion-free areas and those hosting the whitish and brownish particle. The chemistry of three different areas is discussed below.

3.2.2.1 CHEMISTRY OF INCLUSION-FREE AREAS AND THOSE CONTAINING WHITISH PARTICLES

GIA Reference Sample 206-N

In untreated sapphires, natural Be associated with high field strength elements (such as Zr, Nb, Hf, Ta, W, and Th) may be found in cloudy areas [Shen *et al.* 2007, Lu and Shen 2011]. The Baw Mar samples from the Northern zone rarely exhibit dense particulate areas. However, one of the samples in this study, sample 206-N, did contain dense whitish particles. Therefore it was analyzed using LA-ICP-MS in two different areas; a visually inclusion-free zone and one containing the whitish particles (Figure 114). When the results from both areas were compared the particulate area (Table 6, bottom) showed significantly higher Ti and slightly higher Fe concentrations, whereas Mg, V, and Ga concentrations were comparable to those within the clean area (Table 6, top). Other trace elements, including Be, Cr, Sn and various high field strength elements, were generally below the detection limits in both areas. The data in Table 6, indicates that Ti is the main element present within the whitish particles, and hence rutile as their likely identity.

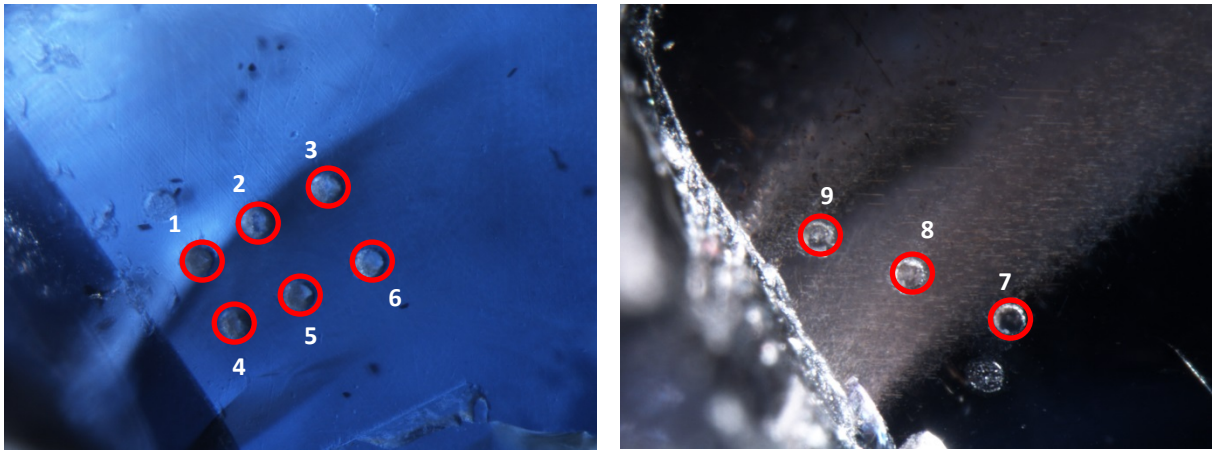

Figure 114: Sample 206-N showing the location of the 6 spots within the visually inclusion-free area (left, FOV 0.80 mm) and another 3 spots (right, FOV 1.00 mm) within the whitish particulate area. Photo: C. Khowpong © GIA.

Table 6: LA-ICP-MS results in ppma on GIA reference sample #206-N. Spots 1 to 6 were obtained from an inclusion-free area, while spots 7 to 9 were positioned within a particulate area. 'BDL' stands for 'below detection limit' and 'BQL' for 'below quantification limit'.

VISUALLY INCLUSION-FREE AREA

Sample 206-N Spot number	Concentration in ppma													
	9Be	24Mg	47Ti	51V	53Cr	57Fe	69Ga	90Zr	93Nb	120Sn	178Hf	181Ta	182W	232Th
SP1 (clean, blue area)	BDL	6.66	18.4	0.29	BDL	1782	21.6	BDL	BQL	BDL	BDL	0.00	BDL	BDL
SP2 (clean, blue area)	BQL	7.52	21.5	0.33	BDL	1855	22.0	BDL	BDL	BDL	BDL	0.00	BDL	BDL
SP3 (clean, blue area)	BDL	7.36	21.3	0.27	BQL	1760	20.9	BDL	BQL	BDL	BDL	BDL	BDL	BDL
SP4 (clean, blue area)	BDL	6.48	18.8	0.28	BQL	1829	21.8	0.00	BDL	BDL	BDL	BDL	BDL	BDL
SP5 (clean, blue area)	BDL	7.45	19.8	0.27	BQL	1756	21.4	BDL	BDL	BDL	BDL	BDL	BDL	BDL
SP6 (clean, blue area)	BDL	7.33	21.2	0.34	BQL	1745	21.2	BDL	BQL	BDL	0.00	0.00	BDL	BDL
Average	-	**7.13**	**20.2**	**0.30**	-	**1788**	**21.5**	-	-	-	-	-	-	-
Standard Deviation	-	**0.45**	**1.4**	**0.03**	-	**44**	**0.4**	-	-	-	-	-	-	-

WHITISH PARTICULATE CLOUD AREA

Sample 206-N Spot number	Concentration in ppma													
	9Be	24Mg	47Ti	51V	53Cr	57Fe	69Ga	90Zr	93Nb	120Sn	178Hf	181Ta	182W	232Th
SP7 (particle area)	BDL	8.98	52.8	0.38	BDL	1851	17.9	BDL	BDL	BQL	0.00	0.00	BDL	BDL
SP8 (particle area)	BDL	10.7	77.1	0.36	BDL	1961	18.2	0.00	BDL	BDL	BDL	0.00	BDL	BDL
SP9 (particle area)	BDL	10.3	60.9	0.40	BDL	1979	17.4	BQL	BDL	BQL	BDL	0.00	BDL	BDL
Average	-	**10.0**	**63.6**	**0.38**	-	**1930**	**17.9**	-	-	-	-	-	-	-
Standard Deviation	-	**0.9**	**12.4**	**0.02**	-	**69**	**0.4**	-	-	-	-	-	-	-

Detection limit	*0.05*	*0.09*	*0.71*	*0.03*	*1.57*	*70.11*	*0.02*	*0.00*	*0.00*	*0.03*	*0.00*	*0.00*	*0.00*	*0.00*

GIA Reference Sample 723-S

In order to compare the trace element chemistry of Baw Mar sapphires from the Southern area, visually inclusion-free and whitish particulate areas were analyzed in sample 723-S (Figure 115 and Table 7). The chemical profiles of the dense whitish particles showed comparable amounts of Fe and Ga to those of the clean area, whereas the cloudy area examined showed significantly greater Mg and Ti content and slightly higher V content than those of inclusion-free area. Small quantities of high field strength elements, including Zr, Nb, Hf, Ta, W and Th, were only detected within the particulate area. Be was present in some spots from both the clean and cloudy areas. Cr was not detected in any of the areas examined. The data in Table 7, indicates that Mg and Ti are the main elements present within the whitish particles and hence, rutile is the likely identity of some particles while other minerals containing Mg are also likely associated with the rutile.

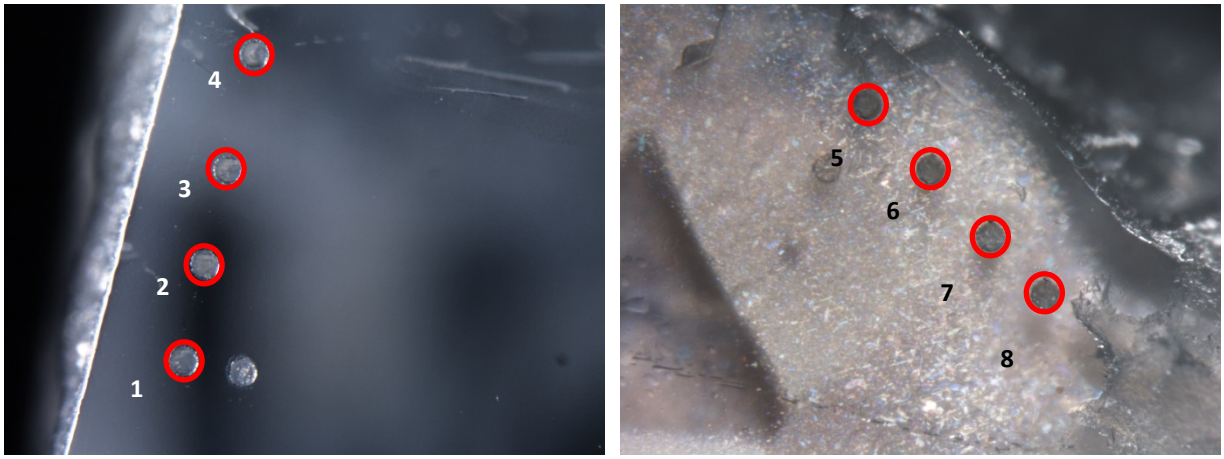

Figure 115: Sample 723-S showing the location of the 4 spots within a visually inclusion-free area (left, FOV 1.00 mm), and another 4 spots within a whitish particulate area (right, FOV 1.00 mm). Photo: C. Khowpong © GIA.

Table 7: LA-ICP-MS results in ppma on GIA reference sample 723-S. 'BDL' stands for 'below detection limit' and 'BQL' for 'below quantification limit'.

VISUALLY INCLUSION-FREE AREA

Sample 723-S Spot number	Concentration in ppma													
	9Be	24Mg	47Ti	51V	52Cr	57Fe	69Ga	90Zr	93Nb	120Sn	178Hf	181Ta	182W	232Th
SP1 (clean, blue area)	BDL	28.4	15.1	1.00	BDL	409	18.5	BDL	BDL	BDL	BDL	BDL	BDL	BDL
SP2 (clean, blue area)	BDL	31.4	17.1	1.05	BDL	416	17.7	BDL	BDL	BQL	BDL	BDL	BDL	BDL
SP3 (clean, blue area)	BDL	27.8	15.7	1.07	BDL	402	18.2	BDL	BDL	BDL	BDL	BDL	BDL	BDL
SP4 (clean, blue area)	0.32	29.5	16.7	0.89	BQL	405	17.9	BDL	BDL	BDL	BDL	BDL	BDL	BDL
Average	-	**29.3**	**16.2**	**1.00**	-	**408**	**18.1**	-	-	-	-	-	-	-
Standard Deviation	-	**1.6**	**0.9**	**0.08**	-	**6**	**0.3**	-	-	-	-	-	-	-

WHITISH PARTICULATE CLOUD AREA

Sample 723-S Spot number	Concentration in ppma													
	9Be	24Mg	47Ti	51V	52Cr	57Fe	69Ga	90Zr	93Nb	120Sn	178Hf	181Ta	182W	232Th
SP5 (particle area)	0.17	216	439	2.06	BDL	431	18.9	0.85	5.20	0.09	0.02	2.61	26.7	0.23
SP6 (particle area)	0.14	122	312	1.94	BDL	383	17.4	0.80	4.83	BQL	0.01	2.56	25.7	0.25
SP7 (particle area)	BDL	94.8	127	1.85	BDL	398	18.4	0.19	1.36	BQL	0.00	0.95	21.2	0.20
SP8 (particle area)	0.12	44.5	43.9	1.19	BDL	383	17.4	0.02	0.05	BDL	BDL	0.03	3.75	0.06
Average	-	**119**	**230**	**1.76**	-	**399**	**18.0**	**0.46**	**2.86**	-	-	**1.54**	**19.4**	**0.19**
Standard Deviation	-	**72**	**178**	**0.39**	-	**22**	**0.8**	**0.42**	**2.55**	-	-	**1.27**	**10.7**	**0.09**

Detection limit	*0.03*	*0.02*	*0.27*	*0.05*	*0.47*	*3.62*	*0.02*	*0.00*	*0.00*	*0.03*	*0.00*	*0.00*	*0.00*	*0.00*

The Baw Mar blue sapphires studied occasionally included clouds of whitish minute particles as previously mentioned, whereas other metamorphic blue sapphires, such as those from Sri Lanka and Madagascar, typically showed fine-grained clouds area [Suthiyuth *et al.* 2016, Sudarat *et al*. 2016]. Table 8 shows the results obtained from LA-ICP-MS analysis of the inclusion-free and particulate areas from various metamorphic blue sapphire sources; Baw Mar in this study; Ilakaka, Madagascar; and Elahera, Sri Lanka. A comparison of the data from the whitish particulate cloud areas shows that Baw Mar and Sri Lankan material sometimes show trace amounts of high field strength elements (such as Zr, Nb, Hf, Ta, W and Th), while Madagascan samples commonly contain significant concentrations of these elements. Additionally, significant levels of Sn were detected within particulate areas in Madagascan sapphires, while Sn concentrations were generally below the detection limits in Baw Mar and Sri Lankan stones. Other than the high field strength elements, small amounts of Be were present within particulate areas of Madagascan and Sri Lankan samples, whereas Be was generally below the detection limits or just above within whitish particulate areas of Baw Mar blue sapphires.

Table 8: Chemical composition of metamorphic blue sapphires from Baw Mar (Myanmar), Ilakaka (Madagascar) and Elahera (Sri Lanka), using LA-ICP-MS within inclusion-free and whitish particulate areas. 'BDL' stands for 'below detection limit' and 'BQL' for 'below quantification limit'.

Element	Concentrations in ppma[a]							
	Baw Mar-North (1 sample)		Baw Mar-South (3 samples)		Ilakaka, Madagascar[b] (26 samples)		Elahera, Sri Lanka[c] (44 samples)	
	clean	whitish particles	clean	whitish particles	clean	whitish particles	clean	whitish particles
^{9}Be	BDL-BQL	**BDL**	BDL-0.3	**BDL-0.2**	BDL-0.7	**0.01-18**	BDL-0.6	**BDL-3.53**
^{24}Mg	6.5-7.5 *(7.1±0.5)*	**9.0-10.7** ***(10.0±0.9)***	28-98 *(44±19)*	**44-216** ***(92±48)***	19-196	**33-245**	16-162	**28-169**
^{47}Ti	18-22 *(20±1)*	**53-77** ***(64±12)***	15-55 *(36±16)*	**44-439** ***(154±113)***	19-690	**73-2577**	15-112	**20-1393**
^{51}V	0.27-0.34 *(0.30±0.03)*	**0.36-0.40** ***(0.38±0.02)***	0.8-1.2 *(1.0±0.1)*	**0.8-2.1** ***(1.4±0.4)***	3-18	**1-22**	2-54	**0.9-22**
^{53}Cr	BDL-BQL	**BDL**	BDL-BQL	**BDL-BQL**	5-10	**2-14**	BDL-51	**BDL-14**
^{57}Fe	1745-1855 *(1788±44)*	**1851-1979** ***(1930±69)***	402-1030 *(611±286)*	**383-1179** ***(686±347)***	73-719	**81-876**	53-716	**42-643**
^{69}Ga	21-22 *(21.5±0.4)*	**17.4-18.2** ***(17.9±0.4)***	18-27 *(23±4)*	**17-28** ***(24±4)***	9-37	**8-42**	4-42	**5.5-25**
^{90}Zr	BDL-0.00	**BDL-0.00**	BDL-0.01	**0.00-0.8** ***(0.2±0.3)***	0.001-0.04	**0.003-1.44**	BDL-0.07	**BDL-0.19**
^{93}Nb	BDL-BQL	**BDL**	BDL	**BDL-5.2**	0.001-0.05	**0.001-6.85**	BDL-0.04	**BDL-0.13**
^{120}Sn	BDL	**BDL-BQL**	BDL	**BDL-0.09**	0.17-0.26	**0.11-20**	BDL	**BDL-0.7**
^{178}Hf	BDL	**BDL-0.00**	BDL	**BDL-0.02**	0.001-0.01	**0.001-0.07**	BDL-0.01	**BDL-0.03**
^{181}Ta	BDL-0.00	**0.00-0.00**	BDL	**BDL-2.6**	0.001-0.27	**0.001-4.4**	BDL-0.08	**BDL-0.24**
^{182}W	BDL	**BDL**	BDL-0.001	**BDL-27**	0.001-0.8	**0.001-1.2**	BDL-0.15	**BDL-0.48**
^{232}Th	BDL	**BDL**	BDL-0.001	**BDL-0.3**	0.001-0.08	**0.001-8.2**	BDL-0.93	**BDL-2.4**

[a]Data reported in minimum and maximum values, with average values and standard deviations in parentheses.
[b]Data from Saeseaw *et al*. 2016 [c]Data from Suthiyuth *et al*. 2016

3.2.2.2 CHEMISTRY OF INCLUSION-FREE AREAS AND THOSE CONTAINING BROWNISH PARTICLES

GIA Reference Sample 728-S

LA-ICP-MS analysis was performed on a visually inclusion-free area and on the brownish particles just below the surface of sample 728-S for chemical data comparison (Figure 116). The concentrations of each element were relatively consistent in the inclusion-free area, whereas they varied greatly from spots 5 to 8 within the brownish particulate cloud area (Table 9). This is possibly due to the inhomogeneity of the sampled areas in the dense brownish particulate zone tested. However, the results between the visually inclusion-free and brownish particulate cloud areas varied considerably. A comparison of the data from the inclusion-free area with that from the brownish particulate area shows the amounts of Mg, Ti and Fe in the latter were significantly greater, and the amounts of V and Ga were slightly higher. In addition, Be, Nb, Zr, Hf, Ta, W and Th were present in relatively low concentrations within the brownish particulate area. Cr and Sn were generally below detection limits within both areas. The data presented in Table 9, indicates that the brownish particles mainly consist of Mg, Fe and Ti which mean that ilmenite ($FeTiO_3$), and hematite (Fe_2O_3) as well as other minerals containing Mg are present.

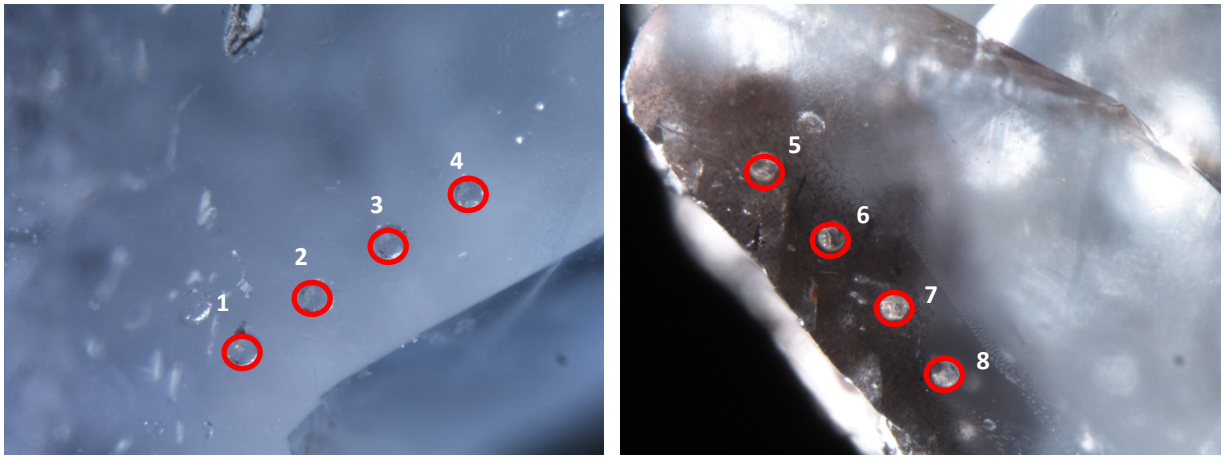

Figure 116: Sample 728-S showing the location of the 4 spots within the visually inclusion-free area (left, FOV 1.00 mm), and another 4 spots within the brownish particulate area (right, FOV 1.00 mm). Photo: C. Khowpong © GIA.

Table 9: LA-ICP-MS results in ppma on GIA reference sample 728-S. 'BDL' stands for 'below detection limit' and 'BQL' for 'below quantification limit'

VISUALLY INCLUSION-FREE AREA

Sample 728-S Spot number	Concentration in ppma													
	9Be	24Mg	47Ti	51V	52Cr	57Fe	69Ga	90Zr	93Nb	120Sn	178Hf	181Ta	182W	232Th
SP1 (clean, blue area)	BQL	70.6	71.1	0.98	BDL	613	20.3	BDL	BDL	BDL	BDL	BDL	BDL	BDL
SP2 (clean, blue area)	0.27	72.5	71.6	0.99	BQL	610	19.7	BDL	0.00	BDL	BDL	BDL	BDL	0.00
SP3 (clean, blue area)	BQL	74.7	71.6	0.99	1.12	613	19.2	BDL	BDL	BDL	BDL	BDL	BDL	BDL
SP4 (clean, blue area)	0.25	71.0	76.2	1.04	BQL	624	19.5	BDL	BDL	BDL	BDL	BDL	BDL	BDL
Average	-	**72.2**	**72.6**	**1.00**	-	**615**	**19.7**	-	-	-	-	-	-	-
Standard Deviation	-	**1.9**	**2.4**	**0.03**	-	**6**	**0.5**	-	-	-	-	-	-	-

BROWNISH PARTICULATE CLOUD AREA

Sample 728-S Spot number	Concentration in ppma													
	9Be	24Mg	47Ti	51V	52Cr	57Fe	69Ga	90Zr	93Nb	120Sn	178Hf	181Ta	182W	232Th
SP5 (particulate cloud)	1.13	1510	307	2.19	BQL	3041	33.3	BDL	0.07	BQL	0.00	0.01	0.00	0.05
SP6 (particulate cloud)	0.25	107	460	2.02	BDL	1486	29.5	0.20	0.10	BDL	BQL	0.01	0.01	0.09
SP7 (particulate cloud)	0.68	656	1018	2.24	BDL	2906	29.5	0.34	0.27	BDL	0.00	0.02	0.02	0.11
SP8 (particulate cloud)	BQL	87.2	102	1.61	1.38	1106	24.3	0.00	0.00	BDL	BDL	BDL	BDL	0.00
Average	-	**590**	**472**	**2.02**	-	**2135**	**29.2**	-	**0.11**	-	-	-	-	
Standard Deviation	-	**668**	**393**	**0.29**	-	**982**	**3.7**	-	**0.11**	-	-	-	-	

Detection limit	*0.04*	*0.04*	*0.24*	*0.04*	*0.36*	*3.50*	*0.02*	*0.00*	*0.00*	*0.03*	*0.00*	*0.00*	*0.00*	*0.00*

3.2.2.3 CHEMISTRY OF VISUALLY INCLUSION-FREE AREA

GIA Reference Sample 754-S

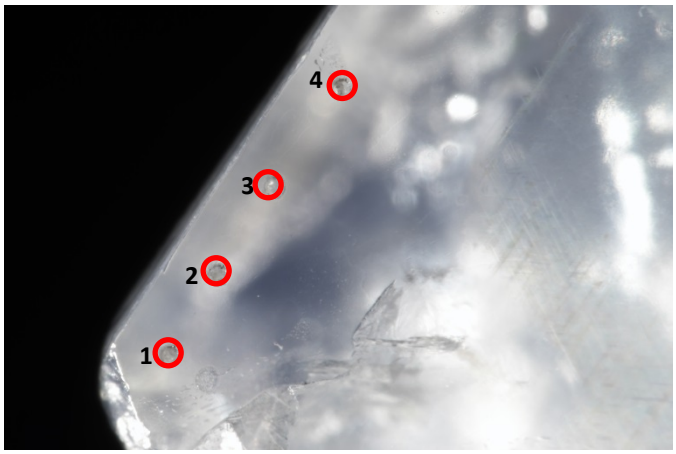

Figure 117: Sample 754-S showing the location of the 4 spots within a visually inclusion-free area, FOV 1.2 mm. Photo: C. Khowpong © GIA.

In the visually inclusion-free area, Be and high field strength elements (such as Zr, Nb, Hf, Ta, W and Th) were generally below the detection limit or slightly above, however, three of the samples (715-S, 719-S and 754-S) revealed small amounts of Be, possibly because of included nanoparticles in the area analyzed, associated with high field strength elements. It was notable to see that significant amounts of Sn were detected within the visually inclusion-free area for sample 754-S (Table 10 and Figure 117).

Table 10: LA-ICP-MS results in ppma from GIA reference sample 754-S. 'BDL' stands for 'below detection limit'.

VISUALLY INCLUSION-FREE AREA

Sample 754-S Spot number	Concentration in ppma													
	9Be	24Mg	47Ti	51V	52Cr	57Fe	69Ga	90Zr	93Nb	120Sn	178Hf	181Ta	182W	232Th
SP1 (clean, blue area)	0.38	49.6	117	0.92	BDL	431	35.4	0.13	0.54	10.6	0.01	0.04	0.15	0.05
SP2 (clean, blue area)	0.70	41.9	89.1	1.49	4.31	643	38.6	0.37	0.09	17.2	0.03	0.02	0.00	0.01
SP3 (clean, blue area)	0.15	33.9	58.5	1.41	4.94	573	35.7	0.15	0.02	8.88	0.02	0.01	0.00	0.00
SP4 (clean, blue area)	BDL	33.0	61.3	1.24	2.01	559	33.3	0.30	0.04	6.61	0.02	0.01	0.02	0.02
Average	**-**	**39.6**	**81.5**	**1.26**	**-**	**551**	**35.8**	**0.24**	**0.17**	**10.8**	**0.02**	**0.01**	**0.01**	**0.01**
Standard Deviation	**-**	**7.8**	**27.5**	**0.25**	**-**	**88**	**2.2**	**0.12**	**0.25**	**4.5**	**0.003**	**0.001**	**0.01**	**0.01**
Detection limit	*0.03*	*0.02*	*0.27*	*0.05*	*0.47*	*3.62*	*0.02*	*0.00*	*0.00*	*0.03*	*0.00*	*0.00*	*0.00*	*0.00*

3.2.2.3 TRACE ELEMENT COMPARISON BETWEEN BLUE SAPPHIRES FROM THE BAW MAR MINES AND OTHER METAMORPHIC SOURCES:

The data presented in Table 11 shows the chemical data results of Baw Mar samples from the Northern and Southern areas, analyzed within inclusion-free areas using LA-ICP-MS. Significant levels of Fe, Ti, Ga, Mg and V were found in the samples from both areas. Nil to insignificant levels of high field strength elements were detected in the samples. When samples from the two different zones are compared, relatively high Fe concentrations are present in Baw Mar North stones, while moderate to high Fe are present in stones from the Southern area (Table 11 and Figure 118). Mg and Ti concentrations were higher in the sapphires from the Southern part than those from the Northern part, while V and Ga concentrations were comparable from both areas.

Table 11: Chemical composition in ppma of Baw Mar blue sapphires within inclusion-free areas using LA-ICP-MS. Data reported in minimum and maximum values, with average and standard deviation in parentheses. 'BDL' stands for 'below detection limit'.

Element	Concentrations	
	Samples from Northern part, FE46 (36 samples, 267 spots)	Samples from Southern Part, FE75 (28 samples, 148 spots)
^{9}Be	BDL-1.5	BDL-8.4
^{24}Mg	6-29 *(10.7±3.9)*	9.6-102 *(52±24)*
^{47}Ti	6-77 *(18.9±8.0)*	6.8-112 *(45.7±26.8)*
^{51}V	BDL-2.4	0.4-2.2
^{53}Cr	BDL-7	BDL-13
^{57}Fe	1092-2118 *(1463±237)*	302-1179 *(548±219)*
^{69}Ga	17-37 *(26.3±3.8)*	4.9-39 *(23±8)*
^{90}Zr	BDL-0.07	BDL-0.4
^{93}Nb	BDL-0.1	BDL-2.1
^{120}Sn	BDL-2.7	BDL-17
^{178}Hf	BDL-0.02	BDL-0.004
^{181}Ta	BDL-0.002	BDL-0.78
^{182}W	BDL-0.2	BDL-9.4
^{232}Th	BDL-0.003	BDL-0.3

The Ga/Mg ratio can be used as a reliable method to help differentiate between magmatic and metamorphic blue sapphires [Peucat *et al*. 2007]. As can be seen in Figure 118, Ga/Mg ratios of the Baw Mar samples varied from 1.3 to 8.0 and 0.1 to 2.9 for Northern and Southern samples, respectively. Values under 10 indicate the samples in this study are of metamorphic origin. It is notable that the range of the Ga/Mg ratios of the Baw Mar samples in this study are vary slightly from the Baw Mar blue sapphires reported on by Kan-Nyunt *et al.* (2013) which stated their Baw Mar samples were of either magmatic or metamorphic origins (Ga/Mg ratios varied from 0.6 to 17).

In cases where no indicative inclusions exist in samples submitted for origin determination, the relationship between trace elements, such as V-Fe plot (Figure 118) and Fe-V-Mg plot (Figure 119) may be used to support other information in order to separate Baw Mar sapphires from other metamorphic blue sapphires, such as Sri Lankan and Madagascan stones, with overlapping properties. The ternary Fe-V-Mg plot (Figure 119) enables the samples studied to be separated of from Sri Lankan and Madagascan sapphires slightly better than when applying the V-Fe plot. However, Fe-V-Mg plotting produced partially overlapping data when trying to differentiate between stones from Ilakaka, Madagascar and Baw Mar samples from the Southern area.

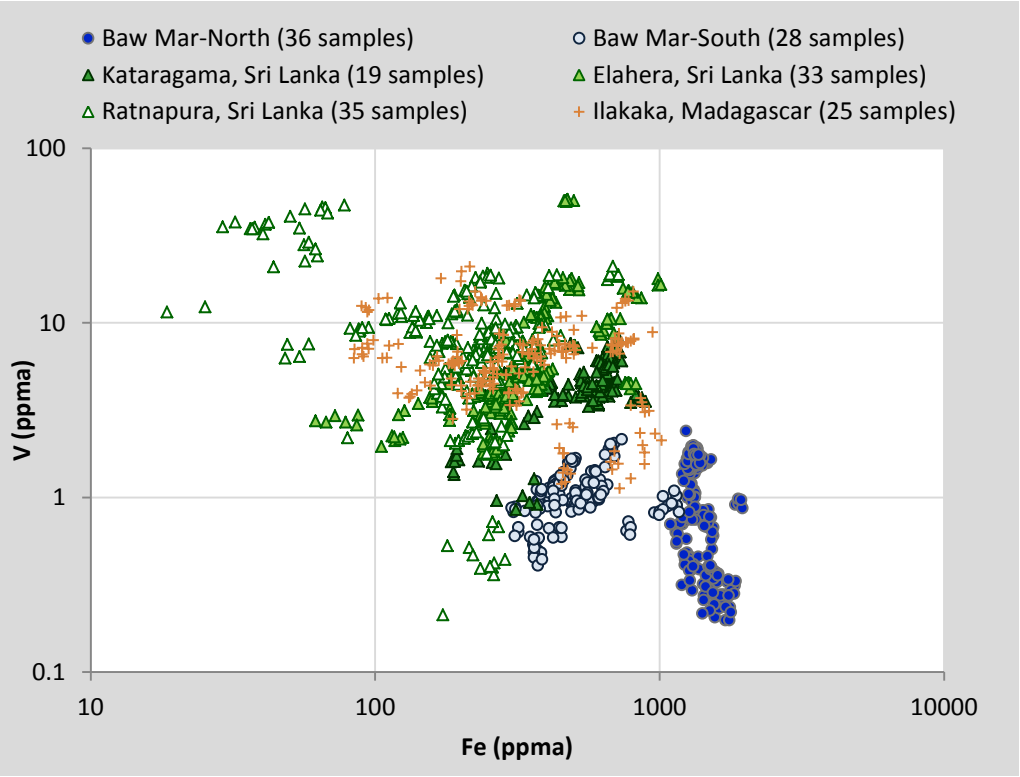

Figure 118: Population field of the elements V vs Fe from blue sapphires from the Southern and Northern areas of Baw Mar mine, Myanmar, compared to data from metamorphic blue sapphires obtained from deposits in Sri Lanka and Madagascar.

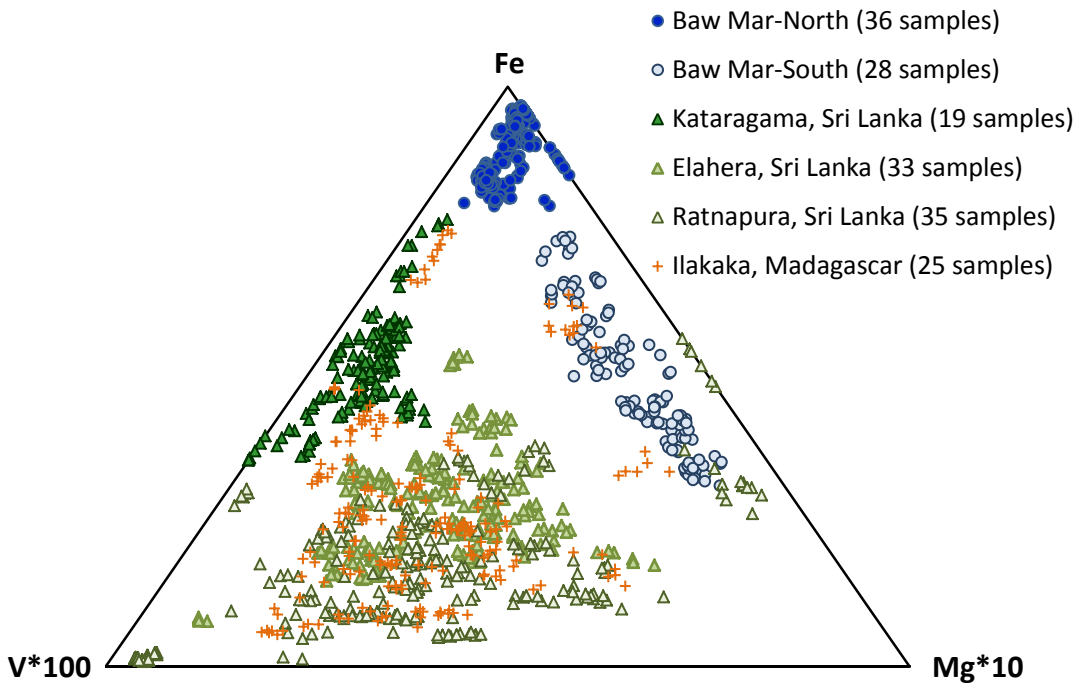

Figure 119: Fe-V-Mg ternary plot of blue sapphires from Baw Mar mine, Myanmar, when compared to data from metamorphic blue sapphires obtained from deposits in Sri Lanka and Madagascar.

3.2.3 FTIR SPECTROSCOPY

3.2.3.1 SAPPHIRES FROM THE NORTHERN AREA OF BAW MAR MINE (FE46):

FTIR spectra obtained from Baw Mar mine samples commonly showed diagnostic features, as listed in Table 12. The FTIR features obtained from the samples indicated the presence of numerous minerals including boehmite and diaspore, kaolinite (typically in association with boehmite features), and gibbsite, and a single weak peak 3309 cm^{-1}.

Table 12: FTIR features obtained from 36 Baw Mar (Northern area) mine samples examined in this study.

GIA Reference #	Orientation between polished wafer and IR beam path	FTIR features				
		Single 3309 cm^{-1}	Boehmite	Diaspore	Kaolinite	Gibbsite
159-N	unoriented	Y (weak)				
160-N	unoriented		Y			
161-N	unoriented		Y			
163-N	unoriented		Y		Y	

GIA Reference #	Orientation between polished wafer and IR beam path	FTIR features				
		Single 3309 cm^{-1}	Boehmite	Diaspore	Kaolinite	Gibbsite
165-N	unoriented	Y (very weak)				
166-N	unoriented	Y (weak)	Y			
168-N	unoriented			Y		
170-N	unoriented		Y		Y	
171-N	unoriented	Y (very weak)		Y		
172-N	unoriented		Y		Y	
173-N	unoriented	Y (very weak)				
174-N	unoriented	Y (very weak)	Y		Y	
175-N	unoriented		Y			
176-N	unoriented			Y		
177-N	perpendicular to c-axis		Y		Y	
178-N	unoriented	Y (very weak)				
179-N	unoriented		Y			
181-N	unoriented		Y			
183-N	unoriented		Y			Y
186-N	unoriented		Y			
188-N	unoriented		Y			
189-N	unoriented	Not diagnostic				
190-N	unoriented	Not diagnostic				
191-N	unoriented	Not diagnostic				
192-N	unoriented		Y		Y	
195-N	unoriented		Y			
200-N	unoriented		Y			
201-N	unoriented		Y		Y	
202-N	perpendicular to c-axis	Y (weak)				
203-N	perpendicular to c-axis	Y (weak)				
205-N	unoriented		Y		Y	
206-N	unoriented		Y		Y	

GIA Reference #	Orientation between polished wafer and IR beam path	FTIR features				
		Single 3309 cm^{-1}	Boehmite	Diaspore	Kaolinite	Gibbsite
207-N	unoriented	Y (weak)	Y			
208-N	unoriented	Y (very weak)				
210-N	unoriented	Y (very weak)				
213-N	unoriented	Y (very weak)	Y			

weak signal intensities: $0.03<\alpha<0.3$, very weak signal: $\alpha<0.03$

3.2.3.2 SAPPHIRES FROM THE SOUTHERN AREA OF BAW MAR MINE (FE 75):

Table 13 lists the FTIR features obtained from the samples from the Southern area of Baw Mar mine. The spectra revealed FTIR features commonly observed in the samples from the Northern area of the mine (Table 12) including boehmite and diaspore, kaolinite (typically in association with boehmite and/or diaspore), and a single weak peak at 3309 cm^{-1}. Interestingly, the samples from the Southern part of Baw Mar mine sometimes showed a single 3161 cm^{-1} peak, as previously observed in blue sapphires from Sri Lanka and Madagascar.

Table 13: FTIR features obtained from 28 Baw Mar (Southern part) mine samples examined in this study.

GIA Reference #	Orientation between polished wafer and IR beam path	FTIR features					
		Single 3309 cm^{-1}	Boehmite	Diaspore	Kaolinite	Gibbsite	Single 3161 cm^{-1}
711-S	unoriented				Y		
712-S	unoriented		Y		Y		
714-S	unoriented			Y	Y		
715-S	unoriented		Y		Y		
716-S	perpendicular to c-axis	Y (very weak)					
718-S	unoriented		Y		Y		
719-S	unoriented				Y		Y (weak)
720-S	unoriented				Y		
721-S	unoriented			Y	Y		Y (weak)
722-S	unoriented				Y		Y (very weak)
723-S	unoriented				Y		
725-S	unoriented		Y	Y	Y		
727-S	unoriented				Y		

GIA Reference #	Orientation between polished wafer and IR beam path	FTIR features					
		Single 3309 cm^{-1}	Boehmite	Diaspore	Kaolinite	Gibbsite	Single 3161 cm^{-1}
728-S	unoriented		Y				
739-S	unoriented			Y	Y		
741-S	perpendicular to c-axis	Y (weak)		Y	Y		
745-S	unoriented		Y	Y	Y		
746-S	unoriented		Y		Y		
749-S	unoriented		Y	Y	Y		
750-S	unoriented		Y		Y		
752-S	unoriented			Y	Y		
754-S	unoriented				Y		
755-S	unoriented		Y		Y		
756-S	unoriented			Y			
757-S	unoriented	Y (very weak)					Y (weak)
760-S	unoriented			Y	Y		
762-S	unoriented			Y			
763-S	perpendicular to c-axis	Not diagnostic					

weak signal intensities: $0.03<\alpha<0.3$, very weak signal: $\alpha<0.03$

PART IV. SUMMARY

In this study, the gemological and spectroscopic properties together with the chemistry, of blue sapphires from two different areas, Northern and Southern parts, of the Baw Mar mine were investigated. Although the samples came from the same mine, some of their properties differed. The samples also showed slightly different characteristics from those expected for classic Burmese blue sapphires.

In general, the samples from the Northern part possessed a medium to dark blue color, whereas those from Southern part were generally of a lighter tone. When exposed to long- and short-wave UV radiation, the samples from Northern part were inert, while those from the Southern part sometimes exhibited a very weak to weak orange zoned fluorescence. The samples from both zones hosted many common inclusions seen in classic Burmese blue sapphires as well Baw Mar blue sapphires as reported by Kan-Nyunt *et al*. (2013). In addition to the classical inclusions, Baw Maw sapphires from the Northern part frequently contained irregular brownish platelets of ilmenite, whereas the samples from the Southern part often hosted dense clouds of short rutile silk and euhedral tabular negative crystals surrounded by thin films.

UV-Vis-NIR spectra of the samples revealed typical features expected for metamorphic blue sapphires, including three Fe absorption peaks and an Fe^{2+}-Ti^{4+} absorption band. Their FTIR spectra typically revealed a single weak 3309 cm^{-1} peak and several absorption features, relating to minerals such as diaspore, boehmite, kaolinite, and gibbsite. Samples from the Southern area sometimes showed a single 3161 cm^{-1} peak in keeping with blue sapphires from Sri Lanka and Madagascar.

Trace element analysis using LA-ICP-MS showed relatively high Fe concentrations in Baw Maw blue sapphires from the Northern area, while moderate to high Fe concentrations were noted in samples from the Southern area. The Ga/Mg ratios varied from 1.3 to 8.0 and 0.1 to 2.9 for Baw Mar samples from the Northern and Southern areas, respectively. Fe-V-Mg ternary diagram plotting helped distinguish the Baw Mar sapphires from other metamorphic blue sapphires with overlapping properties, such as those from Sri Lanka and Madagascar.

Due to the diverse properties of the blue sapphires from the Baw Mar mine, as seen from this study and the work conducted by Kan-Nyunt *et al*. (2013), a large number of blue sapphires from various zones in the mine may be needed to obtain a complete overview of the properties of blue sapphires from the Baw Mar mine.

ACKNOWLEDGEMENTS: The authors would like to thank John Emmett, Sudarat Saeseaw and Nicholas Sturman for their valuable advices and comments, Sasithorn Engniwat for macrophotograph and Jonathan Muyal for sample fabrication. The authors are also grateful for the access to the Baw Mar mine and samples, provided by Baw Mar Gems Co,Ltd.

ABOUT THE AUTHORS: Dr. Wasura Soonthorntantikul (wsoontho@gia.edu) is a staff gemologist. Wim Vertriest (wvertrie@gia.edu) is field gemologist. Dr. Supharart Sangsawong is a research scientist. Victoria Liliane Raynaud-Flattot, Ungkhana Atikarnsakul, Charuwan Khowpong and Vararut Weeramonkhonlert are analysts, all are working in GIA's Bangkok laboratory. Vincent Pardieu is an independent, Bangkok-based gemologist.

PART V. BIBLIOGRAPHY

Dubinsky E.V. and Emmett J.L. (2013), "The colors of corundum" *Gem Guide* **32** (1): 1-11.

Emmett J.L., Scarratt K., McClure S.F., Moses T., Douhit T.R., Hughes R., Novak S., Shigley J.E., Wang W., Bordelon O., Kane R.E. (2003), "Beryllium diffusion of ruby and sapphire" *Gems and Gemology* **39** (2), pp. 84-135.

Ferguson J. and Fielding P. E. (1971), "The origins of the colours of yellow, green and blue sapphires." *Chemical Physics Letters* **10**(3): 262-265.

Ferguson J. and Fielding P. E. (1972), "The origins of the colours of natural yellow, blue, and green sapphires." *Australian Journal of Chemistry* **25**: 1371-1385.

Hughes R. W., Manorotkul W. and Hughes E.B. (2017), *Ruby and sapphire: a gemologist's guide*, 1st edition, RWH Publishing/Lotus Publishing, Thailand, pp. 134-135, 558-559 and 564-565.

Groat, L. A. (Ed.) (2014). *Geology of Gem Deposits* (Second edition ed. Vol. Short Course Series, Vol. 44). Québec: Mineralogical Association of Canada.

Gübelin E. J., and Koivula J. I. (2005). "Photoatlas of inclusions in Gemstones Volume 3", Opinio Publishers, Basel, Switzerland, 672 pp.

Kan-Nyunt H.-P., Karampelas S., Link K., Thu K., Kiefert L., Hardy P. (2013), "Blue sapphires from the Baw Mar mine in Mogok", *Gems and Gemology* **49** (4), pp. 223-232.

Kane E.R., Kammerling, R.C., "Status of Ruby and Sapphire mining in the Mogok Stone track", (1992) Gems & Gemology , Vol. 28, No3, pp.152-174

Kievlenko, E. Y. (2003). *Geology of Gems* (A. Soregaroli, Trans.). Vancouver: Ocean Pictures Ltd.

Krebs J. J. and Maisch W. G. (1971), "Exchange effects in the optical-absorption spectrum of Fe^{3+} in Al_2O_3." *Physical Review B* **4**(3): 757-769.

Lu R., Shen A. (2011), "Unusally High Beryllium in Three Blue Sapphires" *Gems & Gemology*, **47** (3), pp. 232-233.

Peucat J.J, Ruffault P., Fritsch E., Bouhnik-Le Coz M., Simonet C., Lasnier B. (2007), "Ga/Mg ratio as a new geochemical tool to differentiate magmatic from metamorphic blue sapphries" *Lithos*, **98**, pp. 261-274.

Saeseaw S. Weeramonkhonlert V., Khowpong C., Raynaud V. (2016) "Blue sapphires from Ilakaka, Madagascar". Unpublished manuscript.

Shen A., McClure S., Breeding M., Scarratt K., Wang W., Smith C., Shigley J. (2007), "From the GIA Laboratory: Beryllium in Corundum – The Consequences for Blue Sapphire" *GIA Insider*, **9** (2), Jan. 26.

Suthiyuth R., Khowpong C., Weeramonkhonlert V. (2016) "Blue sapphires from Ajith mine in Elahera, Sri Lanka" Unpublished manuscript.

Themelis T. (2008), *Gems and Mines of Mogok*, Thailand, pp. 98-105.

Pardieu V., Dubinsky E. V., Sangsawong S., Chauviré B. (2012), "Sapphire Rush Near Kataragama, Sri Lanka" GIA News from Research. www.gia.edu/gia-news-research-nr50212.

ANNEX A: ADDITIONAL BAW MAR BLUE SAPPHIRE SPECTRA AND CHEMISTRY DATA

BAW MAR SAPPHIRES FROM THE NORTHERN AREA (FE 46)

GIA REFERENCE NUMBER 100305165161-A-3 (161-N):

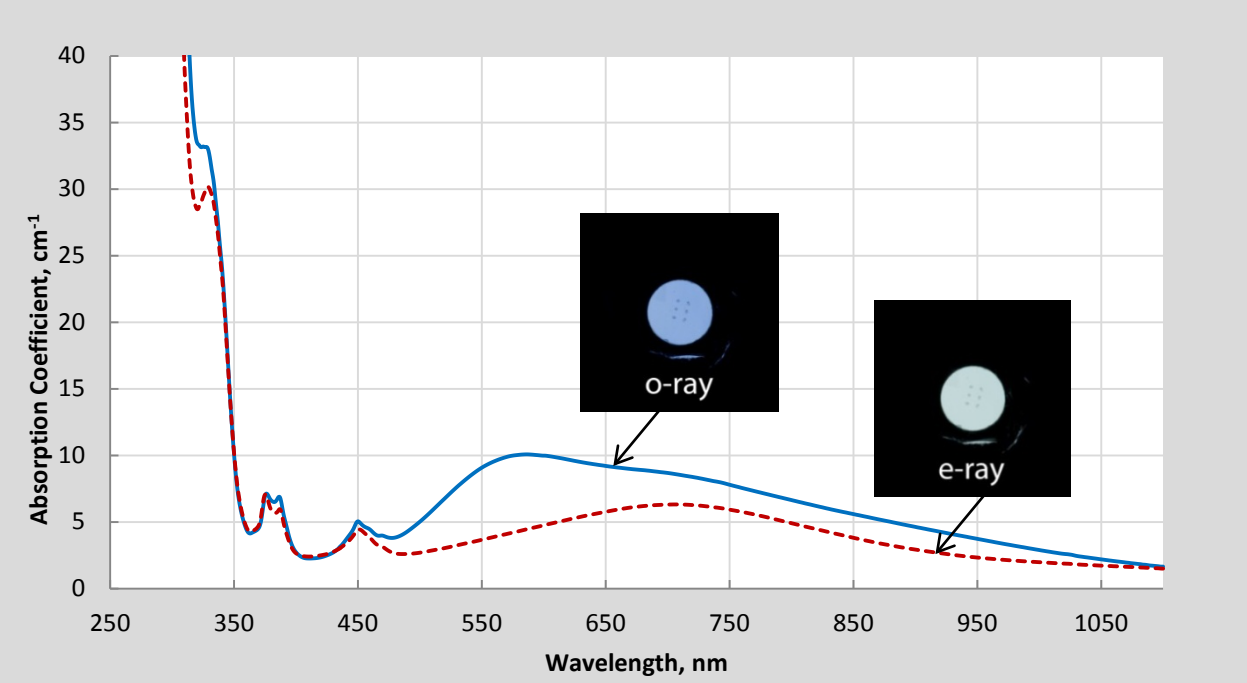

GIA Ref Sample 161-N
Hitachi U-2910 spectrophotometer
Wavelength resolution 1.5 nm
Wafer plane ‖ C-axis
Thickness 1.148 mm
α(max)= 28.5 cm^{-1}

Figure 120: UV-Vis-NIR spectra of sample 161-N with inset color calibrated polarized photos of the beam path area for the o- and e-rays. Optical path length 1.148 mm. Weight 0.340 carat. Color: Even blue.

Table 14: LA-ICP-MS results in ppma on GIA reference sample 161-N. 'BDL' stands for 'below detection limit' and 'BQL' for 'below quantification limit'

Sample 161-N Spot no.	Concentration in ppma																	
	9Be	24Mg	47Ti	51V	53Cr	57Fe	60Ni	69Ga	90Zr	93Nb	120Sn	139La	140Ce	178Hf	181Ta	182W	232Th	283U
SP1 (blue area)	BDL	8.64	15.2	BQL	BDL	1833	BQL	22.7	BDL	0.01	BDL	BQL	BDL	BDL	BDL	BDL	BDL	BDL
SP2 (blue area)	BDL	8.09	14.1	BDL	BQL	1749	BDL	23.1	BDL	0.01	BDL	BQL	BDL	BDL	BDL	BDL	BDL	BDL
SP3 (blue area)	BDL	7.42	13.2	BQL	BDL	1826	BDL	23.4	BDL	0.01	BDL	BQL	BDL	BDL	BDL	BDL	BDL	BDL
SP4 (blue area)	0.32	6.27	12.9	BQL	BDL	1745	BQL	24.3	BDL	0.01	BDL	BDL	BDL	BDL	BDL	BDL	BDL	BDL
SP5 (blue area)	BDL	6.70	13.5	BQL	BDL	1727	BDL	24.3	BDL	0.01	BDL	BQL	BDL	BDL	BDL	BDL	BDL	BDL
SP6 (blue area)	BDL	6.53	12.2	BQL	BDL	1749	BQL	23.9	BDL	0.01	BDL	BQL	BDL	BDL	BDL	BDL	BDL	BDL
SP7 (blue area)	BDL	7.67	13.7	BDL	BQL	1986	BDL	21.2	0.01	0.01	BDL	BDL	BDL	BDL	BDL	BDL	BDL	BDL
SP8 (blue area)	0.34	8.64	16.6	BQL	BDL	1844	BQL	21.2	BDL	BQL	BDL	BQL	BDL	BDL	BDL	BDL	BDL	BDL
SP9 (blue area)	0.34	11.2	18.6	BQL	BDL	1950	BQL	21.6	BDL	0.01	BDL	BQL	BDL	BDL	BDL	BDL	BDL	BDL
SP10 (blue area)	BDL	8.39	15.9	BQL	BDL	1986	BDL	22.1	BDL	0.01	BDL	BQL	BDL	BDL	BDL	BDL	BDL	BDL
SP11 (blue area)	BDL	9.06	19.6	BQL	BQL	1950	BQL	21.7	BDL	BQL	BDL	BQL	BDL	BDL	BDL	BDL	BDL	BDL
SP12 (blue area)	BDL	9.31	19.3	BQL	BQL	2037	BDL	21.4	0.01	0.01	BDL	BQL	BDL	BDL	BDL	BDL	BDL	BDL
Average	-	**8.16**	**15.4**	-	-	**1865**	-	**22.6**	-	-	-	-	-	-	-	-	-	-
SD	-	**1.39**	**2.6**	-	-	**112**	-	**1.2**	-	-	-	-	-	-	-	-	-	-
DL	*0.07*	*0.04*	*0.74*	*0.10*	*1.25*	*6.87*	*0.05*	*0.06*	*0.00*	*0.00*	*0.07*	*0.00*	*0.00*	*0.00*	*0.00*	*0.00*	*0.00*	*0.00*

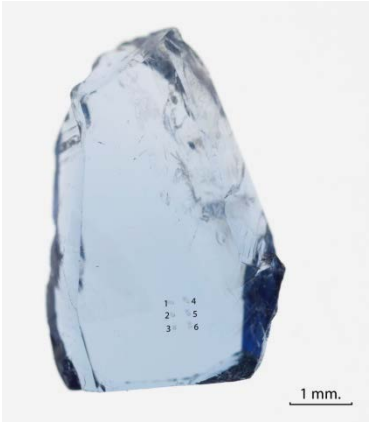

GIA REFERENCE NUMBER 100305165188-A-3 (188-N):

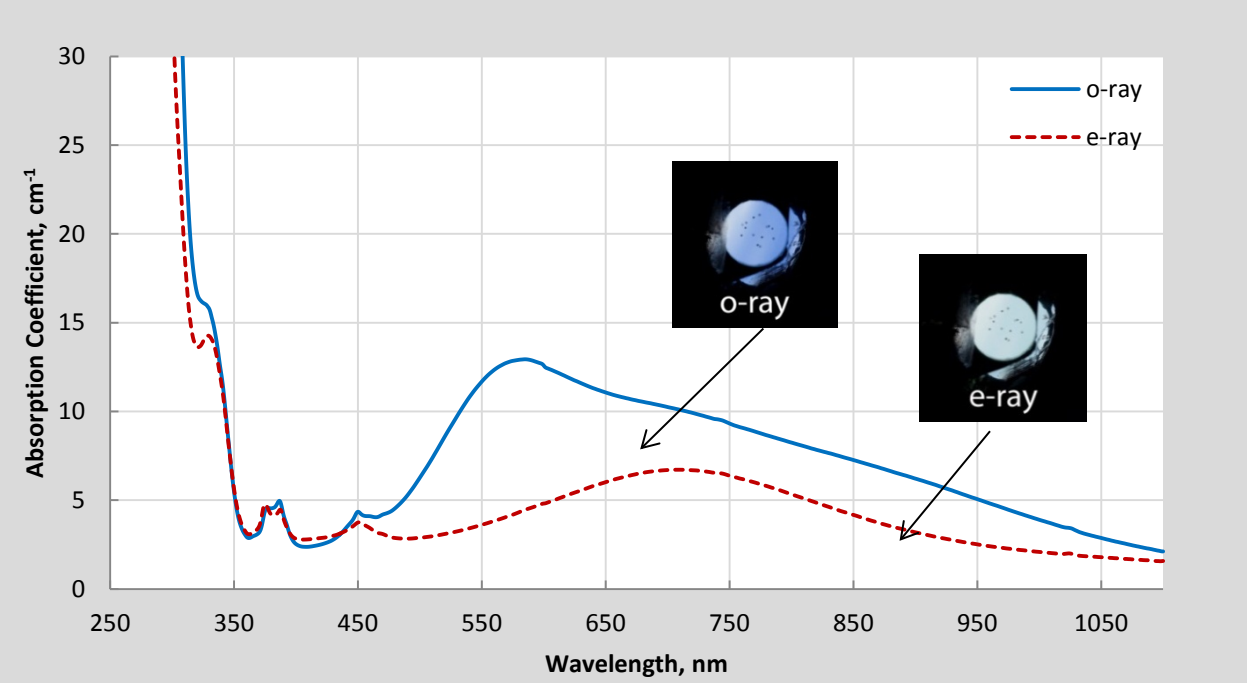

GIA Ref Sample 188-N
Hitachi U-2910 spectrophotometer
Wavelength resolution 1.5 nm
Wafer plane ‖ C-axis
Thickness 1.231mm
α(max)= 26.6 cm^{-1}

Figure 121: UV-Vis-NIR spectra of sample 188-N with inset color calibrated polarized photos of the beam path area for the o- and e-rays. Optical path length 1.231 mm. Weight 0.350 carat. Color: Blue and colorless.

Table 15: LA-ICP-MS results in ppma on GIA reference sample 188-N. 'BDL' stands for 'below detection limit' and 'BQL' for 'below quantification limit'

Sample 188-N Spot no.	Concentration in ppma																	
	9Be	24Mg	47Ti	51V	53Cr	57Fe	60Ni	69Ga	90Zr	93Nb	120Sn	139La	140Ce	178Hf	181Ta	182W	232Th	283U
SP1 (blue area)	BDL	11.2	17.7	1.81	BDL	1274	BDL	26.2	BQL	BDL	BDL	BDL	BDL	BDL	BQL	BDL	BDL	BDL
SP2 (blue area)	BDL	14.5	16.2	1.76	BQL	1413	BDL	27.3	BDL	BDL	BDL	BDL	BDL	BDL	BDL	BDL	BDL	BDL
SP3 (blue area)	BDL	14.6	20.3	1.84	BDL	1289	BDL	26.1	BDL	BDL	BDL	BDL	BDL	BDL	BDL	BDL	BDL	BDL
SP4 (blue area)	BDL	14.8	20.1	1.23	BDL	1293	BDL	26.2	BDL	BDL	BDL	BDL	BDL	BQL	BQL	BQL	0.00	BDL
SP5 (blue area)	BDL	13.8	17.1	1.74	BDL	1245	BDL	25.5	BDL	BDL	BDL	BDL	BDL	BQL	BDL	BDL	BDL	BDL
SP6 (blue area)	BDL	13.5	19.7	1.98	BDL	1384	BDL	27.2	BDL	BDL	BDL	BDL	BDL	BDL	BDL	BDL	BDL	BDL
SP7 (colorless)	BDL	15.9	14.2	1.30	BDL	1336	BDL	26.6	BDL	BDL	BDL	BDL	BQL	BDL	BDL	BDL	BDL	0.00
SP8 (colorless)	BDL	16.4	15.6	1.69	BDL	1234	BDL	25.0	BDL	BDL	BDL	BDL	BDL	BDL	BDL	BDL	BDL	BDL
SP9 (colorless)	BQL	17.3	11.6	1.70	BDL	1274	BDL	24.8	BQL	BDL	BDL	BDL	BDL	BDL	BDL	BQL	BDL	BDL
SP13 (blue area)	BQL	14.5	19.0	1.87	BDL	1293	BDL	26.4	BDL	BDL	BQL	BDL	BDL	BDL	BDL	BDL	BDL	BDL
SP14 (blue area)	BDL	15.2	22.7	2.07	BDL	1303	BDL	25.7	BDL	BQL	BDL	BQL	BDL	BDL	BDL	BDL	BDL	BDL
SP15 (blue area)	BDL	13.3	16.1	1.62	BQL	1274	BDL	25.5	BDL	BDL	BQL	BDL	BDL	BDL	BDL	BQL	BDL	BDL
SP16 (blue area)	BDL	14.1	13.9	1.45	BDL	1293	BDL	24.9	BDL	BQL	BDL	BDL	BDL	BQL	BDL	BQL	BDL	BDL
SP17 (blue area)	BDL	13.0	19.8	2.18	BDL	1311	BDL	24.4	BDL	BDL	BDL	BDL	BDL	BQL	BDL	BQL	BDL	BDL
SP18 (blue area)	BDL	12.1	17.3	1.86	BQL	1373	BDL	26.9	BDL	BDL	BQL	BQL	BDL	BDL	BDL	BDL	BDL	BDL
Average	-	**14.5**	**17.2**	**1.74**	-	**1302**	-	**25.8**	-	-	-	-	-	-	-	-	-	-
SD	-	**1.5**	**2.8**	**0.25**	-	**53**	-	**0.8**	-	-	-	-	-	-	-	-	-	-
DL	*0.21*	*0.11*	*1.34*	*0.27*	*2.10*	*7.20*	*0.19*	*0.14*	*0.02*	*0.02*	*0.03*	*0.00*	*0.00*	*0.00*	*0.00*	*0.00*	*0.00*	*0.00*

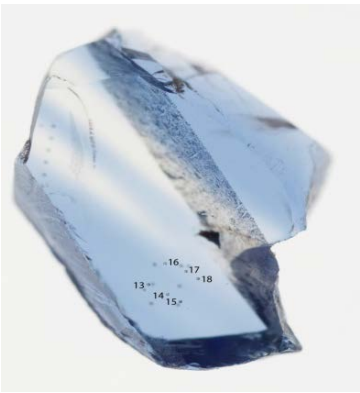

GIA REFERENCE NUMBER 100305165190-A-3 (190-N):

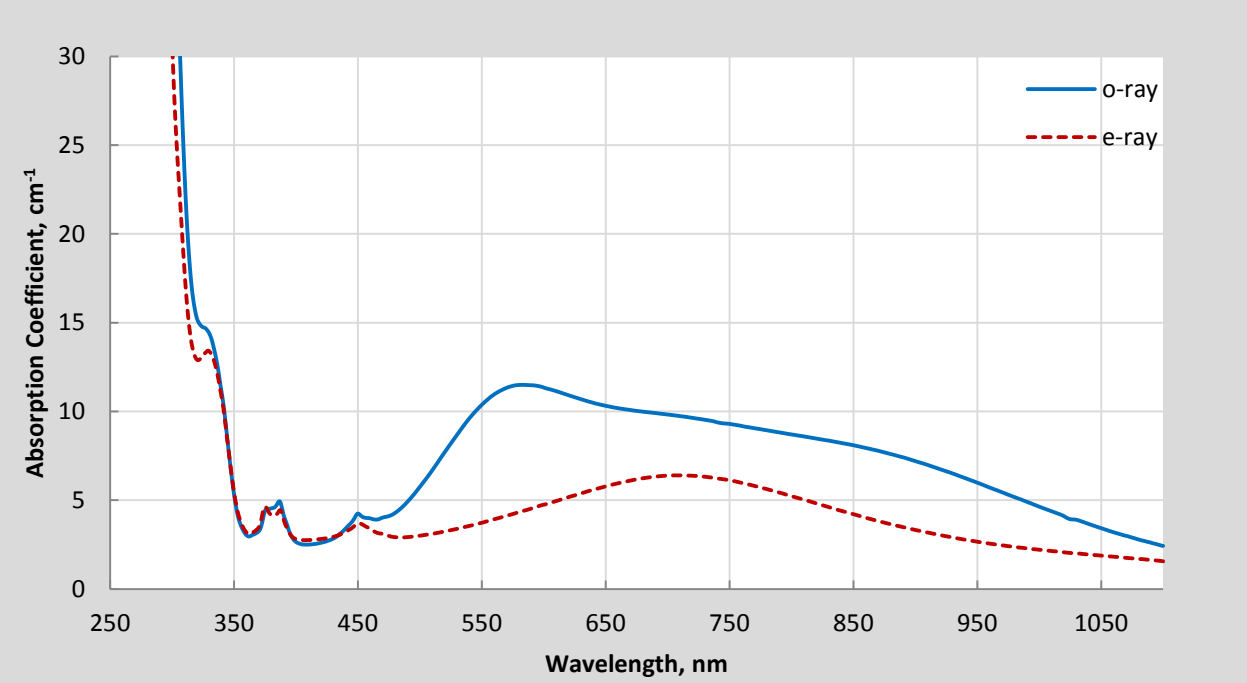

GIA Ref Sample 190-N
Hitachi U-2910 spectrophotometer
Wavelength resolution 1.5 nm
Wafer plane || C-axis
Thickness 1.008 mm
α(max)= 32.4 cm^{-1}

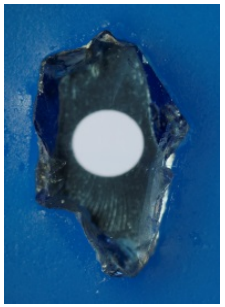

Figure 122: UV-Vis-NIR spectra of sample 190-N. Optical path length 1.008 mm. Weight 0.227 carat. Color: Even blue.

Table 16 LA-ICP-MS results in ppma on GIA reference sample 190-N. 'BDL' stands for 'below detection limit' and 'BQL' for 'below quantification limit'

Sample 190-N Spot no.	Concentration in ppma																	
	9Be	24Mg	47Ti	51V	53Cr	57Fe	60Ni	69Ga	90Zr	93Nb	120Sn	139La	140Ce	178Hf	181Ta	182W	232Th	283U
SP1 (blue area)	BDL	8.16	9.92	1.71	BDL	1362	BDL	26.8	BDL	BDL	BDL	BDL	BQL	BDL	BDL	BDL	BDL	BDL
SP2 (blue area)	1.45	7.81	12.3	1.78	BDL	1238	BDL	27.0	BDL	BDL	BDL	BDL	BDL	BDL	BDL	BQL	BDL	BDL
SP3 (blue area)	BQL	7.33	11.1	1.90	BDL	1260	BDL	25.6	BDL	BDL	BDL	BDL	BDL	BDL	BDL	BDL	BDL	BDL
SP4 (blue area)	BDL	8.64	11.2	1.70	BDL	1300	BDL	26.5	BDL	BDL	BDL	BDL	BDL	BDL	BDL	BDL	BDL	BDL
SP5 (blue area)	BDL	8.37	11.0	1.43	BDL	1289	BDL	27.3	BDL	BDL	BDL	BDL	BDL	BDL	BDL	BDL	BDL	BDL
SP6 (blue area)	BQL	7.40	11.7	1.91	BDL	1314	BDL	26.0	BDL	BDL	BDL	BDL	BDL	BDL	BDL	BDL	BDL	BDL
SP7 (blue area)	BDL	8.72	6.01	1.91	BDL	1249	BDL	26.4	BDL	BDL	BDL	BDL	BQL	BQL	BDL	BDL	0.00	BDL
SP8 (blue area)	BQL	8.36	11.5	1.42	BDL	1289	BDL	26.4	BDL	BDL	BDL	BDL	BDL	BDL	BDL	BQL	BDL	BDL
SP9 (blue area)	BQL	7.28	9.92	1.14	BDL	1150	BDL	22.2	BDL	BDL	BDL	BDL	BDL	BDL	BDL	BDL	BDL	BDL
SP10 (blue area)	BDL	8.25	12.8	1.85	BDL	1333	BDL	27.3	BDL	BDL	BDL	BDL	BQL	BDL	BDL	BDL	BDL	BDL
SP11 (blue area)	BDL	8.30	18.1	1.79	BDL	1340	BDL	26.1	BDL	BDL	BDL	BDL	BDL	BDL	BDL	BDL	BDL	0.00
SP12 (blue area)	BDL	8.72	12.2	1.49	BDL	1220	BDL	25.0	BDL	BQL	BDL	BDL	BDL	BQL	BDL	BDL	0.00	BDL
Average	-	**8.11**	**11.5**	**1.67**	-	**1279**	-	**26.1**	-	-	-	-	-	-	-	-	-	-
SD	-	**0.53**	**2.7**	**0.25**	-	**59**	-	**1.4**	-	-	-	-	-	-	-	-	-	-
DL	*0.21*	*0.11*	*1.34*	*0.27*	*2.10*	*7.20*	*0.19*	*0.14*	*0.02*	*0.02*	*0.03*	*0.00*	*0.00*	*0.00*	*0.00*	*0.00*	*0.00*	*0.00*

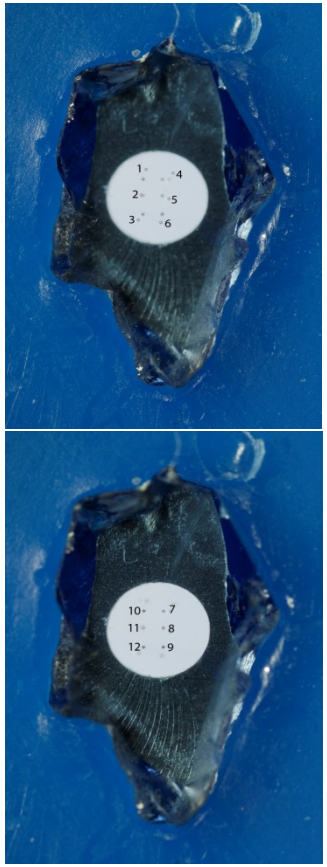

GIA REFERENCE NUMBER 100305165202-A-3 (202-N):

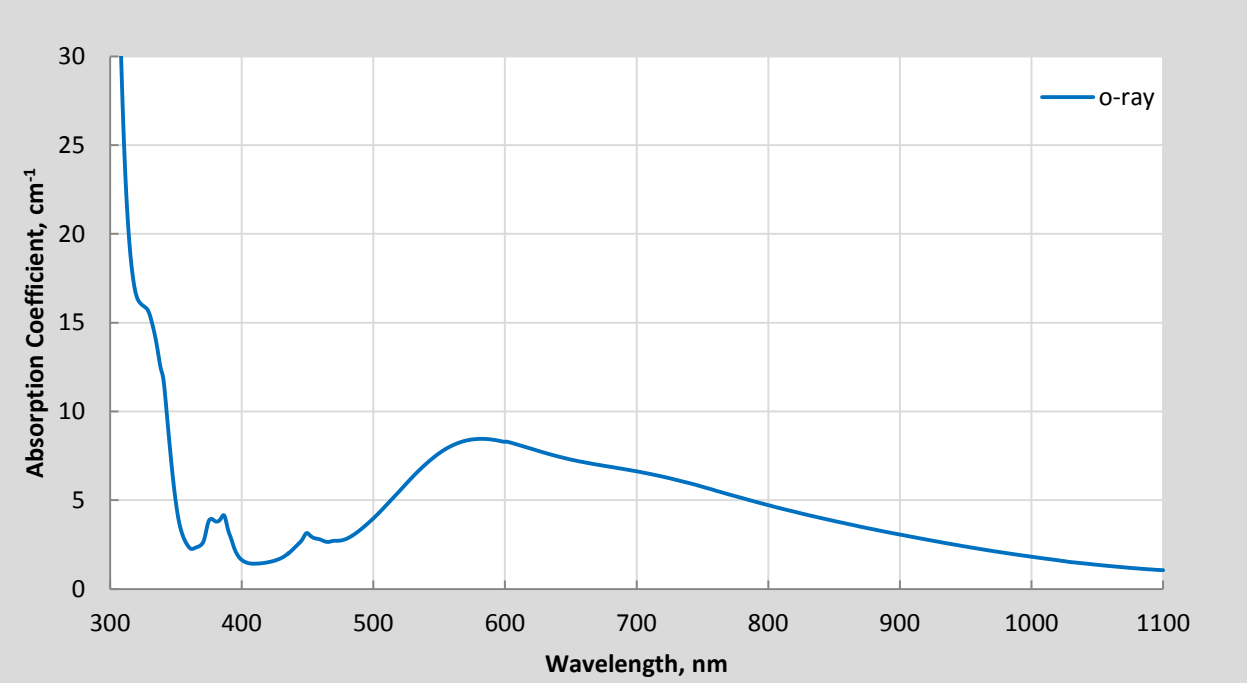

GIA Ref Sample 202-N
Hitachi U-2910 spectrophotometer
Wavelength resolution 1.5 nm
Wafer plane ⊥ C-axis
Thickness 0.899 mm
α(max)= 36.4 cm^{-1}

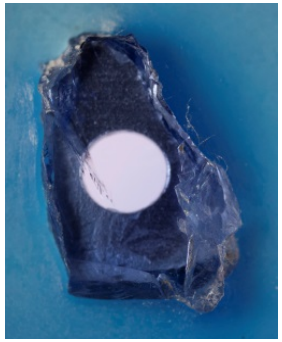

Figure 123: UV-Vis-NIR spectrum of sample 202-N. Optical path length 0.899 mm. Weight 0.277 carat. Color: Even blue.

Table 17 LA-ICP-MS results in ppma on GIA reference sample 202-N. 'BDL' stands for 'below detection limit' and 'BQL' for 'below quantification limit'

Sample 202-N Spot no.	Concentration in ppma																	
	9Be	24Mg	47Ti	51V	53Cr	57Fe	60Ni	69Ga	90Zr	93Nb	120Sn	139La	140Ce	178Hf	181Ta	182W	232Th	283U
SP1 (blue area)	BDL	11.3	14.7	0.45	BDL	1245	BDL	26.4	BDL	BDL	BDL	BDL	BDL	BDL	BQL	BQL	BDL	BDL
SP2 (blue area)	BQL	11.6	15.4	0.41	BQL	1230	BDL	26.8	BDL	BDL	BDL	BQL	BDL	BQL	BQL	BDL	BDL	BDL
SP3 (blue area)	BDL	11.2	14.5	0.42	BQL	1278	BDL	27.0	BDL	BDL	BDL	BDL	BDL	BDL	BDL	BDL	BDL	BDL
SP4 (blue area)	BDL	11.7	14.3	0.42	BQL	1263	BDL	27.9	BDL	BDL	BDL	BQL	BDL	BDL	BDL	BDL	BDL	BDL
SP5 (blue area)	BDL	11.2	15.6	0.54	BDL	1241	BDL	26.7	BDL	BDL	BDL	BQL	BDL	BDL	BQL	BDL	BDL	BDL
SP6 (blue area)	BDL	11.7	15.1	0.39	BQL	1303	BDL	28.4	BDL	BDL	BDL	BDL	BDL	BDL	BQL	BDL	BDL	BDL
SP7 (blue area)	BQL	11.5	14.4	0.35	BQL	1282	BDL	26.6	BQL	BDL	BDL	BQL	BDL	BDL	BDL	BDL	BDL	BDL
SP8 (blue area)	BQL	11.5	16.3	0.42	BDL	1366	BDL	29.5	BDL	BDL	BDL	BDL	BDL	BDL	BQL	BDL	BDL	BDL
SP9 (blue area)	BDL	11.6	16.4	0.38	BQL	1314	BDL	28.4	BQL	BDL	BDL	BDL	BDL	BDL	BDL	0.00	BDL	BDL
SP10 (blue area)	BQL	11.4	14.5	0.40	BQL	1267	BDL	26.3	BDL	BDL	BDL	BQL	BDL	BDL	BDL	BDL	BDL	BDL
SP11 (blue area)	BDL	11.5	15.5	0.38	BDL	1223	BDL	26.6	BDL	BDL	BQL	BDL	BDL	BDL	BQL	BDL	BDL	BDL
SP12 (blue area)	BDL	11.9	17.4	0.44	BQL	1220	BDL	25.2	BDL	BDL	BQL	BDL	BDL	BDL	BQL	BDL	BDL	BDL
Average	-	**11.5**	**15.3**	**0.42**	-	**1269**	-	**27.1**	-	-	-	-	-	-	-	-	-	-
SD	-	**0.2**	**1.0**	**0.05**	-	**43**	-	**1.2**	-	-	-	-	-	-	-	-	-	-
DL	*0.10*	*0.08*	*0.30*	*0.04*	*0.33*	*2.89*	*0.02*	*0.01*	*0.00*	*0.00*	*0.01*	*0.00*	*0.00*	*0.00*	*0.00*	*0.00*	*0.00*	*0.00*

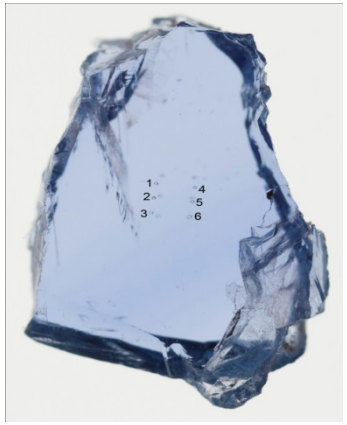

GIA REFERENCE NUMBER 100305165203-A-3 (203-N):

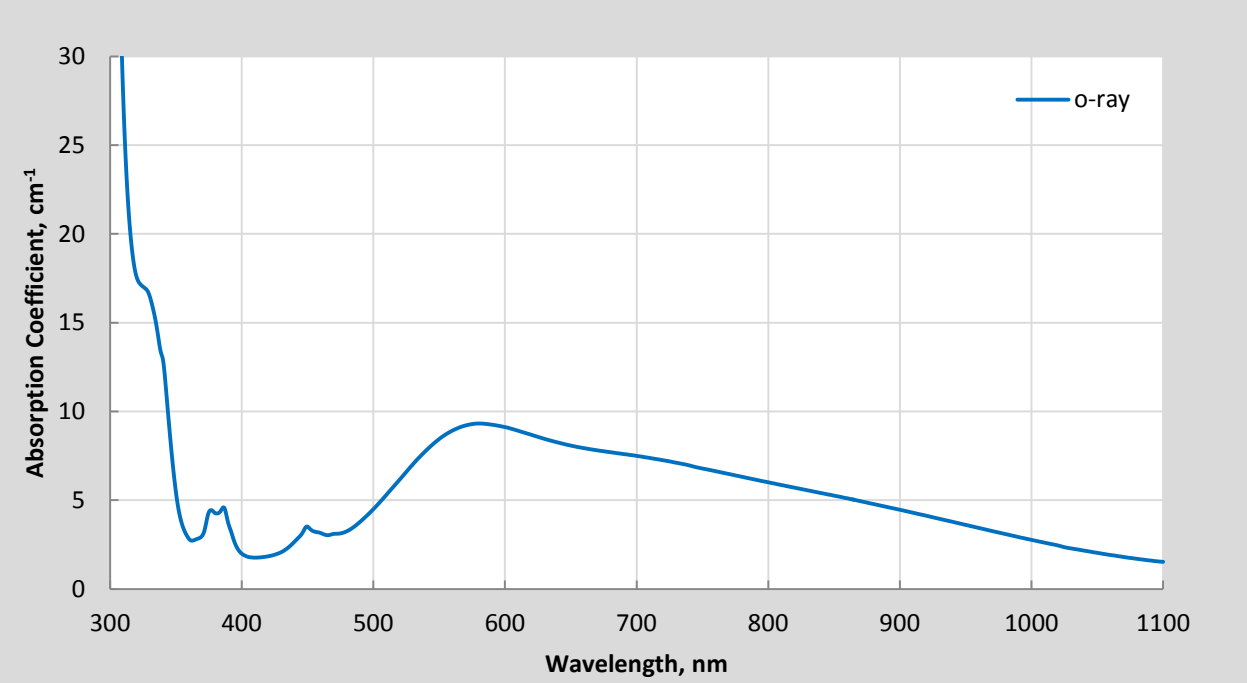

GIA Ref Sample 203-N
Hitachi U-2910 spectrophotometer
Wavelength resolution 1.5 nm
Wafer plane ⊥ C-axis
Thickness 0.836 mm
α(max) = 39.1cm^{-1}

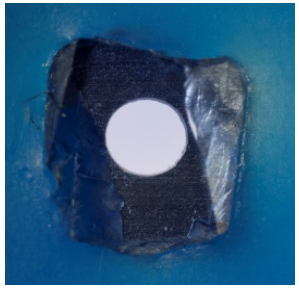

Figure 124: UV-Vis-NIR spectrum of sample 203-N. Optical path length 0.836 mm. Weight 0.183 carat. Color: Even blue.

Table 18 LA-ICP-MS results in ppma on GIA reference sample 203-N. 'BDL' stands for 'below detection limit' and 'BQL' for 'below quantification limit'

Sample 203-N Spot no.	Concentration in ppma																	
	9Be	24Mg	47Ti	51V	53Cr	57Fe	60Ni	69Ga	90Zr	93Nb	120Sn	139La	140Ce	178Hf	181Ta	182W	232Th	283U
SP1 (blue area)	BDL	7.31	14.82	0.81	BQL	1428	BDL	34.8	0.00	BDL	BDL	BDL	BDL	BDL	BDL	BDL	BDL	BDL
SP2 (blue area)	0.21	8.11	11.54	0.66	3.03	1431	BDL	34.8	BDL	BDL	BDL	BDL	BDL	BDL	BDL	BDL	BDL	BDL
SP3 (blue area)	0.21	7.93	12.27	0.75	BQL	1435	BDL	34.8	BDL	BDL	BDL	BDL	BDL	BDL	0.00	BDL	BDL	BDL
SP4 (blue area)	BDL	7.73	16.82	0.68	BQL	1482	BDL	34.5	BDL	BDL	BDL	BDL	BDL	BDL	BDL	BDL	BDL	BDL
SP5 (blue area)	BDL	7.26	14.95	0.74	2.06	1504	BQL	34.8	BDL	BDL	BDL	BDL	BDL	BDL	BDL	BDL	BDL	BDL
SP6 (blue area)	BDL	7.81	12.95	0.65	1.89	1442	BQL	33.3	0.00	BDL	BDL	BDL	0.00	BDL	BDL	BDL	BDL	BDL
SP7 (blue area)	BQL	10.23	12.56	0.74	BQL	1340	BDL	31.3	BDL	BDL	BDL	BDL	BDL	BDL	BDL	BDL	BDL	BDL
SP8 (blue area)	0.48	11.83	13.97	0.75	1.59	1285	BQL	31.6	BDL	BDL	BDL	BQL	BDL	BDL	BDL	BDL	BDL	BDL
SP9 (blue area)	BQL	20.72	19.93	0.77	1.53	1209	BQL	33.1	0.01	0.01	BDL	BDL	BDL	0.00	0.00	0.00	0.00	0.00
SP10 (blue area)	BQL	9.90	13.37	0.75	1.93	1307	BQL	33.1	BDL	BDL	BDL	BDL	BDL	BDL	BDL	BDL	BDL	0.00
SP11 (blue area)	0.29	12.33	14.86	0.88	BQL	1336	BQL	33.6	BDL	BDL	BDL	BDL	BDL	BDL	BDL	BDL	BDL	0.00
SP12 (blue area)	0.29	20.30	20.78	0.85	BQL	1278	BQL	33.1	0.00	0.00	BDL	BQL	BQL	BDL	BDL	BDL	0.00	0.00
Average	-	**11.0**	**14.9**	**0.75**	-	**1373**	-	**33.6**	-	-	-	-	-	-	-	-	-	-
SD	-	**4.8**	**2.9**	**0.07**	-	**93**	-	**1.2**	-	-	-	-	-	-	-	-	-	-
DL	*0.05*	*0.05*	*0.22*	*0.04*	*0.60*	*3.18*	*0.02*	*0.02*	*0.00*	*0.00*	*0.04*	*0.00*	*0.00*	*0.00*	*0.00*	*0.00*	*0.00*	*0.00*

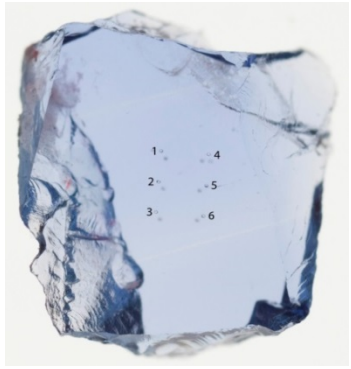

GIA REFERENCE NUMBER 100318470716-A-3 (716-S):

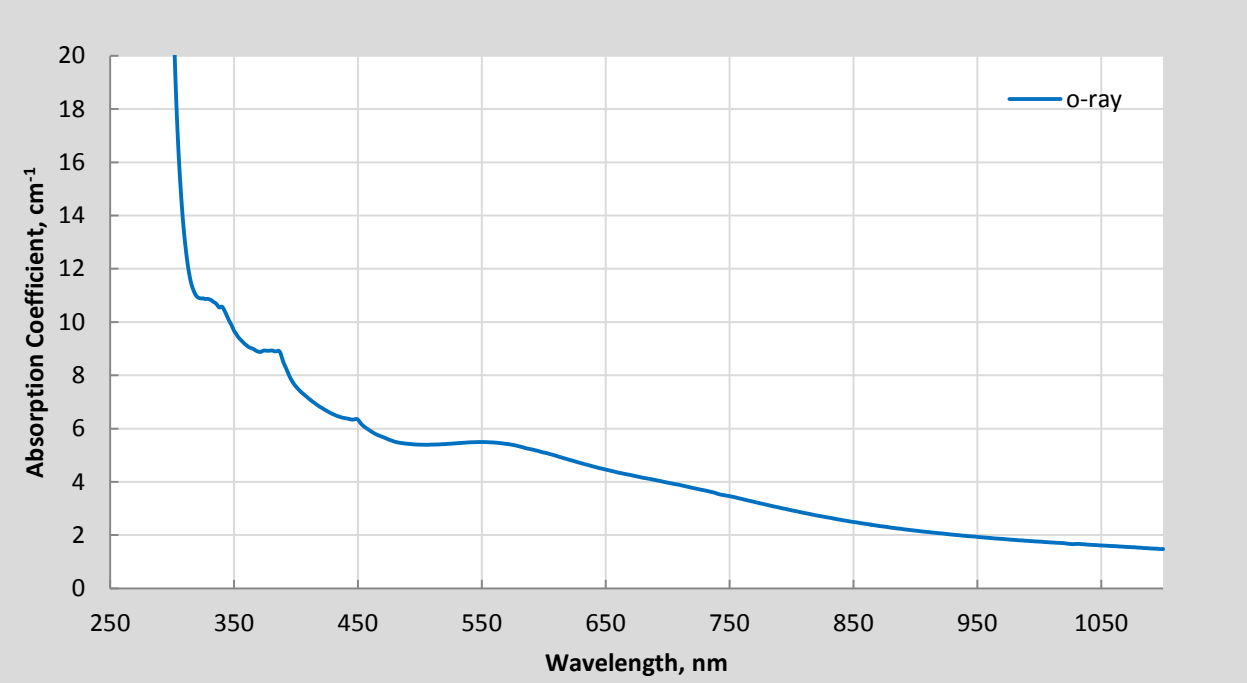

GIA Ref Sample 716-S
Hitachi U-2910 spectrophotometer
Wavelength resolution 1.5 nm
Wafer plane ⊥ C-axis
Thickness 0.696 mm
α(max) = 52.5 cm^{-1}

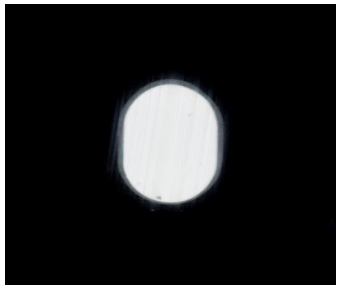

Figure 125: UV-Vis-NIR spectrum of sample 716-S with inset color calibrated polarized photo of the beam path area for the o-ray. Optical path length 0.696 mm. Weight 0.666 carat. Color: Light blue.

Table 19: LA-ICP-MS results in ppma on GIA reference sample 716-S. 'BDL' stands for 'below detection limit' and 'BQL' for 'below quantification limit'

Sample 716-S Spot no.	concentration in ppma																	
	9Be	24Mg	47Ti	51V	53Cr	57Fe	60Ni	69Ga	90Zr	93Nb	120Sn	139La	140Ce	178Hf	181Ta	182W	232Th	283U
SP1 (light blue+particles)	BDL	87.2	92.4	1.59	BDL	478	BDL	33.3	0.00	BDL	BDL	BDL	BDL	BDL	0.00	BDL	0.00	BDL
SP2 (light blue+particles)	BDL	90.6	96.3	1.34	BDL	475	BDL	33.3	0.00	BDL	BDL	0.00	BDL	BDL	0.00	BDL	0.00	BDL
SP3 (light blue+particles)	0.63	93.1	92.0	1.67	BDL	511	BDL	34.5	0.00	BDL	BQL	BDL	BDL	BDL	0.00	BQL	0.00	0.00
SP4 (light blue+particles)	BDL	90.6	95.0	1.61	BDL	482	BDL	33.6	0.00	BDL	BDL	BDL	BDL	BDL	BDL	BDL	0.00	BDL
SP5 (light blue+particles)	BDL	89.8	83.5	1.47	BDL	486	BDL	33.6	BDL	BDL	BDL	BDL	0.00	BDL	BDL	BDL	BDL	BDL
SP6 (light blue+particles)	0.75	89.8	87.7	1.61	BDL	504	BDL	34.2	0.00	BDL	BDL	BDL	BDL	BDL	BDL	BDL	0.00	BDL
SP7 (light blue+particles)	BDL	96.5	103	1.60	BDL	497	BDL	33.6	0.01	BDL	BDL	BDL	0.00	0.00	0.00	BDL	BDL	BDL
SP8 (light blue+particles)	0.36	96.5	103	1.67	BDL	489	BDL	33.9	0.01	BDL	BDL	BDL	BDL	0.00	0.00	BDL	BDL	BDL
Average	-	**91.8**	**94.1**	**1.57**	-	**490**	-	**33.8**	-	-	-	-	-	-	-	-	-	-
SD	-	**3.3**	**6.8**	**0.11**	-	**13**	-	**0.4**	-	-	-	-	-	-	-	-	-	-
DL	*0.03*	*0.02*	*0.27*	*0.05*	*0.47*	*3.62*	*0.02*	*0.02*	*0.00*	*0.00*	*0.00*	*0.00*	*0.00*	*0.00*	*0.00*	*0.00*	*0.00*	*0.00*

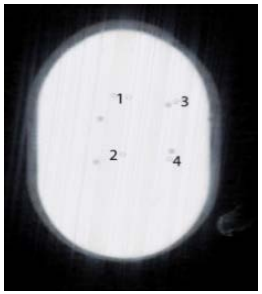

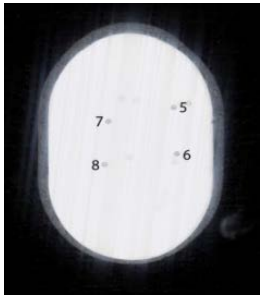

GIA REFERENCE NUMBER 100318470741-A-3 (741-S):

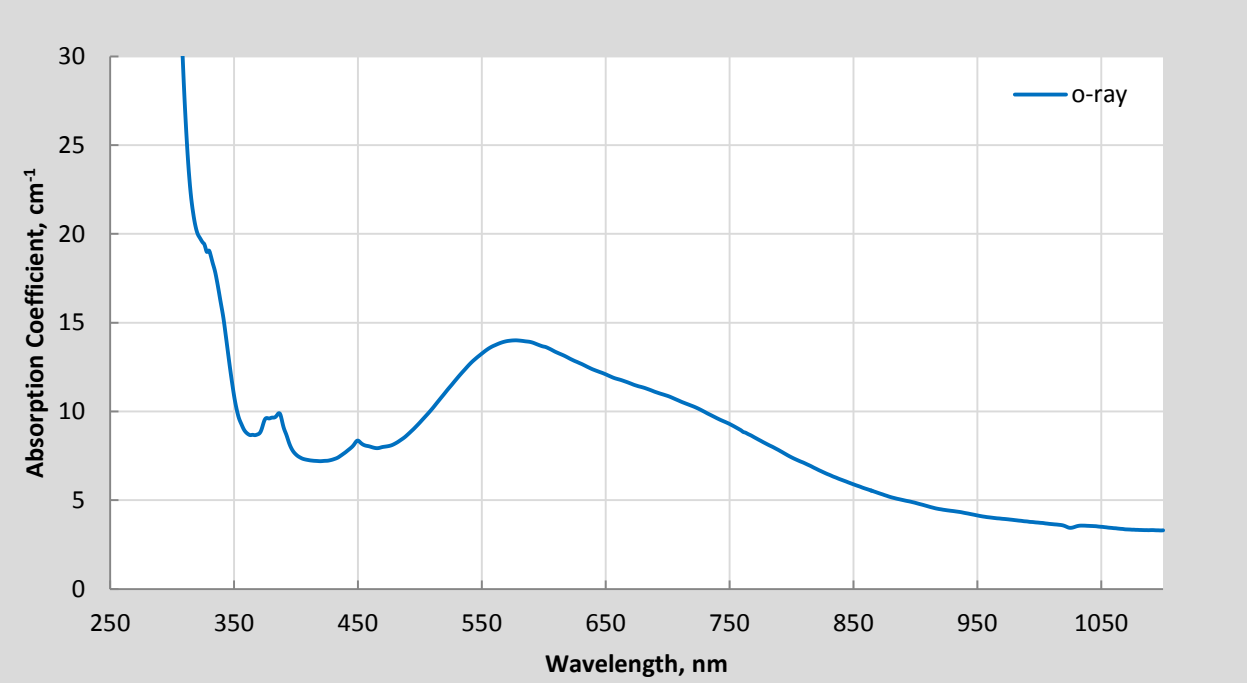

GIA Ref Sample 741-S
Hitachi U-2910 spectrophotometer
Wavelength resolution 1.5 nm
Wafer plane ⊥ C-axis
Thickness 0.666 mm
α(max) = 49.1 cm^{-1}

Figure 126: UV-Vis-NIR spectrum of sample 741-S with inset color calibrated polarized photo of the beam path area for the o-ray. Optical path length 0.666 mm. Weight 0.263 carat. Color: Light blue.

Table 20: LA-ICP-MS results in ppma on GIA reference sample 741-S. 'BDL' stands for 'below detection limit' and 'BQL' for 'below quantification limit'

Sample 741-S Spot no.	Concentration in ppma																	
	9Be	24Mg	47Ti	51V	53Cr	57Fe	60Ni	69Ga	90Zr	93Nb	120Sn	139La	140Ce	178Hf	181Ta	182W	232Th	283U
SP1 (blue area)	BDL	36.2	44.3	0.90	BDL	1154	BDL	32.2	BDL	BDL	BDL	BDL	BDL	BDL	BDL	0.00	BDL	BDL
SP2 (blue area)	0.43	38.4	42.5	1.02	BDL	1150	BDL	32.8	BDL	BDL	BDL	BDL	BDL	BDL	BDL	BDL	BDL	BDL
SP3 (blue area)	0.34	38.5	43.0	1.09	BDL	1128	BDL	32.2	BDL	BDL	BDL	BDL	BDL	BDL	BDL	BDL	BDL	BDL
SP4 (blue area)	BDL	36.4	45.1	0.82	BDL	1172	BDL	33.1	BDL	BDL	BQL	BDL	BDL	BDL	BDL	BDL	BDL	BDL
SP5 (blue area)	BDL	37.4	43.4	0.91	BDL	1110	BDL	31.3	BDL	BDL	BDL	BDL	BDL	BDL	BDL	BDL	BDL	BDL
SP6 (blue area)	0.18	30.3	37.5	1.02	BDL	1030	BDL	29.5	BDL	BDL	BDL	BDL	BDL	0.00	BDL	BDL	BDL	BDL
SP7 (blue area)	BDL	31.8	47.3	0.89	BDL	1066	BDL	31.0	BDL	BDL	BDL	BDL	BDL	BDL	BDL	BDL	BDL	BDL
SP8 (blue area)	BDL	34.2	40.9	0.92	BDL	1103	BDL	31.3	0.00	BDL	BDL	BDL	0.00	BDL	BDL	BDL	BDL	BDL
Average	-	**35.4**	**43.0**	**0.95**	-	**1114**	-	**31.7**	-	-	-	-	-	-	-	-	-	-
SD	-	**3.0**	**2.9**	**0.09**	-	**48**	-	**1.1**	-	-	-	-	-	-	-	-	-	-
DL	*0.03*	*0.02*	*0.27*	*0.05*	*0.47*	*3.62*	*0.02*	*0.02*	*0.00*	*0.00*	*0.03*	*0.00*	*0.00*	*0.00*	*0.00*	*0.00*	*0.00*	*0.00*

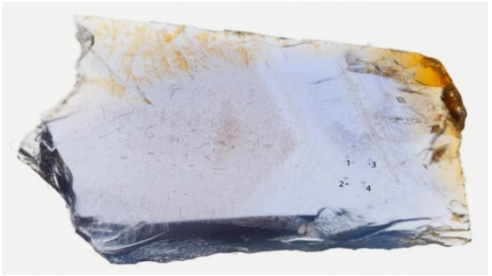

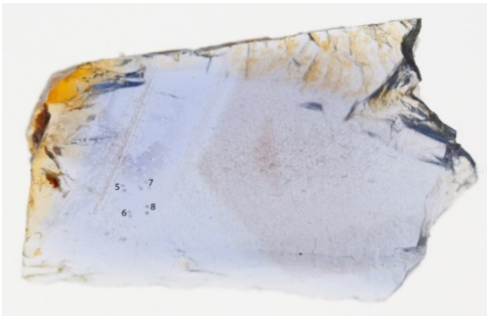

GIA REFERENCE NUMBER 100318470763-A-3 (763-S):

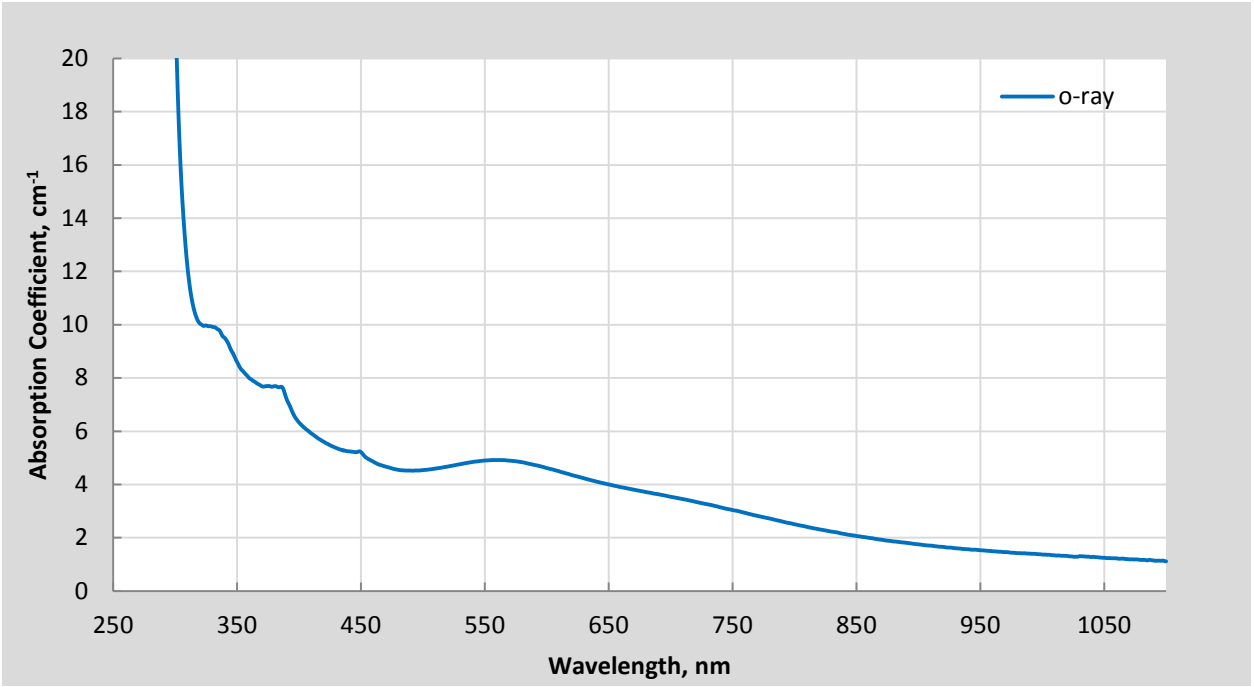

GIA Ref Sample 763-S
Hitachi U-2910 spectrophotometer
Wavelength resolution 1.5 nm
Wafer plane ⊥ C-axis
Thickness 0.405 mm
α(max) = 80.7 cm^{-1}

Figure 127: UV-Vis-NIR spectrum of sample 763-S with inset color calibrated polarized photo of the beam path area for the o-ray. Optical path length 0.405 mm. Weight 0.096 carat. Color: Very light blue.

Table 21: LA-ICP-MS results in ppma on GIA reference sample 763-S. 'BDL' stands for 'below detection limit' and 'BQL' for 'below quantification limit'

Sample 763-S Spot no.	Concentration in ppma																	
	9Be	24Mg	47Ti	51V	53Cr	57Fe	60Ni	69Ga	90Zr	93Nb	120Sn	139La	140Ce	178Hf	181Ta	182W	232Th	283U
SP1 (light blue)	0.45	83.2	101	1.68	BDL	486	BDL	34.5	0.01	BDL	BDL	BDL	BDL	BDL	BDL	BDL	BDL	BDL
SP2 (light blue)	BDL	87.2	91.6	1.45	BDL	460	BDL	31.9	0.00	BQL	BDL	BDL	BDL	BDL	BDL	BDL	BDL	BDL
SP3 (light blue)	0.20	88.9	91.6	1.51	BDL	489	BDL	33.9	BDL	BDL	BDL	BDL	BDL	BDL	BDL	BDL	BDL	BDL
SP4 (light blue)	0.38	89.8	95.8	1.58	BDL	478	BDL	33.1	BDL	BDL	BDL	BDL	0.00	BDL	BDL	BDL	BDL	BDL
SP5 (light blue)	BDL	79.9	83.9	1.40	BDL	467	BDL	33.3	BQL	0.00	BDL	BDL	BDL	0.00	BDL	BDL	0.00	BDL
SP6 (light blue)	BDL	79.5	80.9	1.29	BDL	467	BDL	31.6	BDL	0.00	BDL	BDL	BDL	BDL	BDL	BDL	0.00	BDL
SP7 (light blue)	BDL	78.7	76.7	1.47	BDL	471	BDL	33.6	BDL	BDL	BDL	BDL	BDL	BDL	BDL	BDL	BDL	BDL
SP8 (light blue)	BDL	80.4	80.9	1.44	BDL	453	BDL	31.3	BDL	BDL	BDL	BDL	BDL	BDL	BDL	BDL	BDL	BDL
Average	-	**83.5**	**87.8**	**1.48**	-	**471**	-	**32.9**	-	-	-	-	-	-	-	-	-	-
SD	-	**4.5**	**8.4**	**0.12**	-	**12**	-	**1.2**	-	-	-	-	-	-	-	-	-	-
DL	*0.03*	*0.02*	*0.27*	*0.05*	*0.47*	*3.62*	*0.02*	*0.02*	*0.00*	*0.00*	*0.03*	*0.00*	*0.00*	*0.00*	*0.00*	*0.00*	*0.00*	*0.00*